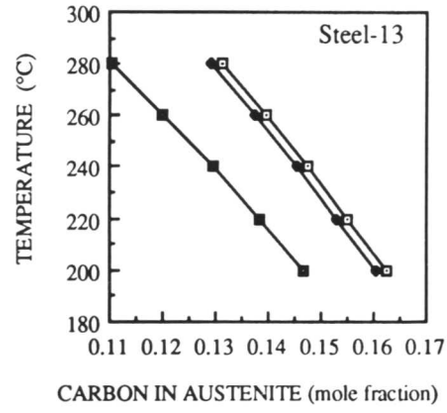

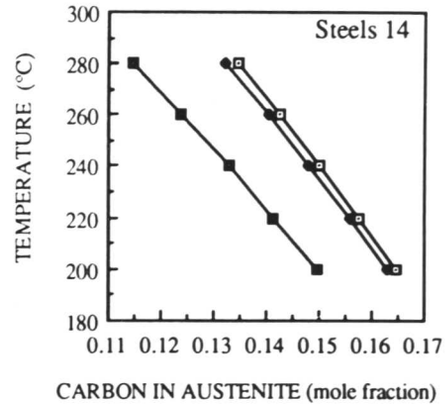

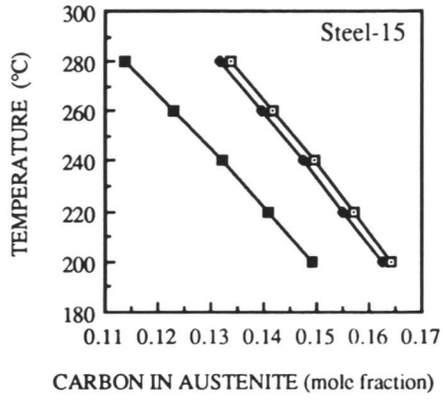

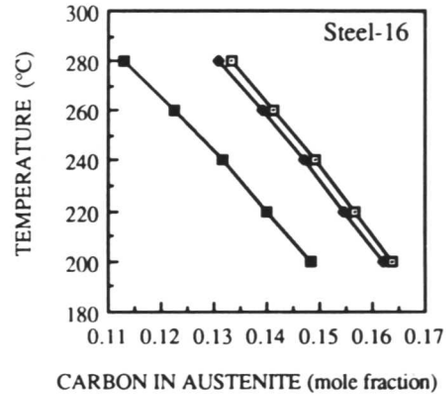

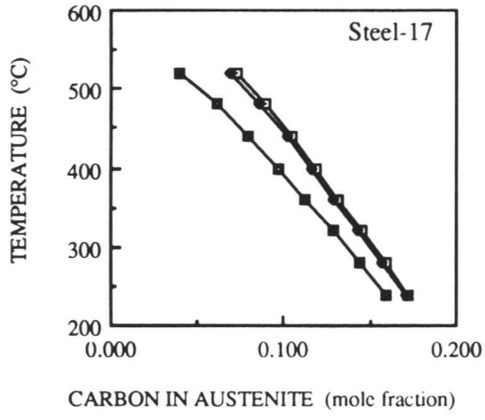

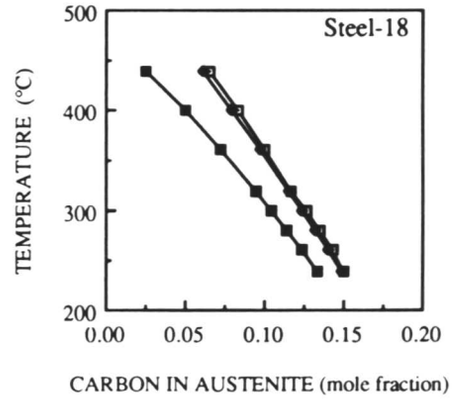

Fig. 9.6: *Continued.....*

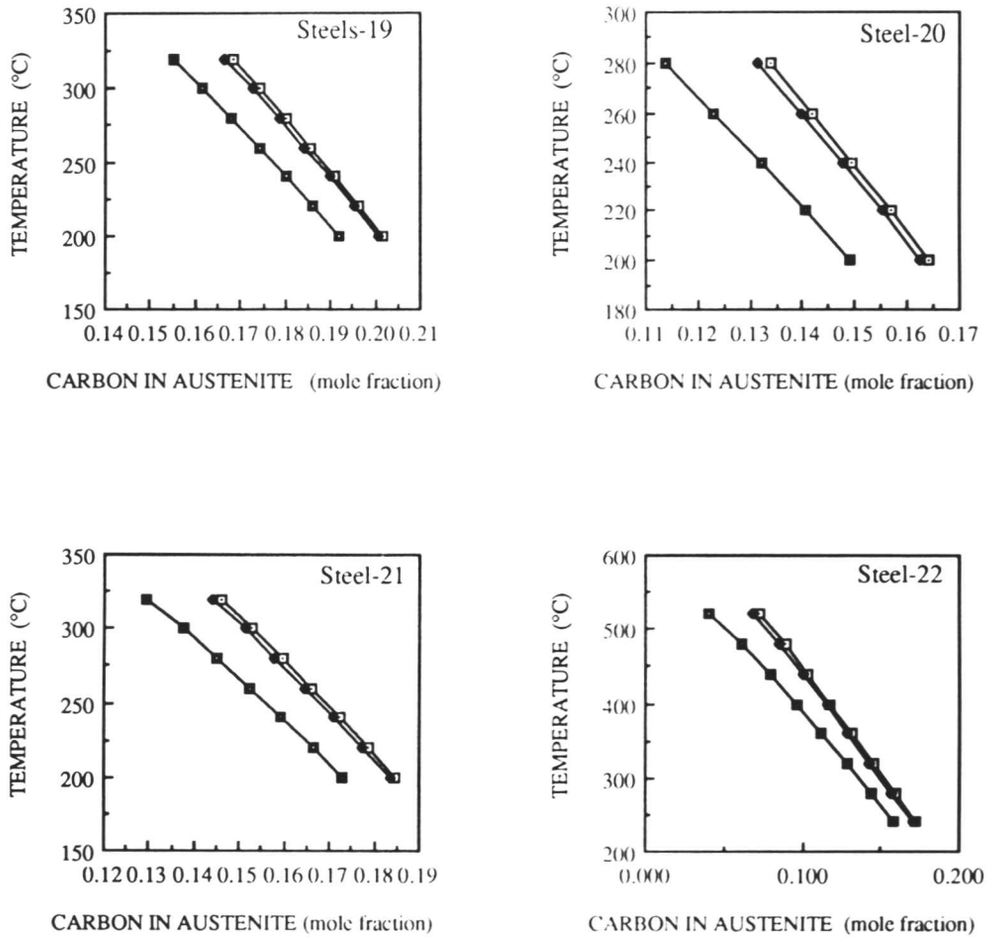

Fig. 9.6: *Effect of stored energy upon carbon content of austenite for the steels in Table 9.1.*

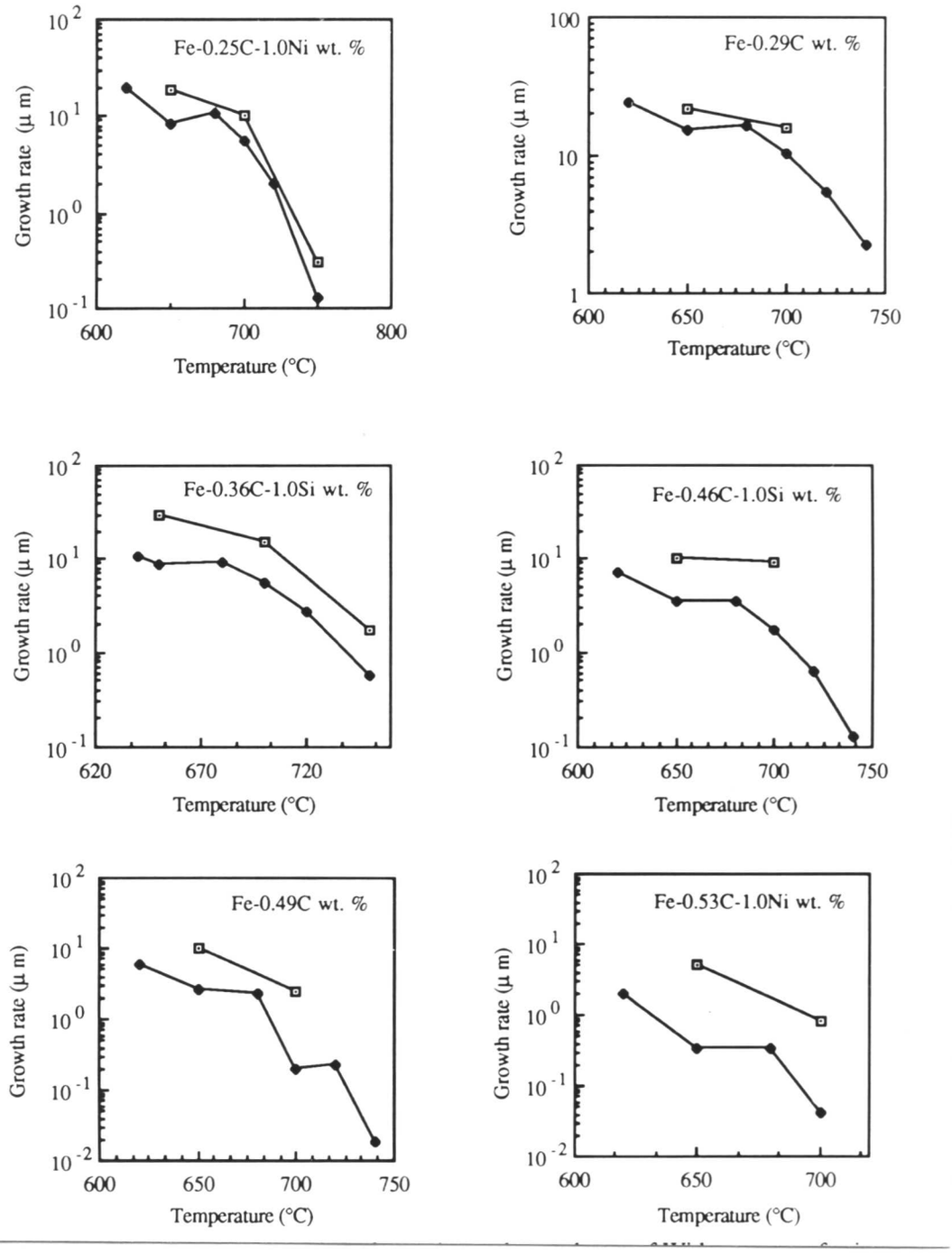

Fig. 9.7: *Continued.....*

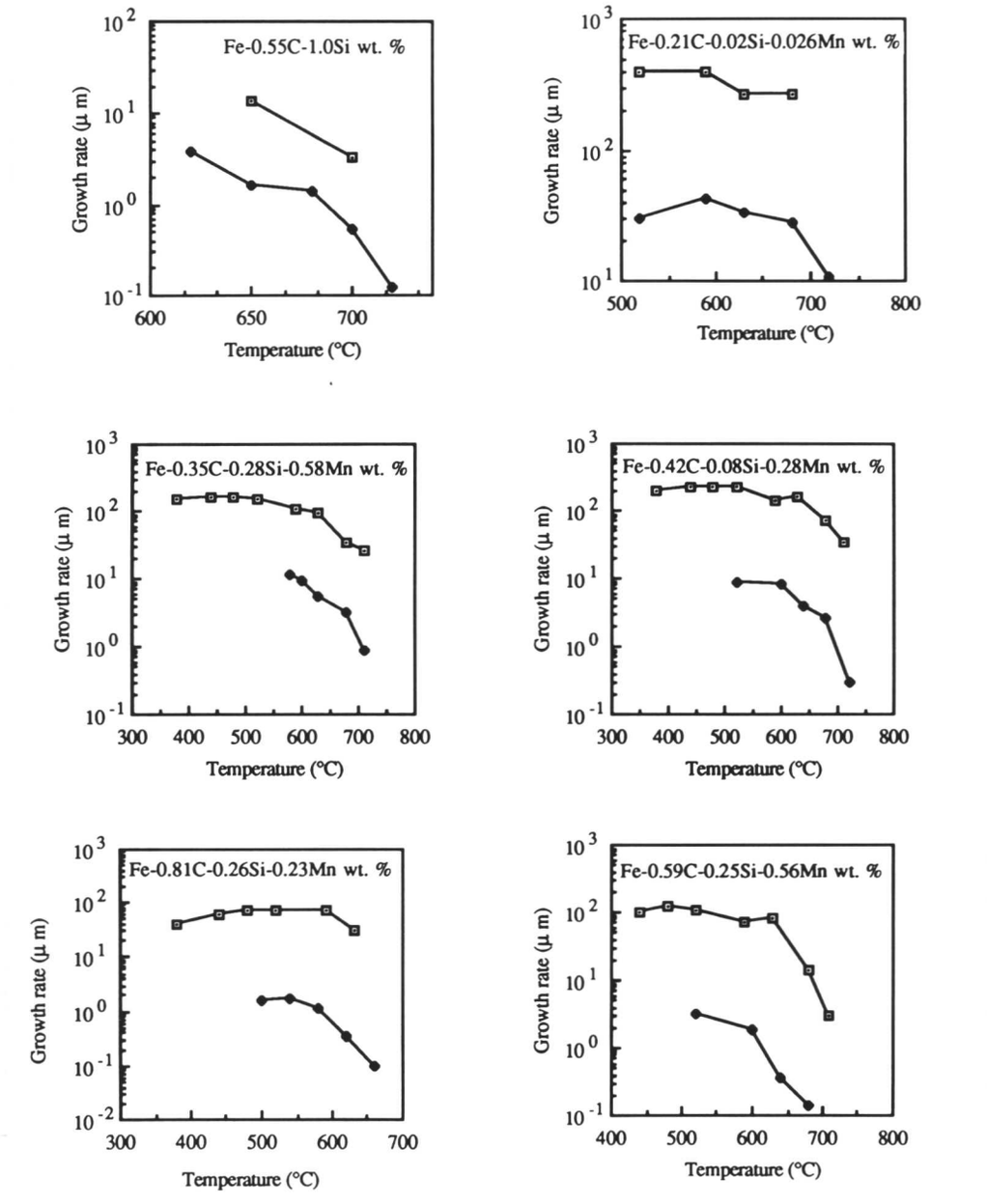

Fig. 9.7: *Calculated and experimental growth rates of Widmanstätten ferrite plates. Experimental data due to Hillert, [1960] and growth rates calculated using carbon diffusion controlled growth rate theory assuming a plate morphology of Widmanstätten ferrite and taking into account a stored energy of 50 J mol^{-1}.*

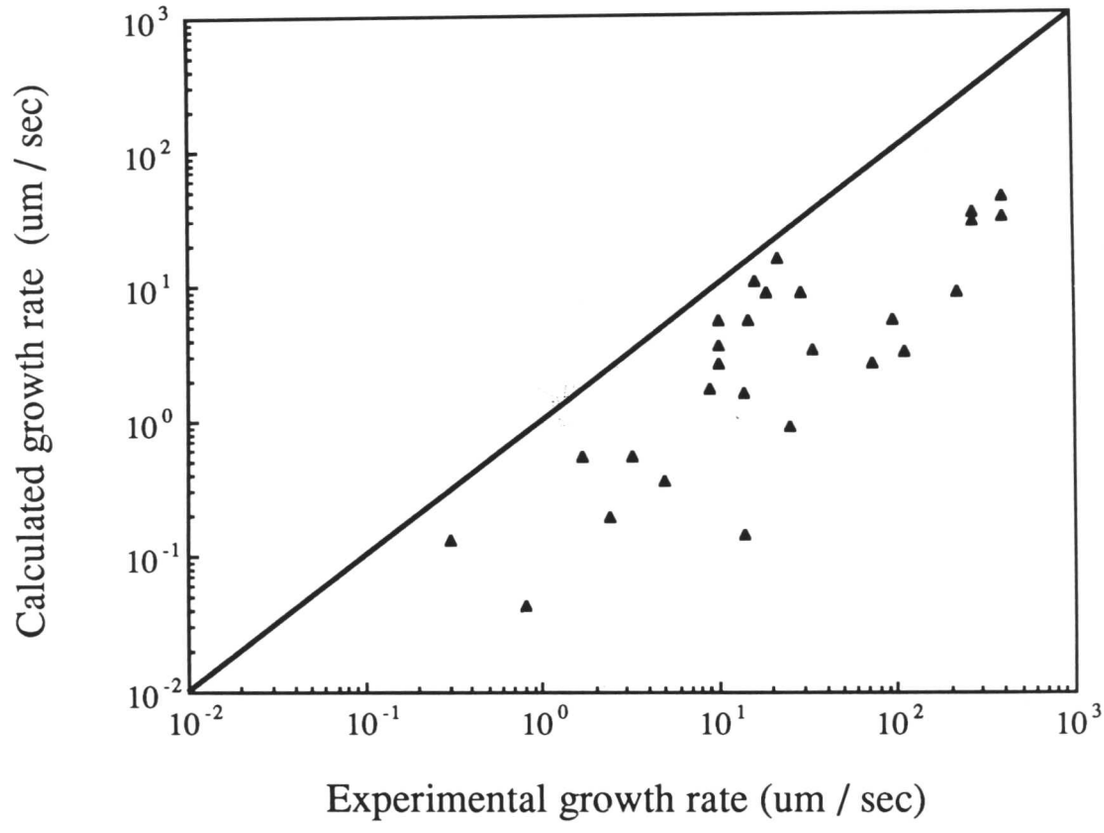

Fig. 9.8: *Combined graph of calculated and experimental growth rates of Widmanstätten ferrite plates. Experimental data due to Hillert, [1960] and growth rates calculated using carbon diffusion-controlled growth rate theory assuming plate morphology of Widmanstätten ferrite and taking into account a stored energy of 50 J* mol^{-1}.

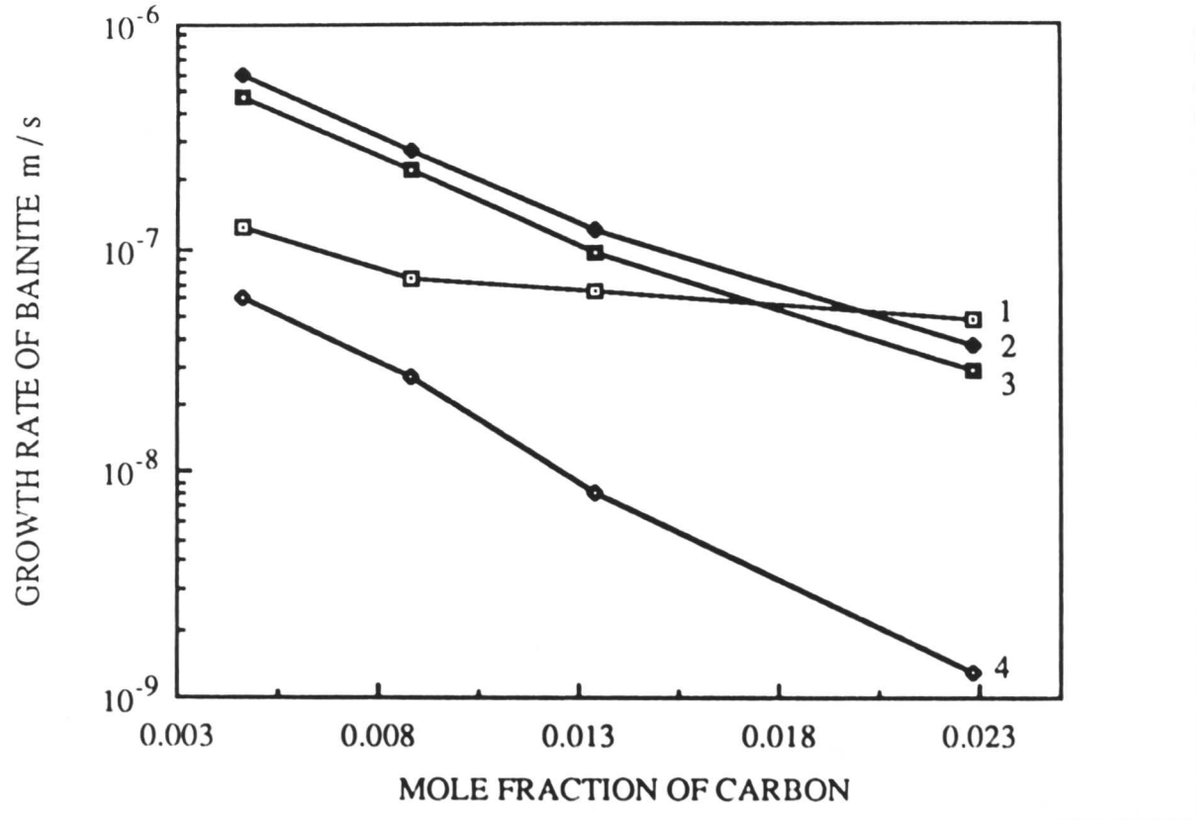

Fig. 9.9: *Comparison of experimental (curve 1) and calculated bainite growth rates. Curves 2-4 are calculated using stored energies of 0, 50, 400 J mol^{-1} respectively. The experimental data are due to Goodenow et al. [1963].*

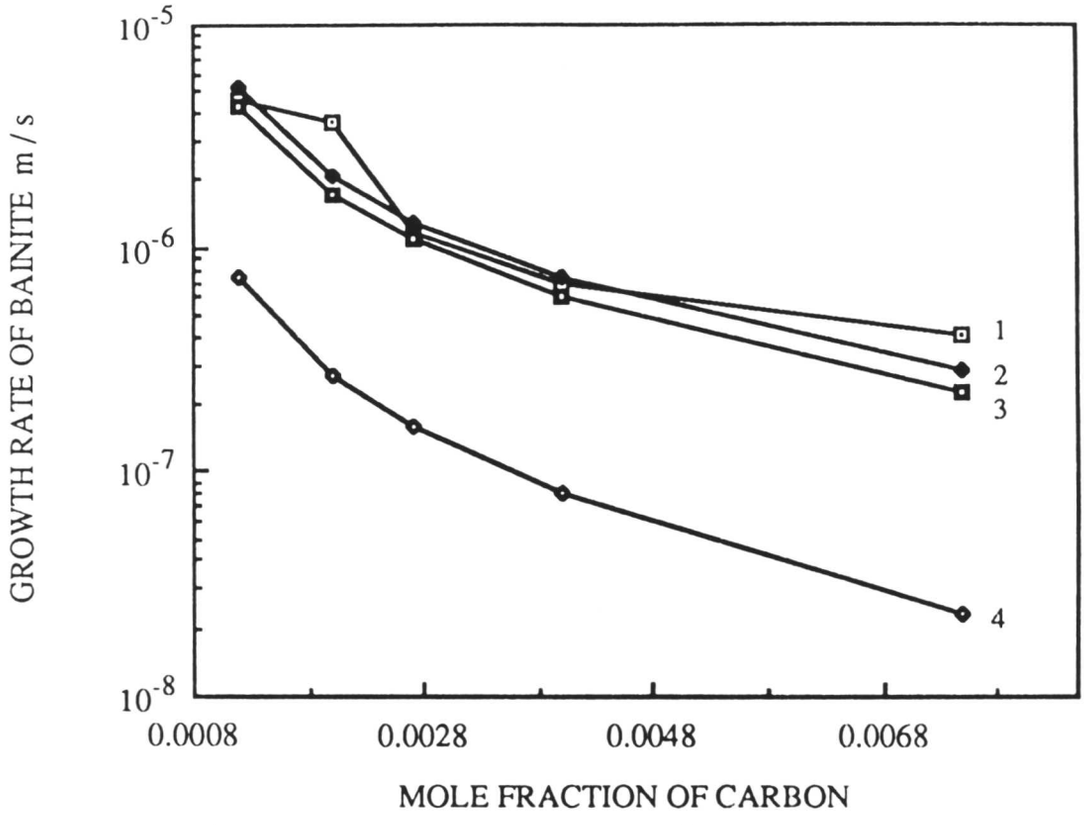

Fig. 9.10: *Comparison of experimental (curve 1) and calculated bainite growth rates. Curves 2-4 are calculated using stored energies of 0, 50, 400 J mol^{-1} respectively. The experimental data are due to Rao and Winchell [1967].*

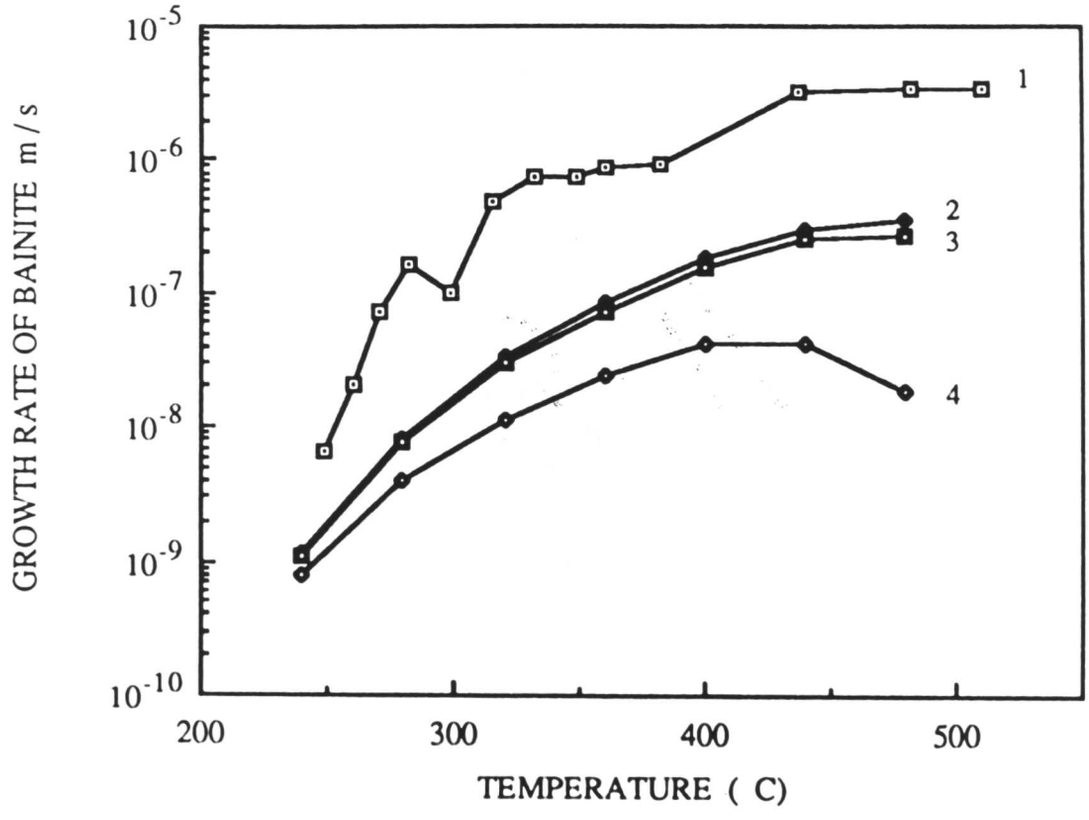

Fig. 9.11: *Comparison of experimental (curve 1) and calculated bainite growth rates. Curves 2-4 are calculated using stored energies of 0, 50, 400 J mol^{-1} respectively. The experimental data are due to Oblak and Hehemann [1967] (Table 9.1 steel-22).*

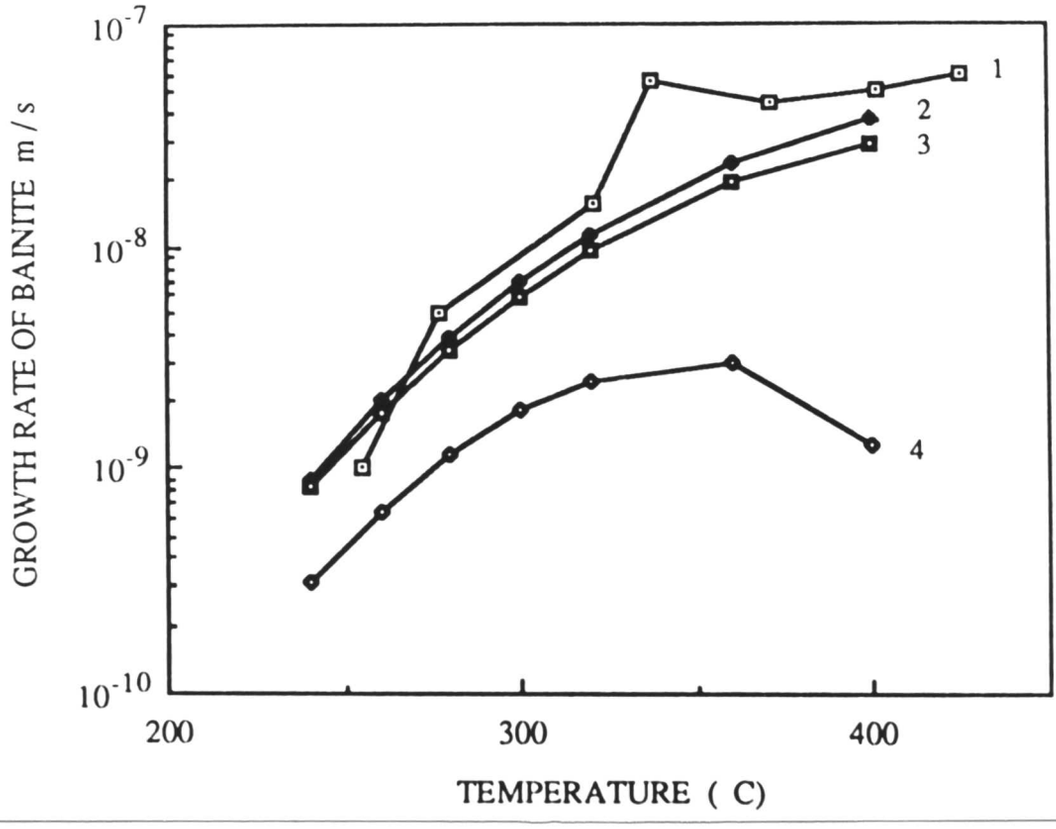

Fig. 9.12: *Comparison of experimental (curve 1) and calculated bainite growth rates. Curves 2-4 are calculated using stored energies of 0, 50, 400 J mol^{-1} respectively. The experimental data are due to Oblak and Hehemann [1967] (Table 9.1 steel-23)*

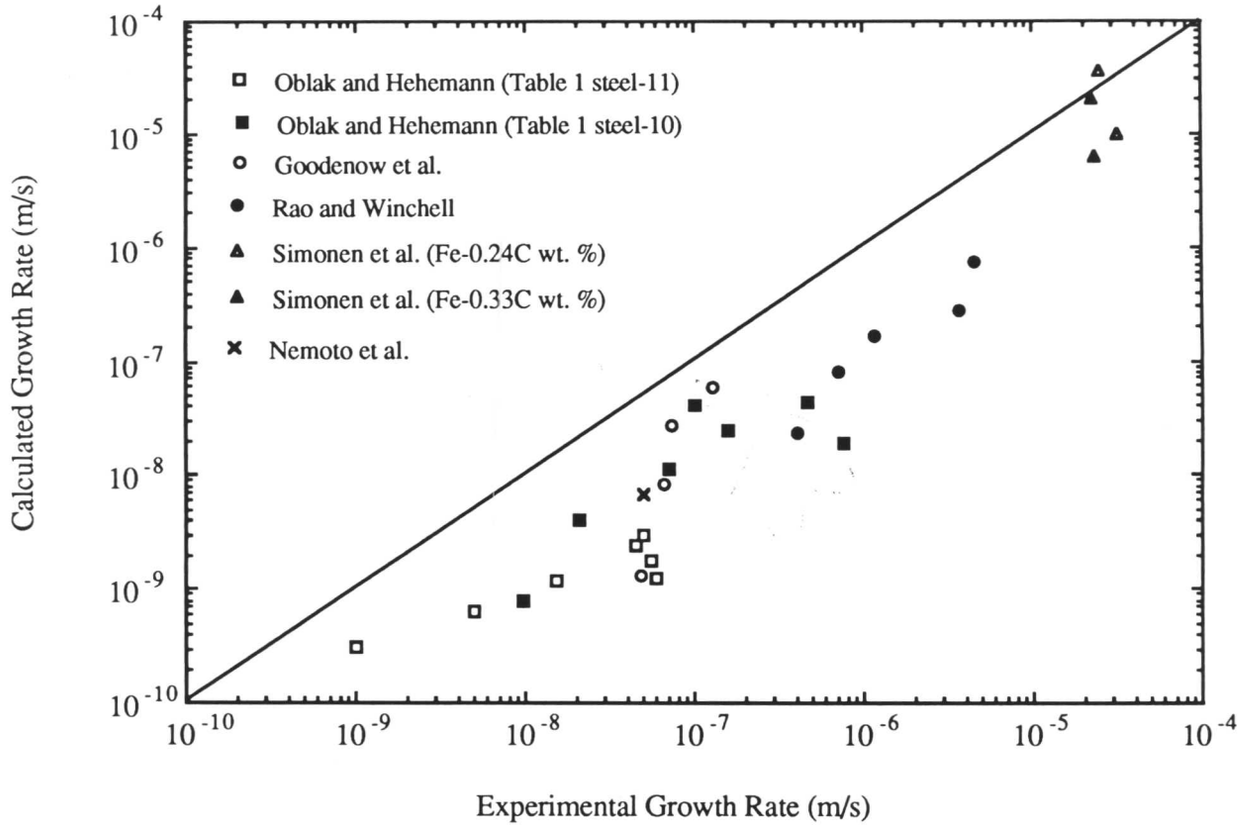

Fig. 9.13: *Comparison of experimentally measured growth rate of bainite sheaves with the growth rates calculated by carbon diffusion-controlled growth theory.*

It is evident from a comparison of the experimental data with the 4th curve on each figure, that the growth rate of bainite sheaves always exceeds that expected on the basis of carbon diffusion-controlled paraequilibrium transformation. This might intuitively be expected to be the case since there are now considerable data to indicate that bainite forms by diffusionless transformation, the excess carbon in the bainitic ferrite being partitioned or precipitated subsequent to transformation [Bhadeshia and Waugh, 1982, Christian and Edmonds, 1984]. However, the lengthening rate of a *sheaf* of bainite does not depend just on the rate of subunit lengthening, but also on the rate at which new subunits are nucleated. The overall lengthening rate of a sheaf may in fact be very low if the nucleation rate of subunits is sufficiently small, even though individual subunits may grow rapidly.

If it is assumed that a subunit reaches its limiting size in a time interval t, and

that the time Δt elapsed before another subunit nucleates at the tip of the original subunit, then the lengthening rate V_s of a sheaf is given by:

$$V_s = \frac{V}{1 + \frac{\Delta t}{t}} \tag{9.5}$$

where V is the average lengthening rate of a subunit. Because the growth of a subunit is diffusionless, V is expected to exceed the rate v calculated on the basis of carbon diffusion-controlled growth, although V_s will only be greater than v if the factor $[1+(\Delta t/t)]$ is sufficiently small (i.e., if the time interval between the nucleation of subunits is small in comparison with the time required for the subunits to reach their limiting size). The results in general indicate that $V_s >> v$ so that it can be safely concluded that the growth rate of the subunits is much faster than expected from carbon diffusion-controlled transformation. This is consistent with direct high-resolution observations on the growth of bainite subunits in an Fe-Mn-Si-C alloy [Bhadeshia, 1984]. The results also indicate that solute/interface interactions are not strong enough to slow down interface motion to velocities less than v, and that there is no special nickel-atom/interface interaction in Fe-Ni-C alloys, as has been suggested in the past [Rao and Winchell, 1967, Purdy and Hillert, 1984]. This conclusion also applies to Cr which is a significant alloying element in some of the steels analysed in the present.

9.7 Conclusions

It has been found that the lengthening rates of sheaves of bainite in alloys steels are far greater than expected from calculations based on carbon diffusion-controlled paraequilibrium transformation. Furthermore, it is found that the lengthening rates of individual bainite subunits within the sheaves must also be faster than carbon diffusion-controlled growth. The results are consistent with the proposed mechanism of the bainite transformation in which the growth of the bainite subunits is diffusionless, with the partitioning of carbon into the residual austenite occurring immediately after transformation.

Chapter 10
ON THE FORMATION OF INTRAGRANULAR WIDMANSTÄTTEN FERRITE PLATES IN ULTRA HIGH STRENGTH STEELS

10.1 Introduction

A number of ferrite morphologies are observed in wrought steels and steel weld deposits, when austenite is allowed to transform isothermally below the Ae_3 temperature depending upon for example, the austenitisation conditions, alloy chemistry, and cooling rates. These austenite decomposition products can be allotriomorphic ferrite, Widmanstätten ferrite, bainite or acicular ferrite. Widmanstätten ferrite usually grows either from prior austenite grain boundaries or from the already transformed grain boundary allotriomorphic ferrite and form in parallel formations *i.e.,* several plates nucleate and grow parallel to each other in packets. The final mechanical properties of the steel or weld deposits are closely related to the proportions of these phases in the microstructure.

Many observations have demonstrated that during cleavage failure, the cracks propagate virtually undeviated across individual sheaves of bainite in low–carbon, low–alloy steels [Pickering, 1967]. Similar results have been reported for low–carbon, low–alloy weld deposits, where qualitative evidence suggests that cleavage cracks propagate undeflected across packets of identically orientated bainite platelets but have to reinitiate on encountering sheaf boundaries [Chandel *et al.* 1985]. The size of cleavage facets obtained by brittle fracture is found to correlate well with the width of bainite sheaves, *i.e.,* the packet size [Naylor and Krahe, 1974], although there are other results which suggest that the *unit crack path* is somewhat larger than the packet size [Ohmori *et al.* 1974; Brozzo *et al.* 1977]. The unit crack path length is defined simply as the region within which the crack propagates in a nearly straight fashion [Matsuda *et al.* 1968, 1972]. The fact that the path length tends to be somewhat larger than the sheaf width, may have something to do with the fact that adjacent bainite sheaves, which are different variants of the orientation relationship with austenite may still have their cleavage planes fairly parallel [Brozzo *et al.* 1977]. Thus, any discrepancy between the packet size and unit crack path length does not weaken the basic argument that having a set of parallel ferrite plates in identical orientation is bad for toughness. Instead, it leads to a more general condition that groups of plates with a common cleavage plane should be avoided.

The idea that a " chaotic" microstructure (rather than one in which the ferrite plates are neatly arranged into packets) is better for toughness is very prominent in the welding industry [Savage and Aaronson, 1966; Rodrigues and Rogerson, 1977; Garland and Kirkwood, 1975; Billy *et al.* 1980]. Hence, controlled quantities of specific kinds of nonmetallic inclusions are tolerated in weld deposits, because they serve to stimulate the intragranular nucleation of ferrite platelets which radiate in many different directions from the inclusion nucleation sites; such a microstructure in welds is denoted " acicular ferrite", although it is now appreciated that acicular ferrite is nothing but intragranularly nucleated bainite [Bhadeshia, 1989]. A propagating crack then has to traverse plates in many different crystallographic orientations. Nonmetallic inclusions are otherwise regarded as harmful, since they can in many circumstances, be responsible for initiating cleavage or void nucleation. Using the same reasoning, deliberate additions of titanium oxide particles have recently been made to wrought steels in order to induce the intragranular nucleation of acicular ferrite [Yamamoto *et al.* 1987; Chijiiwa *et al.* 1988; Bhadeshia, 1989].

In quenched and tempered martensitic steels, fractographic measurements indicate that the dominant microstructural feature in the process of cleavage fracture is the size of the martensite packet [Roberts, 1970]. For heavily–alloyed ultra high-strength steels, ausformed martensites have been demonstrated to have a more chaotic spatial and size martensitic microstructures [Hornbogen, 1989]. This is one of the reasons why ausformed steels also have a higher level of strength without unduly sacrificing the toughness. Tomita and Okabayashi [1983, 1985] demonstrated improvements in the mechanical properties of martensitic steels, when the austenite grain structure was first partitioned into smaller regions by partial transformation to bainite. The small quantity of grain boundary nucleated bainite sheaves effectively refined the austenite grains prior to martensitic transformation.

The purpose of the work presented here was to investigate an alternative method of achieving the same effect, suggested by recent research on Fe–Cr–Mo–C weld deposits [Babu and Bhadeshia, 1990]. The intragranular nucleation can be stimulated if the austenite grain boundaries are removed as potential heterogeneous nucleation sites, by decorating them with thin layers of allotriomorphic ferrite (Fig. 10.1).

For the technique to work, the allotriomorphic ferrite must not act as a substrate for either secondary Widmanstätten ferrite or bainite, since both of these are in the form of undesirable packets of parallel platelets, and indeed, consume austenite which should be preserved for intragranularly nucleated transformation

products. The allotriomorphic ferrite can be rendered innocuous if austenite stabilising elements partition during its growth. This method of stimulating intragranular nucleation is particularly relevant in the context of high–strength steels, because unlike weld deposits, they have to be cleaner in order to ensure adequate toughness, so that the number of oxide particles present can be very limited indeed. It is their high strength which makes them much more susceptible to nonmetallic inclusions as fracture initiators. The experiments reported here are consequently conducted on high purity steels, with the aim of producing a microstructure in which the packets of martensite are refined by the presence of intragranularly nucleated Widmanstätten ferrite.

10.2 Experimental Procedures

Initially the material selected for this study were medium carbon high hardenability alloys. which were heavily alloyed with Si and Mn. These materials were purposely selected because of two reasons. Because they contain a high content of Mn which is austenite stabiliser thus can increased the incubation time for high temperature ferrite products and the silicon is a ferrite stabiliser. The high silicon content also made the carbide precipitation sluggish so that ferrite or bainite reaction can be studied without any interruption of the cementite precipitation. The chemical composition of material used are given in Table 10.1.

Table 10.1: *Chemical compositions (wt.%) of the alloys used in this investigation.*

	C	Si	Mn	Mo	Al	Ti	O
A1	0.22	2.07	3.00	–	0.011	0.004	0.0035
A2	0.22	2.05	3.07	0.70	0.005	0.004	0.0057

The alloys A1 and A2 were hot rolled round bars of 10 mm diameter in the as received condition. Throughout this investigation two types of specimens were used. One set had the form of 10 mm long rods of 3 mm diameter§ for isothermal heat treatments and optical study. The other samples were square sections with 10 mm edges, for surface relief experiments§.

§ 3 mm diameter was selected to facilitate transmission electron microscopy at any stage of the experiments.

§ The specimen preparation methods have been described in Chapter 3.

Fig. 10.2 illustrates schematically the types of heat treatment cycles were used during the present study. Before any isothermal transformation austenitisation treatments generally performed at 1100 or 1300 ^{o}C for 15 min to produce larger austenite grains, while the specimens were sealed in quartz capsules under a partial pressure of pure argon. After austenitisation the samples were taken out from the furnace, the quartz capsule was carefully broken and then immediately quenched into a fluidized bed, which was maintained at the reaction temperature (controlled to $\pm$ 3 ^{o}C), reacted for different time durations and then finally quenched into iced-water. The heat-treatment schedules are given in Table 10.2.

For surface relief experiments, specimens were mechanically polished to a $\frac{1}{4}$ μm finish, and sealed in quartz capsules. The heat treatments were carried out in the same way as described in the previous section except that after austenitisation, the quartz capsules were not broken but simply transferred to the fluidized bed maintained at the reaction temperature, reacted for the predetermined time and then the capsule was quenched into ice cooled water.

Any surface relief effects were imaged using the Nomarski differential interference technique with a Ziess optical microscope. The tilt sense was determined by through focusing experiments, using grain boundary grooves for reference. Upward upheavals consisting of two adjacent and opposing invariant-plane strains referred to as "tent-like" compared with a similar net depression of the free surface which are referred to as "vee-shaped" surface relief effects.

Optical microscopy of the heat treated specimens were carried out using conventional metallography techniques. Optical specimens were etched in 2nital solution and were examined using an Olympus microscope, fitted with Olympus 35 mm camera.

Thin foil specimens were prepared from the heat treated samples for electron microscopy by the methods given in Chapter 3, and examined in a PHILIPS EM400T transmission electron microscope operated at 120 kV, equipped with a LINK 860 energy dispersive analysis system to facilitate microanalysis. Standard thin foil correction programmes were used to compensate for X-ray detection efficiency and absorption. For quantitative analysis the specimen was tilted to 35^{o} towards the detector. Since this reduced the astigmatism in the image and improved the working resolution.

10.3 Theoretical Analysis of Transformation Characteristics

It is found that Widmanstätten ferrite can nucleate at a detectable rate when

[Bhadeshia, 1981]

$$G_{max} \leq G_N. \tag{10.1}$$

G_{max} represents the free energy change during nucleation, assuming that the nucleus adopts a composition which maximises this change. G_N is a nucleation function (linear with temperature and common to all steels) representing the free energy change which has to be exceeded before Widmanstätten ferrite can form at a detectable rate. In addition to this condition, growth should also be thermodynamically possible, so that the free energy change for growth ($\Delta G^{\gamma \rightarrow \gamma + \alpha}$) should exceed the stored energy of Widmanstätten ferrite

$$\Delta G^{\gamma \rightarrow \gamma' + \alpha} < -50 \text{ J mol}^{-1}. \tag{10.2}$$

Since the nucleation of bainite and Widmanstätten ferrite is described by the same function G_N, the nucleus is assumed to develop into bainite if the driving force for growth is sufficient to permit its diffusionless growth. Thus, bainite and Widmanstätten ferrite are normally represented by the same C–curve on the time–temperature–transformation (TTT) diagram, with Widmanstätten ferrite forming between the W_S and B_S (Widmanstätten ferrite–start and bainite–start respectively) temperatures and bainite forming below B_S§. These concepts have already been illustrated schematically in Fig. 7.10.

The aim was to induce the intragranular nucleation of a small volume fraction of Widmanstätten ferrite plates, in such a way that the plates do not grow in parallel formations. Nucleation on inclusions can achieve this because their sub–micron size cannot in general support the formation of more than one plate (although autocatalysis [Olson and Cohen, 1986] can stimulate the formation of other plates in close proximity). Particle nucleation is unlikely to have an opportunity to occur if the austenite grain boundary nucleation sites are active, since they are known [Ricks *et al.* 1982] to be more effective nucleants, so that transformation originating from the grain surfaces can swamp any intragranular events. Grain boundary nucleated (*i.e.,* secondary) Widmanstätten ferrite also has the unfortunate tendency to grow in packets of parallel plates. The boundaries can be rendered ineffective by decorating them with uniform, thin layers of allotriomorphic ferrite [Babu and

§ The TTT diagram can be considered to consist of two 'C' curves, the one at higher temperatures representing reconstructive transformations such as allotriomorphic ferrite and pearlite, and the other, extending to lower temperatures, for displacive reactions such as Widmanstätten ferrite and bainite [Bhadeshia, 1981].

Bhadeshia, 1990] which, due to the partitioning of austenite stabilising elements into the surrounding matrix, can be prevented from acting as substrates for the growth of secondary Widmanstätten ferrite. The steel utilised must therefore be very sluggish in its transformation to allotriomorphic ferrite.

High–strength steels are in this respect eminently suitable, because they are usually heavily alloyed for the sake of hardenability. A less well known effect first predicted theoretically is that the alloying leads to a splitting of the displacive C–curve of the TTT diagram into separate Widmanstätten ferrite and bainite curves [Bhadeshia and Svensson, 1989]. The G_{max} function is significantly curved at high temperatures, so that it can in principle intersect the G_N line at two points (Fig. 10.3). Widmanstätten ferrite ferrite can then form at elevated temperatures above the upper intersection temperature, and bainite at temperatures below the lower intersection (assuming that its growth is thermodynamically possible).

The steels used in the present study exhibit precisely this kind of behaviour, as illustrated in the calculated diagrams presented in Fig. 10.4. The heat–treatments were designed to take advantage of the form of the TTT diagram, which indicates that allotriomorphic ferrite forms long before the onset of Widmanstätten ferrite, although the latter forms over a very narrow temperature range after prolonged heat–treatment. They were also intended to provide further verification of the theory for Widmanstätten ferrite nucleation and growth.

10.4 Results

Fig. 10.4 shows the calculated TTT diagram for both the alloys. The temperature range in which experiments were carried out also marked in the TTT diagrams. The calculated Widmanstätten ferrite, bainite and martensite temperatures are given in Table 10.2.

10.4.1 *General Microstructure and Morphology*

Fig. 10.5 shows that Widmanstätten ferrite plates formed within the prior austenite grains, these are classic lenticular plate shaped with the curved ends because of constraints by the matrix due to the minimisation of the strain energy associated by the formation of these plates. The non parallel formation of these plates suggested that during the initial stage, they nucleate at intragranular nucleation sites such as inclusions and in the latter stage more plates nucleated by the sympathetic nucleation on the existing ferrite plates as shown in Fig. 10.6. It should be noted that these plates are formed in the body of the austenite grains. It is not a section effect produced by primary or secondary Widmanstätten ferrite plates

Table 10.2: *Heat–treatment schedules.*

Identification	Heat–treatment
A1-1	1100 °C @ 15 min → 680 °C @ 264 h → water quench
A1-2	1100 °C @ 15 min → 680 °C @ 600 h → water quench
A1-3	1100 °C @ 15 min → 700 °C @ 53 h → water quench
A1-4	1100 °C @ 15 min → 700 °C @ 100 h → water quench
A1-5	1100 °C @ 15 min → 700 °C @ 144 h → water quench
A1-6	1100 °C @ 15 min → 700 °C @ 216 h → water quench
A1-7	1100 °C @ 15 min → 720 °C @ 120 h → water quench
A1-8	1100 °C @ 15 min → 720 °C @ 346 h → water quench
A1-9	1100 °C @ 15 min → 740 °C @ 240 h → water quench
A1-10	1100 °C @ 30 min → 680 °C @ 264 h → water quench
A1-11	1100 °C @ 30 min → 700 °C @ 264 h → water quench
A1-12	1100 °C @ 30 min → 720 °C @ 264 h → water quench
A1-13	1100 °C @ 30 min → 740 °C @ 264 h → water quench
A1-14	1300 °C @ 15 min → 680 °C @ 264 h → water quench
A1-15	1300 °C @ 15 min → 740 °C @ 264 h → water quench
A2-1	1100 °C @ 15 min → 680 °C @ 600 h → water quench
A2-2	1100 °C @ 15 min → 700 °C @ 600 h → water quench
A2-3	1100 °C @ 15 min → 720 °C @ 240 h → water quench
A2-4	1100 °C @ 15 min → 740 °C @ 240 h → water quench
A2-5	1100 °C @ 30 min → 680 °C @ 264 h → water quench
A2-6	1100 °C @ 30 min → 700 °C @ 264 h → water quench
A2-7	1100 °C @ 30 min → 720 °C @ 264 h → water quench
A2-8	1100 °C @ 30 min → 740 °C @ 264 h → water quench
A2-9	1300 °C @ 15 min → 680 °C @ 264 h → water quench
A2-10	1300 °C @ 15 min → 740 °C @ 264 h → water quench

Table 10.3: *Calculated transformation temperatures (°C) [Bhadeshia, 1981a, 1981b, 1981c; Bhadeshia and Edmonds, 1980].*

	Ae_3	Ae'_3	W_S	B_S	M_S
A1	812	773	700	477	338
A2	818	777	700	469	324

originating from austenite grain boundaries or grain boundary allotriomorphic ferrite, above or below the plane of polishing. They were never seen to cross the austenite grain boundaries. These intragranularly nucleated ferrite plates can cross pearlite-austenite boundaries as shown in Fig. 10.7. It can be noted that the plate has sharp boundaries in austenite region while plate boundaries has disappeared in pearlite region, suggesting that pearlite has nucleated from these ferrite plate.

10.4.2 *Effect of Transformation Temperature*

The isothermal transformation temperature play an important role in determining the ambient temperature microstructure. This is clear from the micrographs shown in Fig. 10.8, all specimens were austenitised at 1100 °C for 15 minutes and isothermally transformed at various temperatures. It is depicted from Fig. 10.8, that these plates only form in a particular vicinity of the temperature range but below the W_S temperature for the alloy concerned, above this temperature grain boundary allotriomorphic ferrite grow and less number of plates were observed. While temperature at below 700 °C pearlite was formed in both the alloys as shown in Figure 10.11. Intragranular ferrite plates are often grouped in star-like and more complex configurations at lower reaction temperatures. The transformation temperature also affects the size and number of these plates. At higher transformation temperatures these plates are longer than those observed at the low temperatures as shown in Fig. 10.9a. The thickness of these plates is also very much dependent on the transformation temperature; as the transformation temperature decreases the thickness of these plates also increases Fig. 10.9b.

10.4.3 *Effect of Transformation Time*

In order to examine the effect of transformation time on the progress of transformation and on the morphology of these plates and to ensure that the plates are not a result of the transformation during cooling, specimens were quenched after transforming to various transformation time periods. It is clear that in the early stages of the reaction grain boundary allotriomorphs appeared on the prior austenite grain boundaries, and with the passage of time these allotriomorphs grow along the austenite boundaries and form a continuous layer of ferrite. Further increase in the transformation time does not effect grain boundary allotriomorphs very much but the nucleation of ferrite plates occurs within the body of the austenite grains as shown in the micrographs in Fig. 10.10a.

10.4.4 *Effect of Austenitisation Temperature*

The effect of austenitisation temperature is to control the austenite grain size, the higher austenitisation temperature leading to a larger austenite grain size, thus providing a large surface to volume ratio (Fig. 9.11). The austenitisation temperature influences both the transformation products and the morphology of these plates. The volume fraction of grain boundary allotriomorphic ferrite clearly decreases with larger austenite grain size. This promotes the subsequent intragranular nucleation of plates of ferrite. Thus, in the specimens austenitised at 900 or 1000 ^{o}C, the smaller austenite grain size has suppressed intragranular nucleation and only grain boundary allotriomorphic ferrite and equiaxed ferrite grains formed.

10.4.5 *Transmission Electron Microscopy (TEM)*

Using Transmission electron microscopy it was possible to find inclusions within some of ferrite plates (Fig. 10.12), inclusions which were presumably responsible for the heterogeneous intragranular nucleation of ferrite plates. The probability of observing such nucleation sites is rather small, so that inclusions need not be observed in all the plates even though they may be present. The plates have an apparent length of gently curved boundaries to giving the lenticular outline of the plates (Fig. 10.13). The tips of the plates were also found to be smoothly curved (Fig. 10.14). These morphological observation are consistent with the displacive mechanism in which the lenticular plates shape of ferrite arises through the need to minimise the strain energy associated with the shape deformation. These observations are inconsistent with the growth involving a ledge mechanism since the α/γ interface is certainly not found to be facetted in any way.

10.5 Discussion

A selected set of metallographic results are discussed here, to illustrate the fact that the heat treatment leads first to the growth of polycrystalline layers of allotriomorphic ferrite at the austenite grain surfaces, followed after a time lag, by the intragranular nucleation and growth of Widmanstätten ferrite. More extensive data were collected for alloy A1, which is discussed first. The results are presented in Fig. 10.10c, which shows that the first six days (144 h) of the heat treatment at 700 °C are used up in forming the allotriomorphic layers and that this is followed by the profuse precipitation of intragranularly nucleated Widmanstätten ferrite. With very few exceptions (Fig. 10.10d), the allotriomorphs themselves do no seem to stimulate the growth of secondary Widmanstätten ferrite plates, probably because they are in the wrong crystallographic orientation§ and because of the solute diffusion field associated with their growth (austenite stabilising elements are expected to be displaced into the matrix as the ferrite grows). In fact, there appeared to be a "precipitate–free zone" along the vast majority of the allotriomorphic ferrite/austenite interface (Fig. 10.15).

Theory indicates that in alloy A1, Widmanstätten ferrite should form only over a very narrow temperature range, approximately 690–700 °C, as illustrated in Fig. 10.4. Consistent with this, isothermal transformation at 680 °C produced a microstructure consisting mostly of allotriomorphic ferrite and pearlite, with very few plates of Widmanstätten ferrite (Fig. 10.8a). Plenty of Widmanstätten ferrite plates were however, found after transformation at 720 °C (Fig. 10.8b) and although this is in slight disagreement with the calculated transformation temperature range, examination of the 740 °C sample (Fig. 10.8d) shows clearly that the amount of Widmanstätten ferrite decreases as the temperature increases.

Quantitative metallographic measurements confirm these general trends; to make the measurements easier, the time at the austenitising temperature of 1100 °C was increased from 15 to 30 min (samples A1-10 to A1-13). The abrupt appearance of Widmanstätten ferrite after a long incubation time is also confirmed by the histogram presented in Fig. 10.16a, which represents a quantitative analysis of the number of Widmanstätten ferrite plates counted per unit area of sample,

§ Widmanstätten ferrite, because of its displacive growth mechanism, always has an orientation relationship with the parent austenite, which is close to the classical Kurdjumov–Sachs or Nishiyama–Wasserman relationships. Consequently, secondary Widmanstätten ferrite plates can only develop if the allotriomorph from which they grow happens to have such an orientation.

using optical microscopy at a magnification of ×100. Consistent with the general " C " shape of the Widmanstätten ferrite TTT curve (Fig. 10.4), both the maximum length (Fig. 10.16b) and the number density of Widmanstätten ferrite plates (Fig. 10.16c), show peaks in plots versus the transformation temperature.

Experiments using Alloy A2 revealed the same general trends, with the exception that the rate of reaction decreased in all respects, Fig. 10.16. This is consistent with the known effect of molybdenum in retarding the reaction rate, and it is notable that the retardation is evident in spite of the fact that alloy A2 has a somewhat larger oxygen concentration, corresponding to a larger oxide particle density. It is the oxides which seem to provide sites for the heterogeneous nucleation of Widmanstätten ferrite. This latter point is extremely difficult to prove on a statistical basis because of the very small probability of observing an inclusion in a plate of ferrite [Bhadeshia, 1989], but supporting evidence was nevertheless gathered using carbon extraction replicas for transmission electron microscopy. Fig. 10.17 shows an example where it can be reasonably claimed that clusters of Widmanstätten ferrite plates radiate in many directions from an inclusion. Microanalysis of the inclusions extracted on the replica indicate that they are predominantly aluminium oxides. The mean chemical composition of the inclusions are given in Table 10.4.

Table 10.4: *Average chemical compositions of the three inclusions analysed.*

Inclusion No.	EDX analysis (wt. %)			
	Fe	Si	Mn	Al
A1-12	5.6	53.3	–	41.0
A1-8	35.1	58.1	4.3	2.3
A1-8	2.2	1.0	–	96.76

10.6 Conclusions

A method has been developed to refine the microstructure of clean, high–strength martensitic steels by partitioning the austenite grain structure with intragranularly nucleated plates of Widmanstätten ferrite. The plates were induced to nucleate heterogeneously on oxide particles present in the steels, by first forming uniform, thin layers of inactive allotriomorphic ferrite at the austenite grain surfaces. This effectively removed the austenite grain boundaries as potential sites for

the nucleation of Widmanstätten ferrite, which consequently nucleated intragranularly on oxide particles, with ferrite plates radiating in many directions from the oxide particles in such a way as to subdivide the remaining austenite into fine blocks. Quenching after this partial transformation to allotriomorphic and Widmanstätten ferrite resulted in the martensitic decomposition of the blocks of residual austenite, leading to a generally very refined overall microstructure.

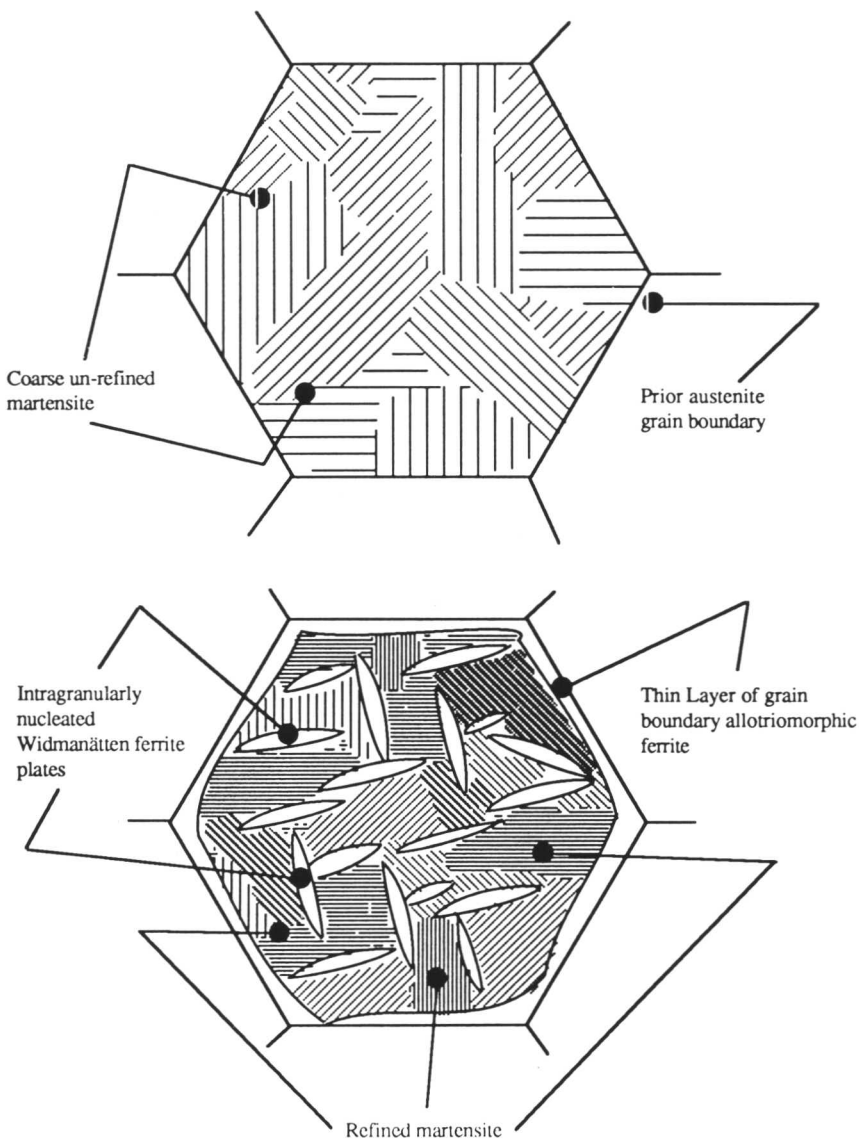

Fig. 10.1: *Schematic illustration of the proposed method of refining the martensitic microstructure with intragranularly nucleated plates of Widmanstätten ferrite.*

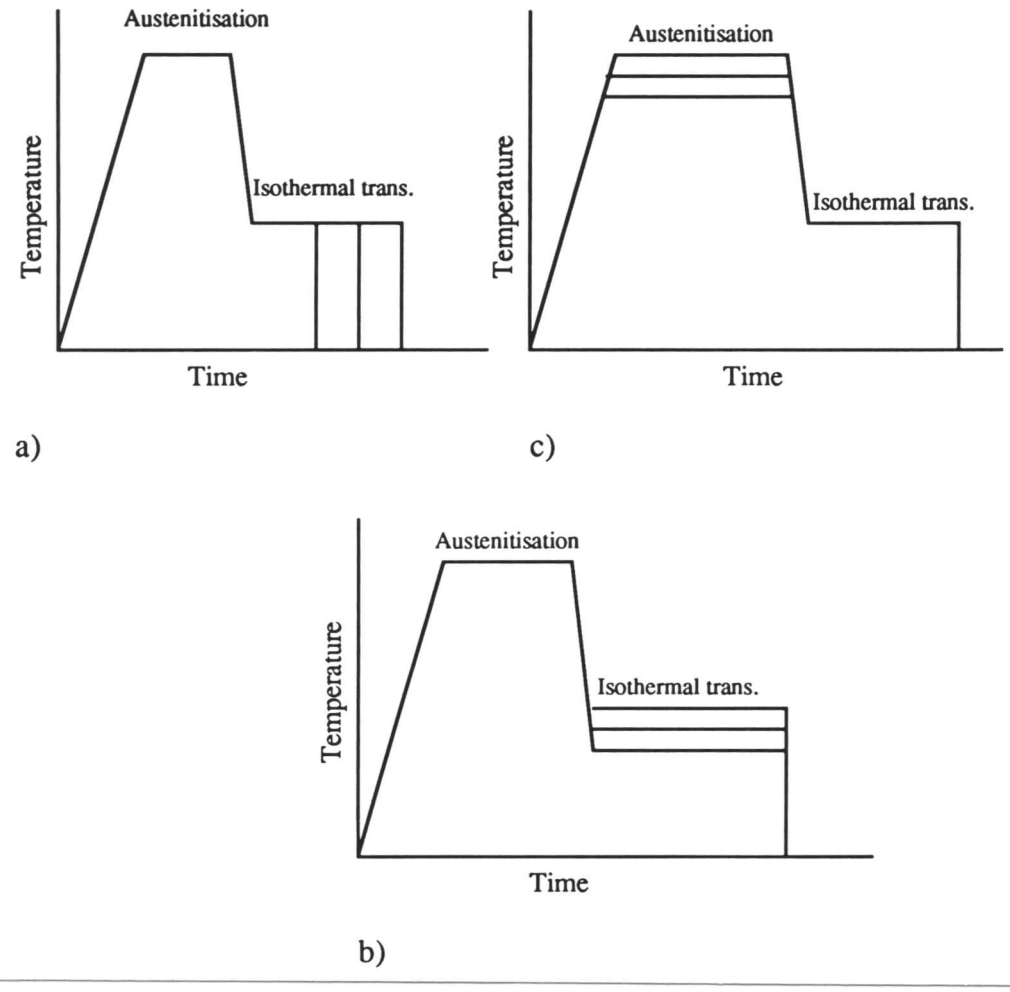

Fig. 10.2: *Schematic illustration of the heat treatments used. (a) Variation of isothermal transformation time. (b) Variation of isothermal transformation temperature. (c) Effect of austenitisation temperature.*

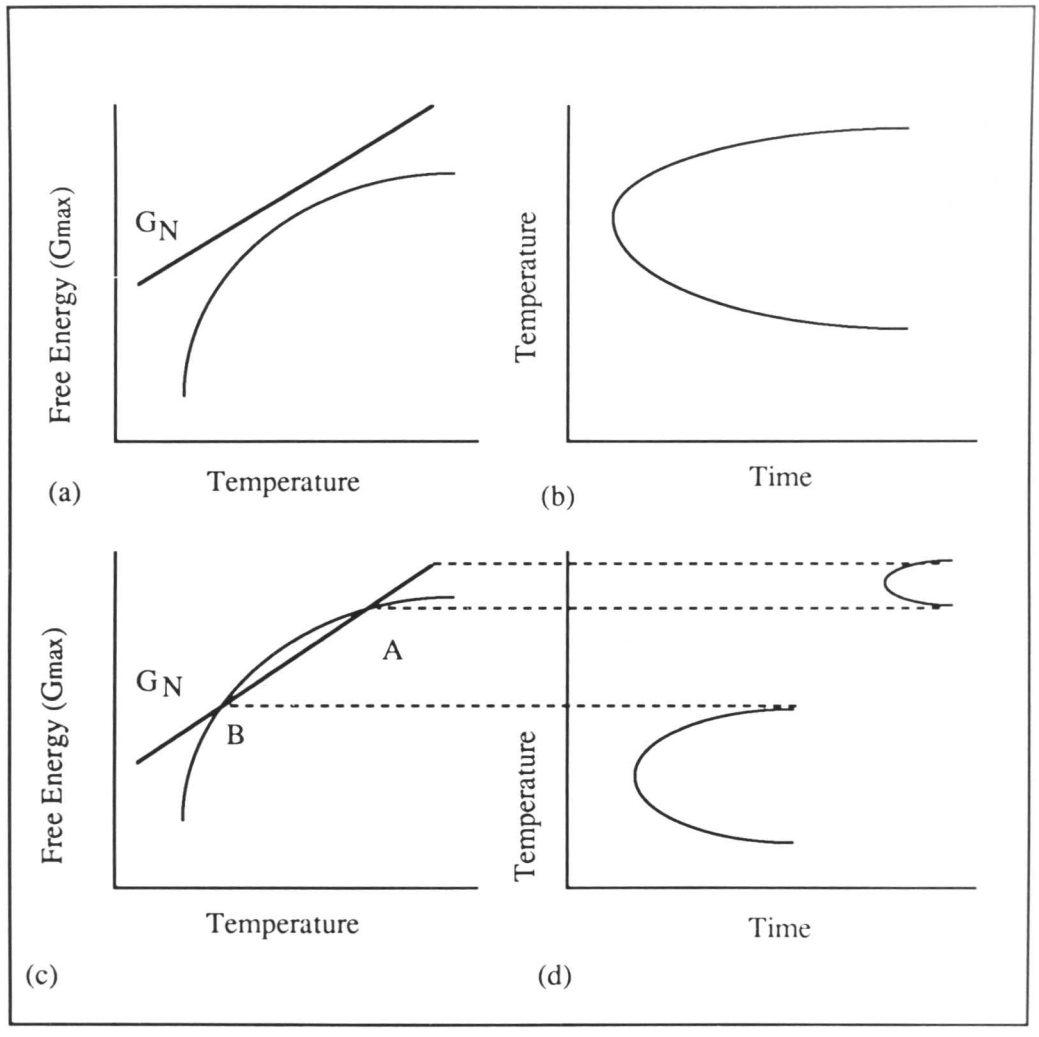

Fig. 10.3: *Schematic illustration of how the double intersection of the G_{max} curve with the nucleation function G_N leads to a splitting of the displacive C–curve into two regions, one for Widmanstätten ferrite and the other for bainite. (a) Represent the case where nucleation of Widmanstätten ferrite or bainite is possible over the whole temperature range, hence both Widmanstätten ferrite and bainite exhibit a single TTT curve and (b) is the case where the nucleation of displacive transformation products is not possible between the temperatures A and B, and hence TTT diagram splits into two C-curves, one for Widmanstätten ferrite and the other one for bainite.*

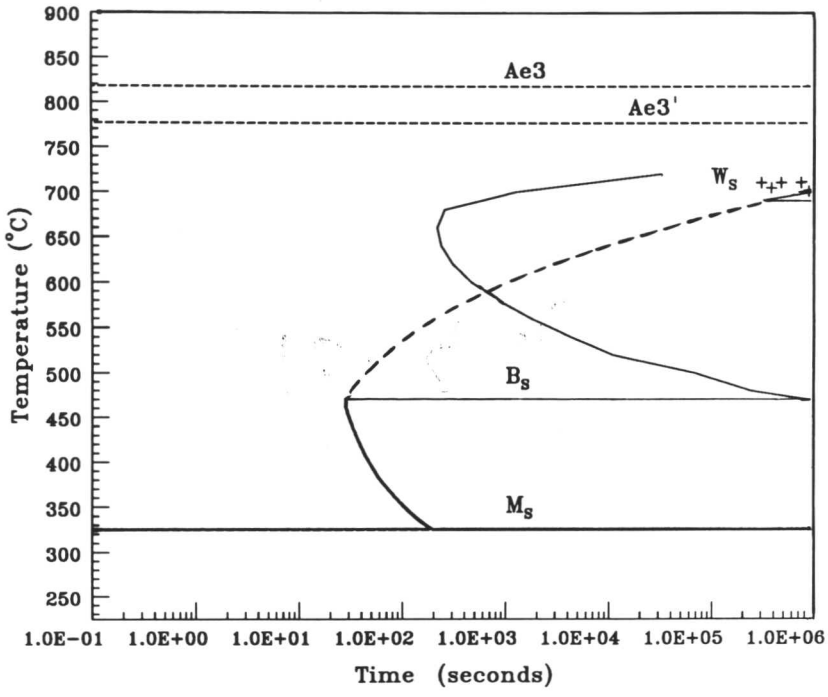

For alloy A1

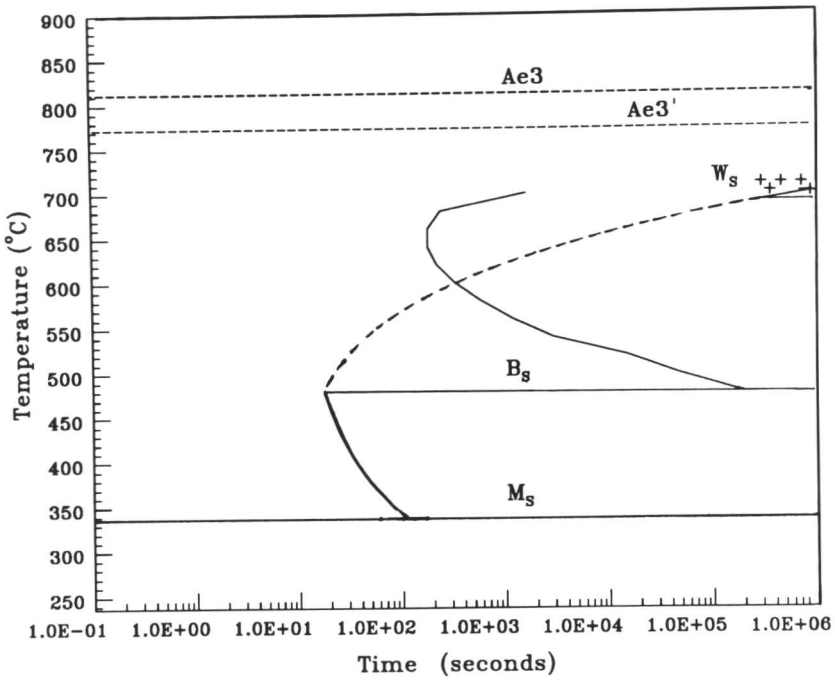

For alloy A2

Fig. 10.4: *Calculated TTT diagrams for the two steels used in the present study.*

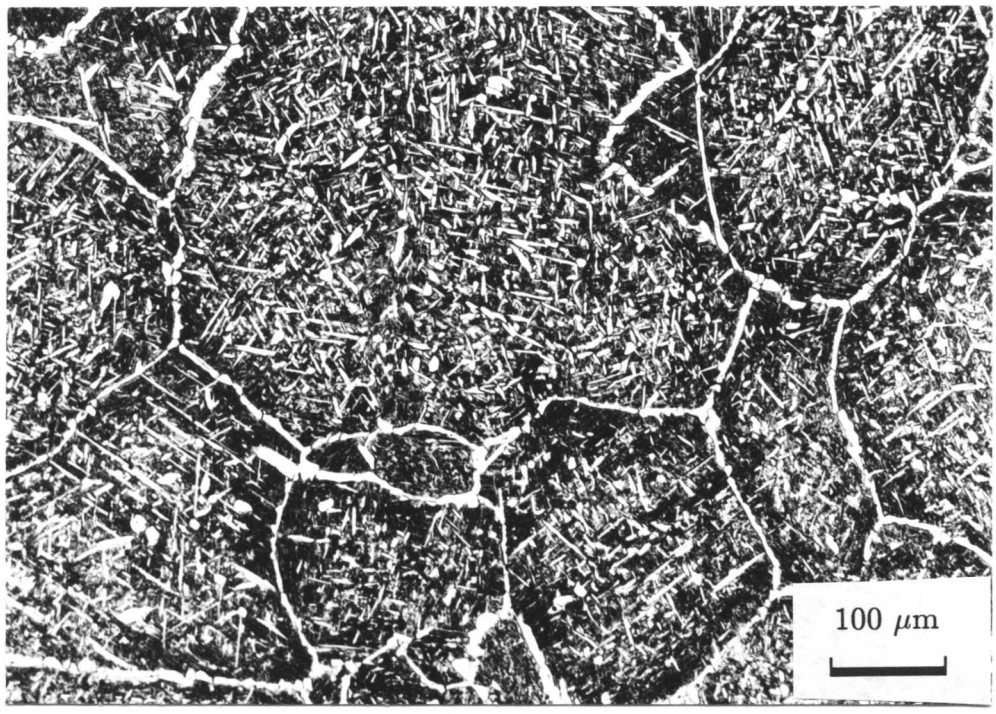

(a)

(b)

Fig. 10.5: *Optical micrographs showing the formation of Widmanstätten ferrite plates in alloys (a) A1 and (b) A2. 1100 °C @ 15* min → *700 °C @ 9* days.

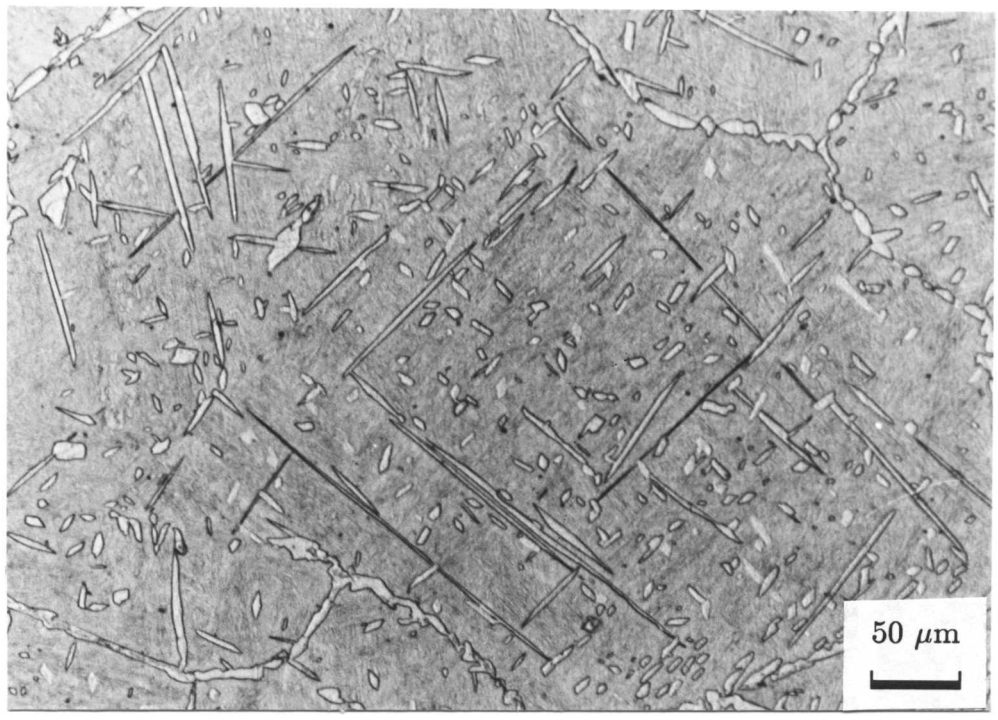

Fig. 10.6: *Optical micrographs showing the sympathetic nucleation of Widmanstätten ferrite plates in alloys A2 (A2-2).*

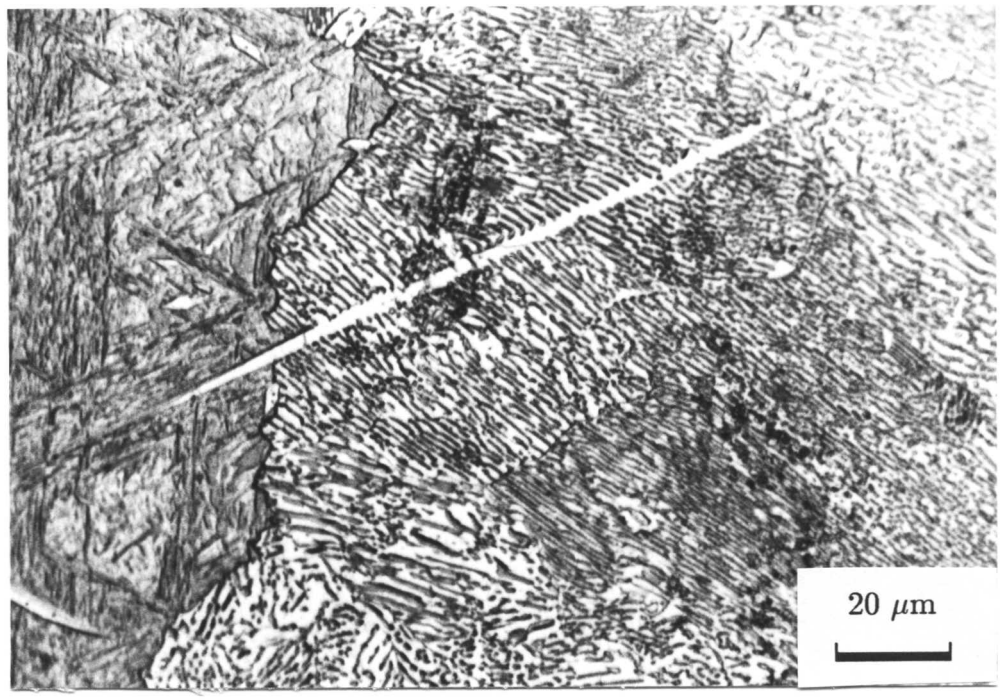

Fig. 10.7: *An illustration of a pearlite colony growing around a intragranularly nucleated Widmanstätten ferrite plate (A2-1).*

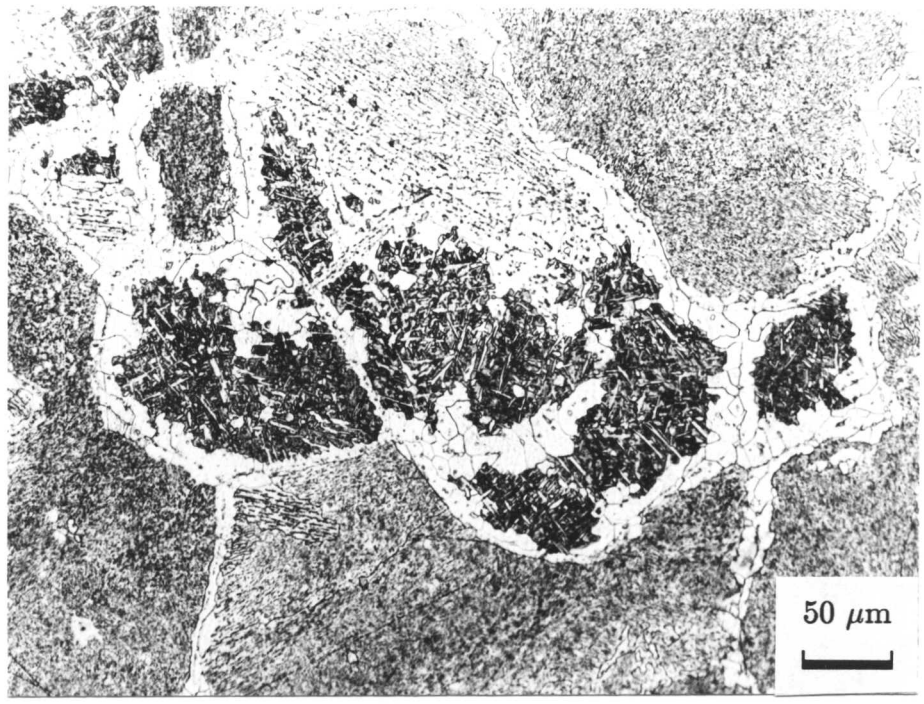

(a)

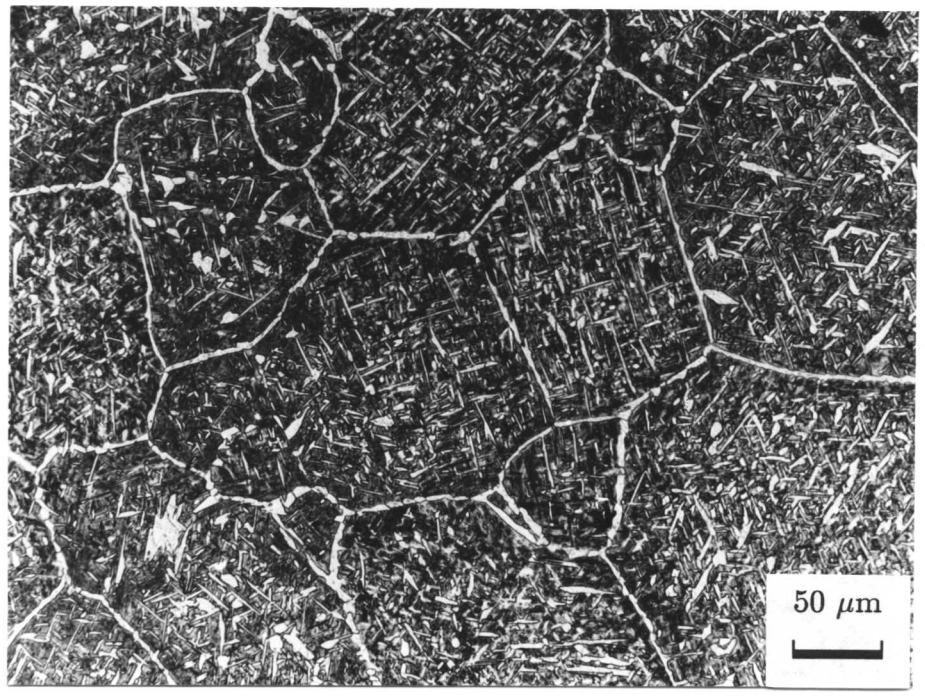

(b)

Fig. 10.8: *Continued* .....

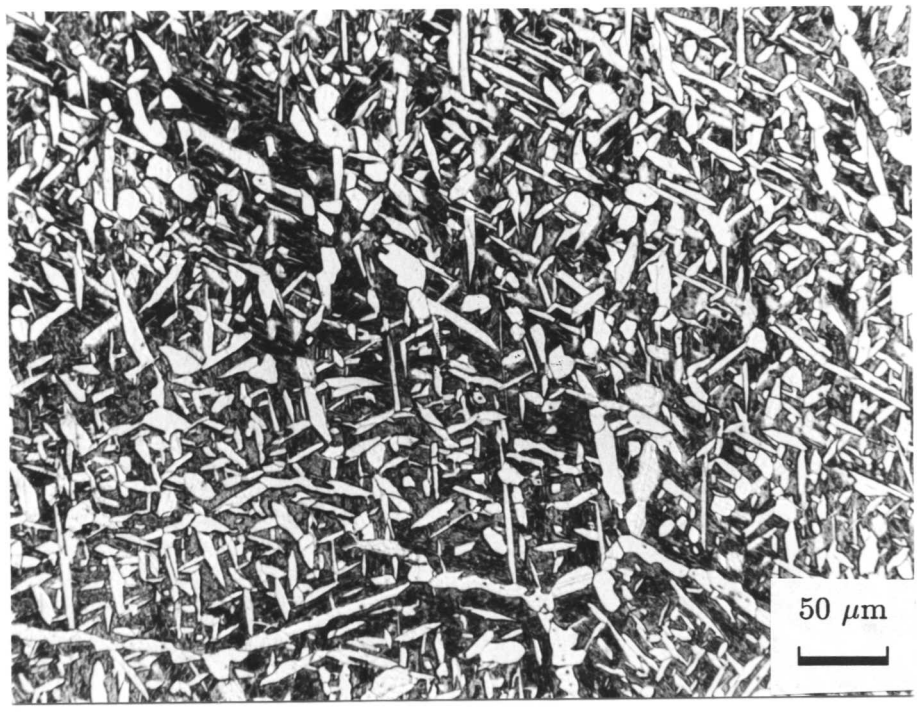

(c)

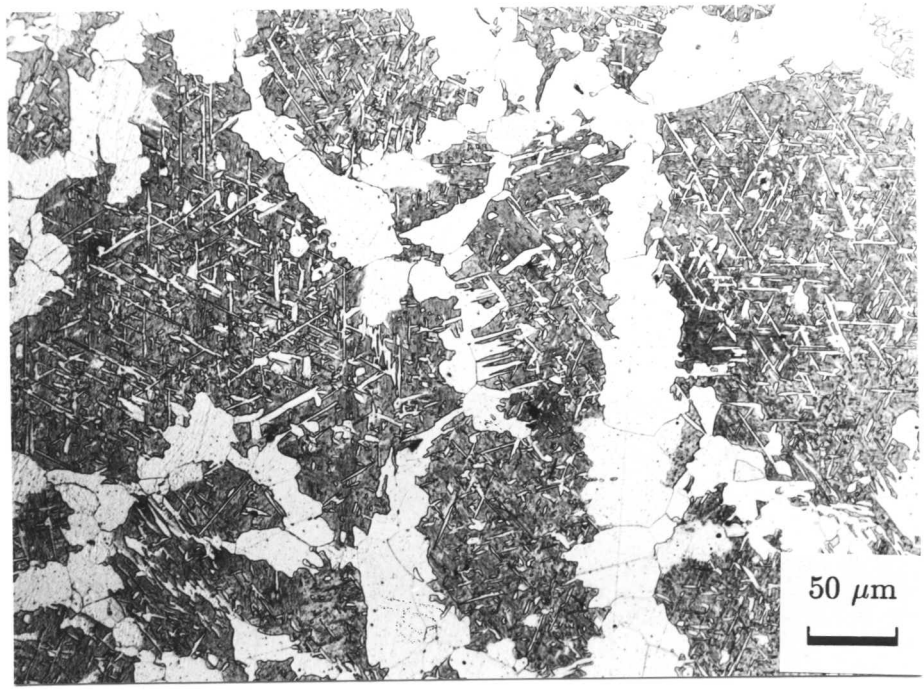

(d)

Fig. 10.8: *Effect of transformation temperature on the formation of intragranular Widmanstätten ferrite plates. All specimens were austenitised at 1100 °C for 15* min *and isothermally transformed at (a) 680 °C @ 11* days *(b) 700 °C @ 9 days (c) 720 °C 346 @* hr *(d) 740 °C @ 10 days.*

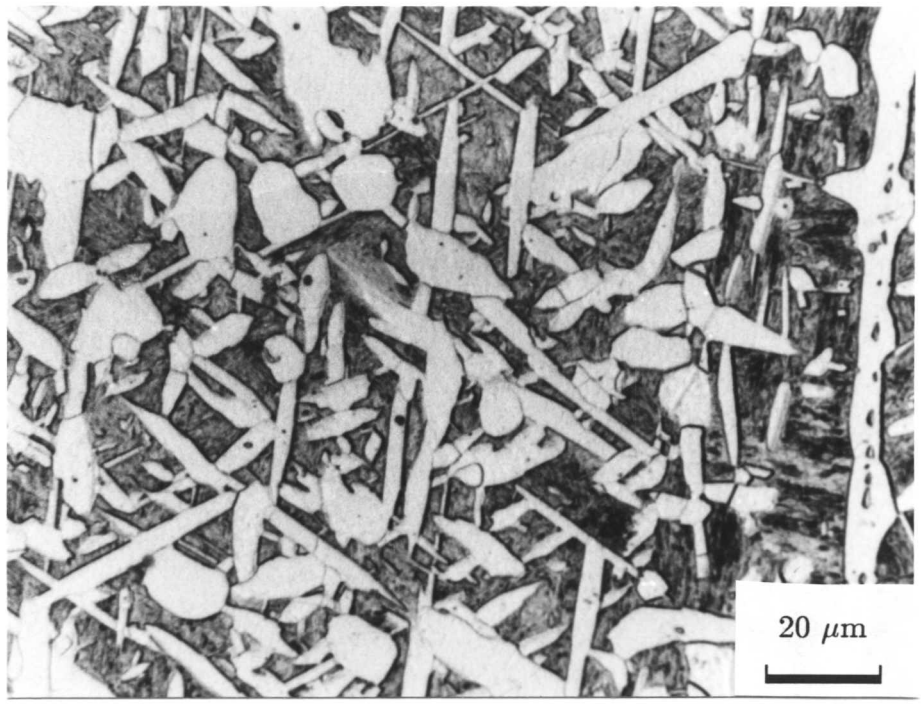

(a)

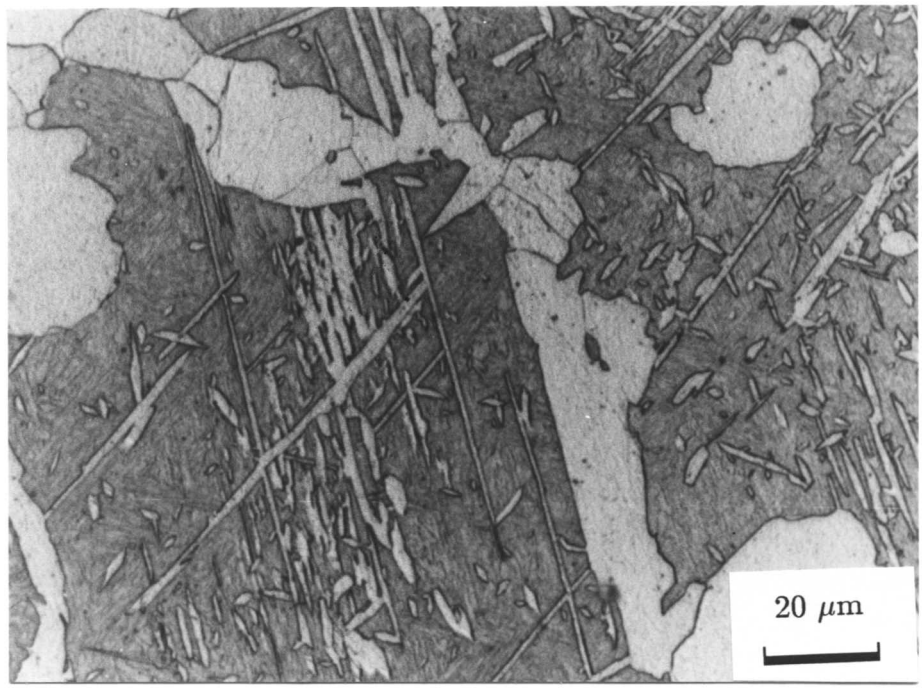

(b)

Fig. 10.9: *Effect of transformation temperature on the size, distribution and thickness of intragranular Widmanstätten ferrite plates. All specimens were austenitised at 1100 °C for 15* min *and isothermally transformed at (a) 720 °C @ 346* hr *(b) 740 °C @ 10 days.*

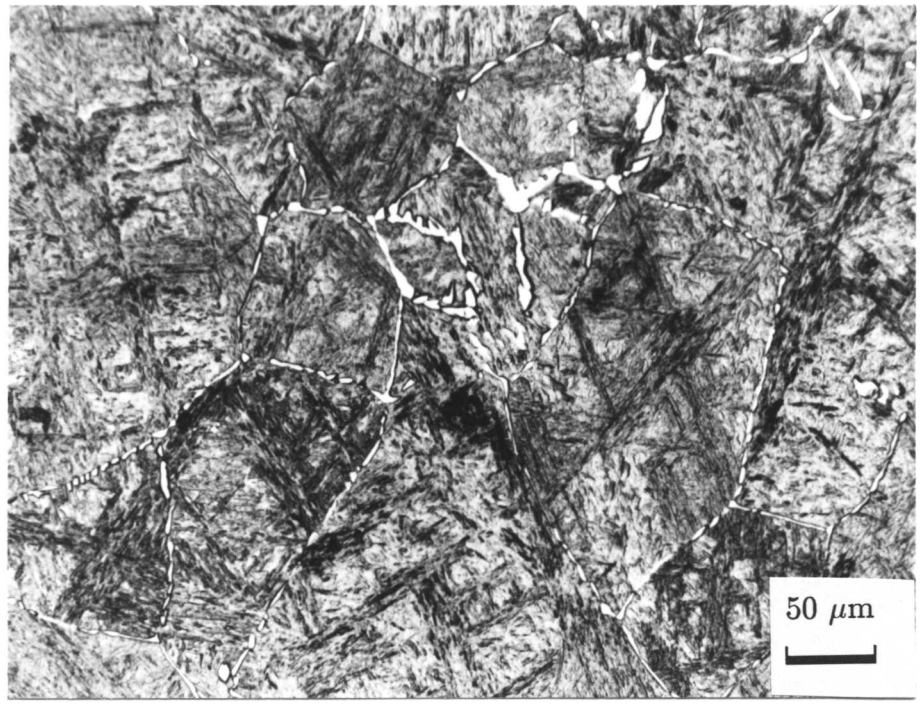

(a)

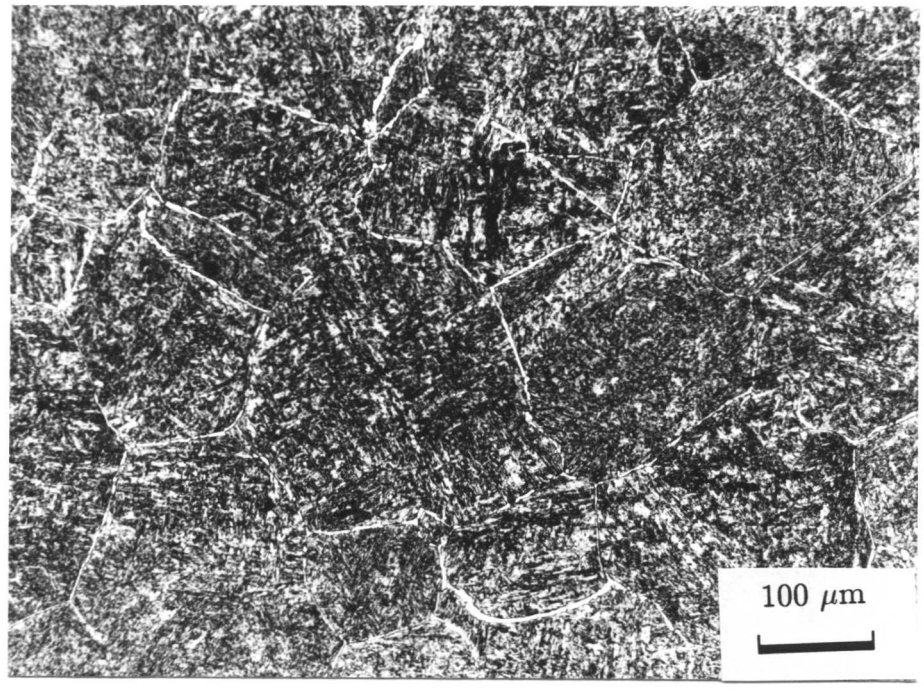

(b)

Fig. 10.10: *Continued .....*

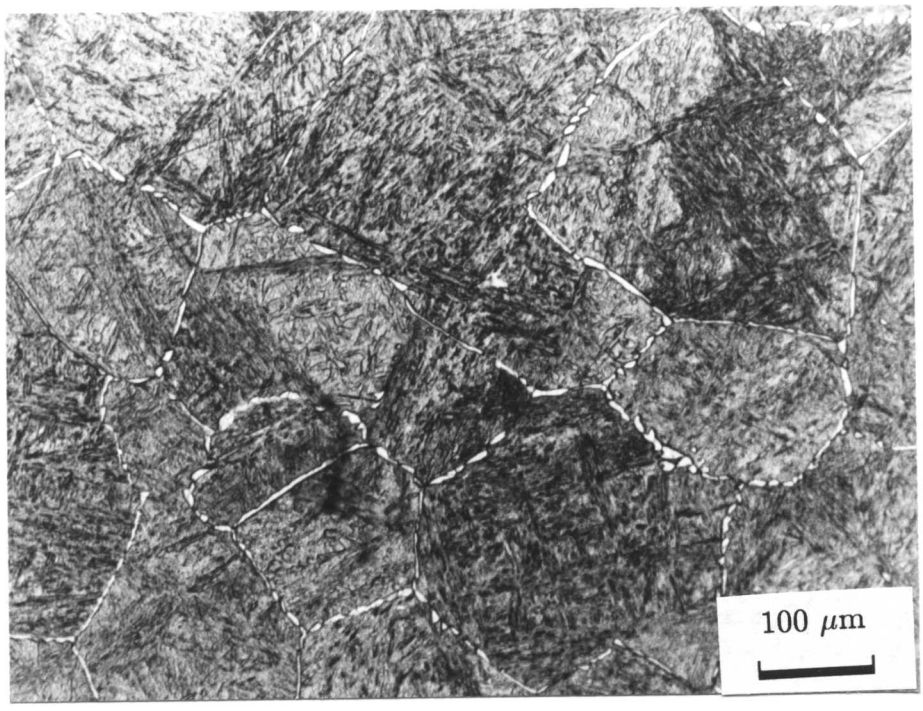

(c)

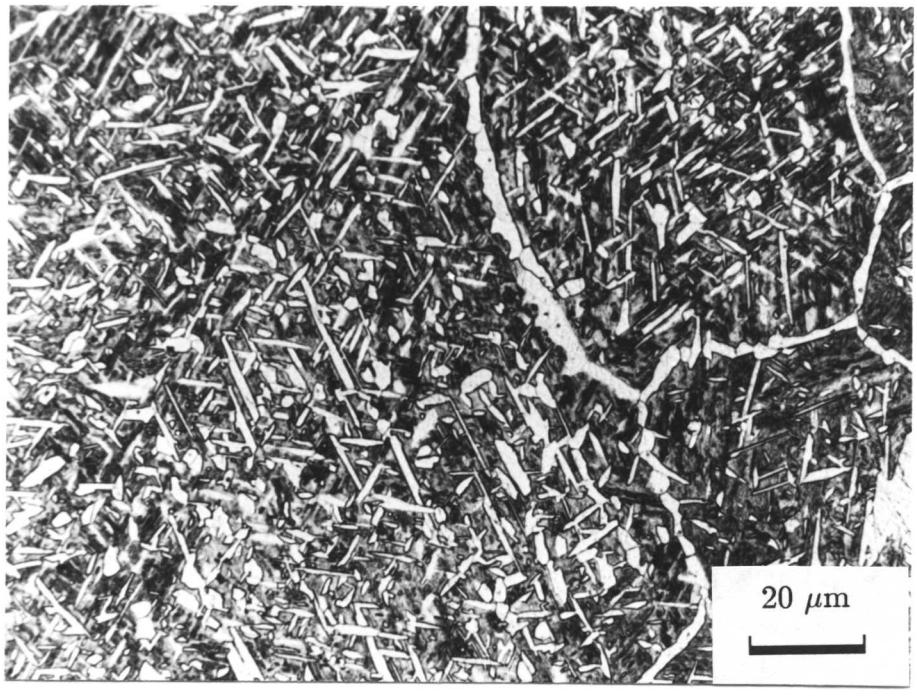

(d)

Fig. 10.10: *Effect of transformation time on the formation of intragranular Widmanstätten ferrite plates. All specimens were austenitised at 1100 °C for 15* min *and isothermally transformed at 700 °C for (a) 53* hr *(b) 100* hr *(c) 6* days *(d) 9* days.

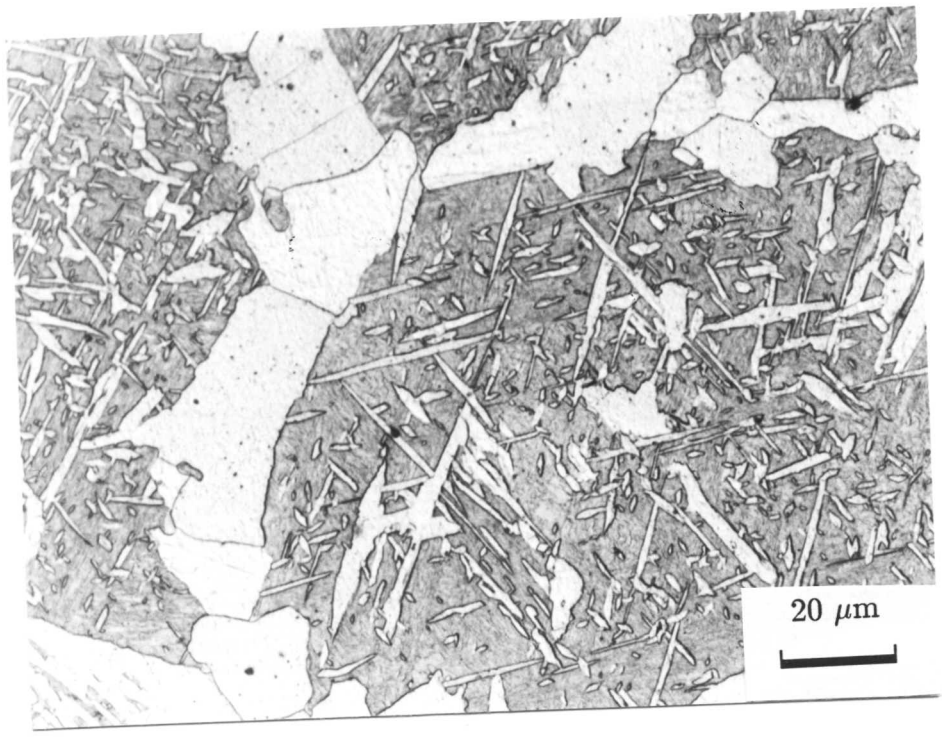

(a)

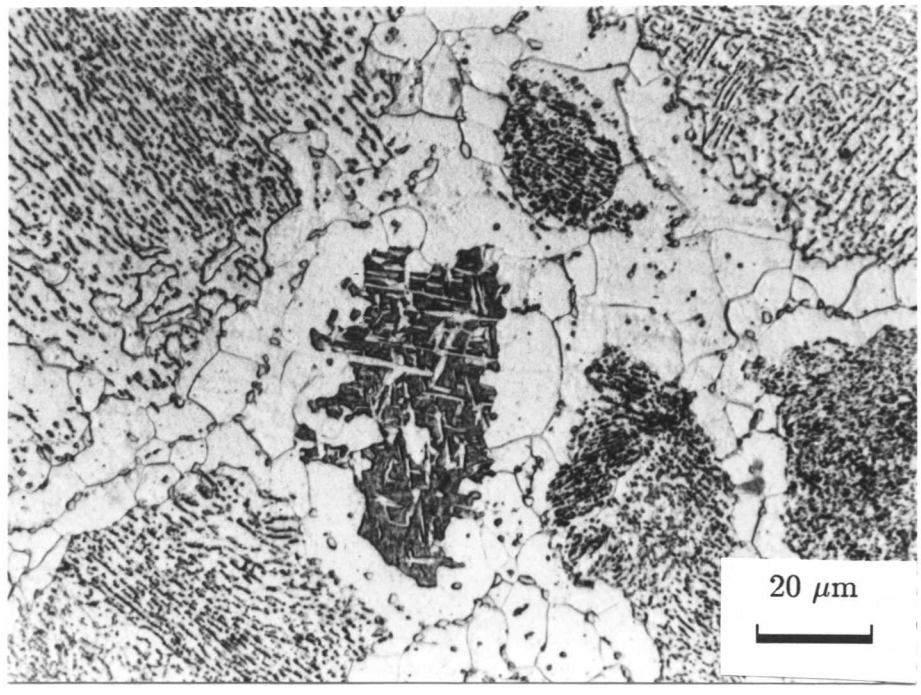

(b)

Fig. 10.11: *Continued* .....

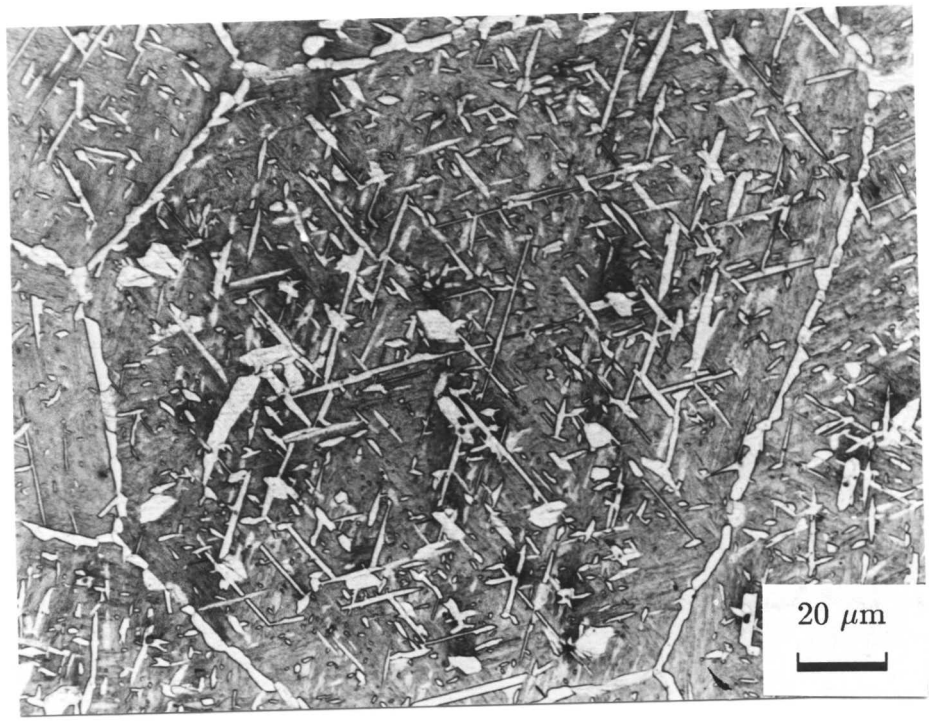

(c)

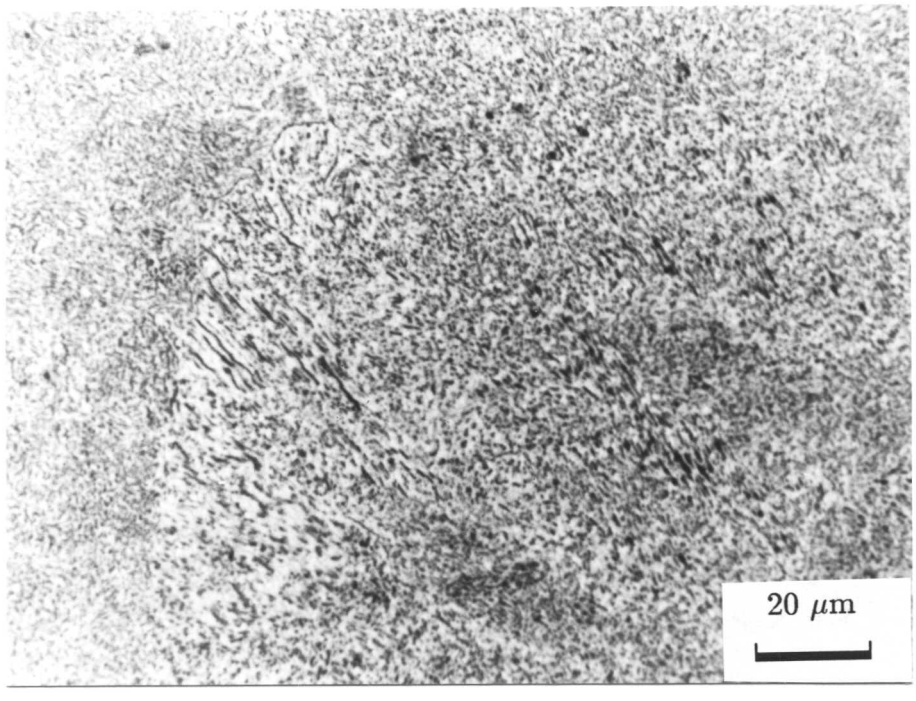

(d)

Fig. 10.11: *Effect of austenitisation temperature on the formation of intragranular Widmanstätten ferrite plates. Specimens were isothermally transformed at 740 °C for 10* days *after austenitisation for 15* min *at (a) 1100 °C (b) 1300 °C and 680 °C for 11* days *after 15* min *of austenitisation at (c) 1100 °C (d) 1300 °C.*

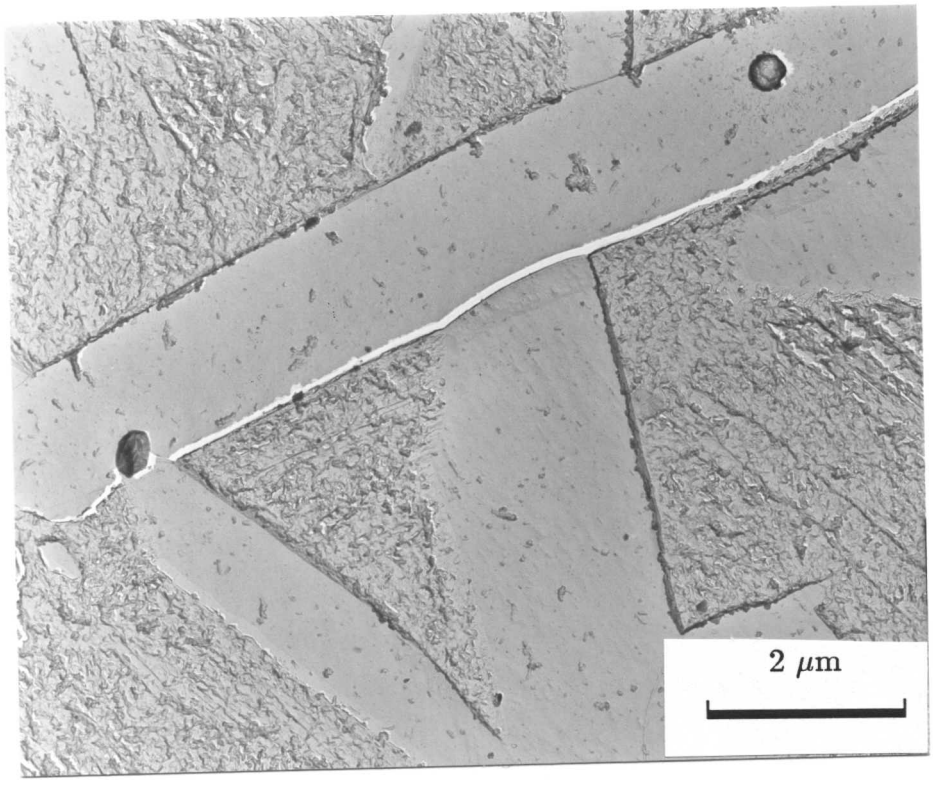

Fig. 10.12: *Replica electron micrograph of an inclusion of the type which were presumably responsible for the intragranular nucleation of Widmanstätten ferrite plates.*

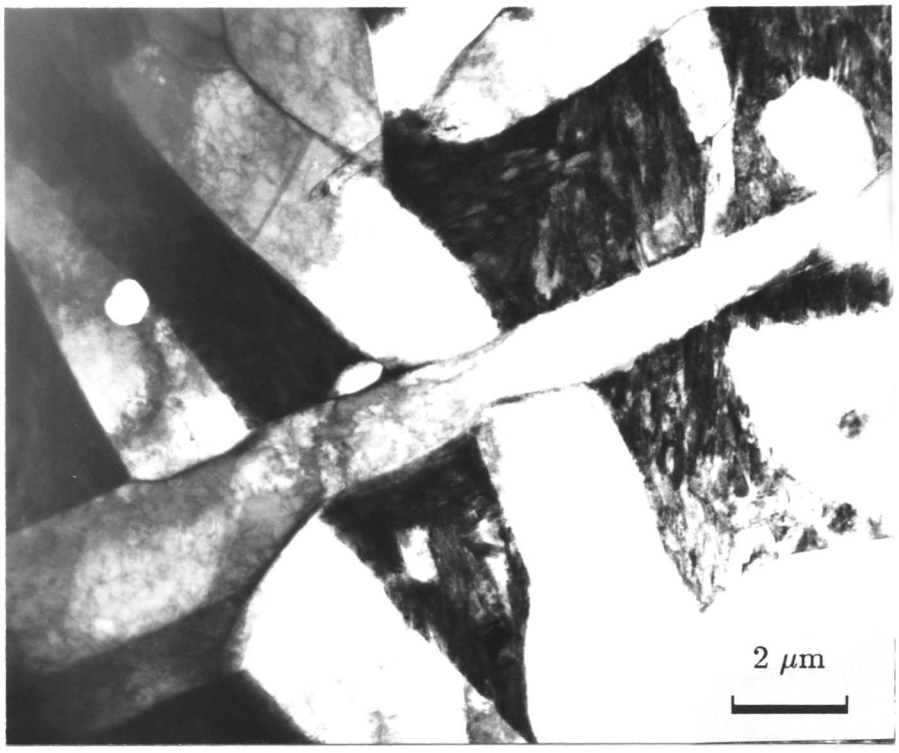

(a)

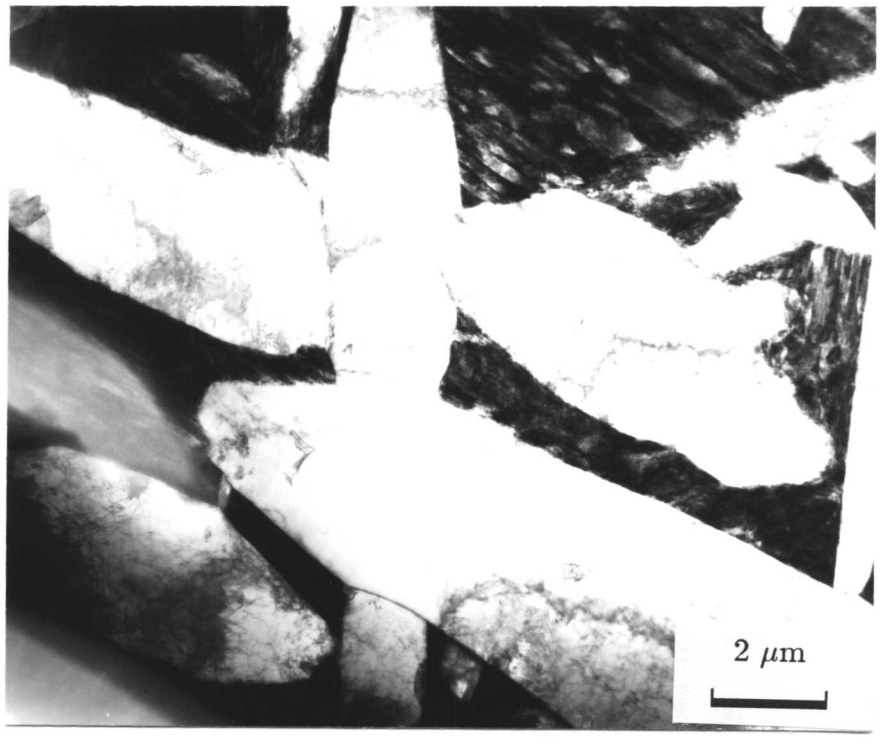

(b)

Fig. 10.13: *TEM micrograph showing the autocatalytic nucleation of intragranularly nucleated Widmanstätten ferrite plates.*

Fig. 10.14: *TEM micrographs showing that intragranularly nucleated plates have smoothly curved lenticular plate morphology.*

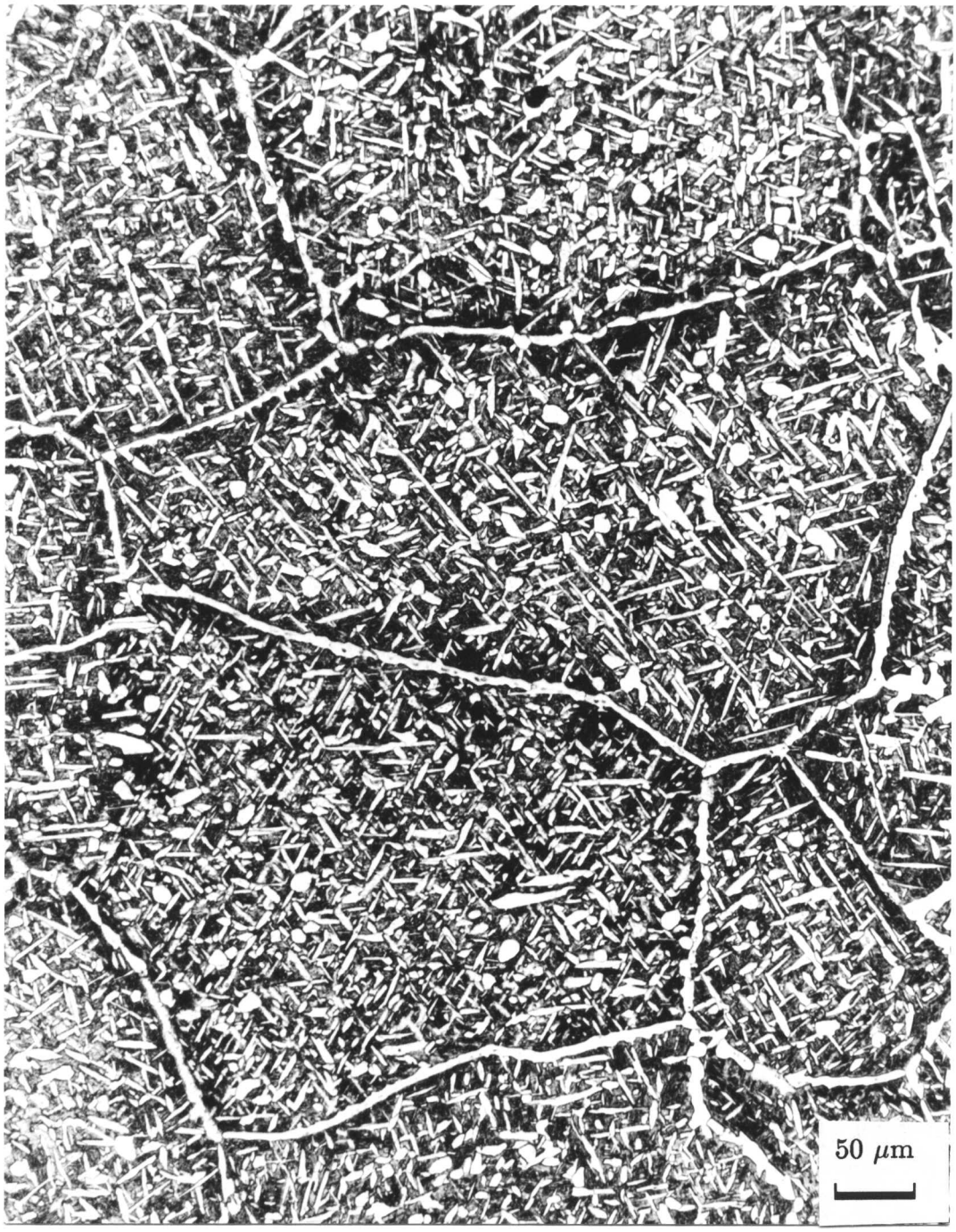

Fig. 10.15: *Optical micrograph showing a precipitate free zone between the grain boundary allotriomorphic ferrite layers and intragranularly nucleated Widmanstätten ferrite plates.*

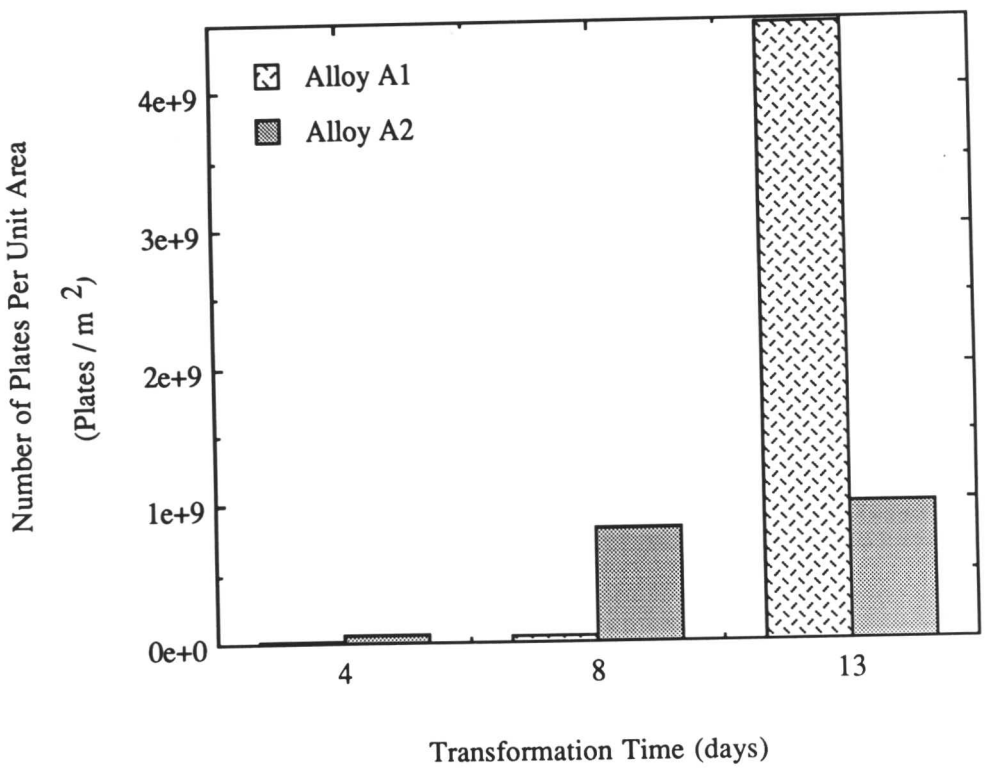

(a)

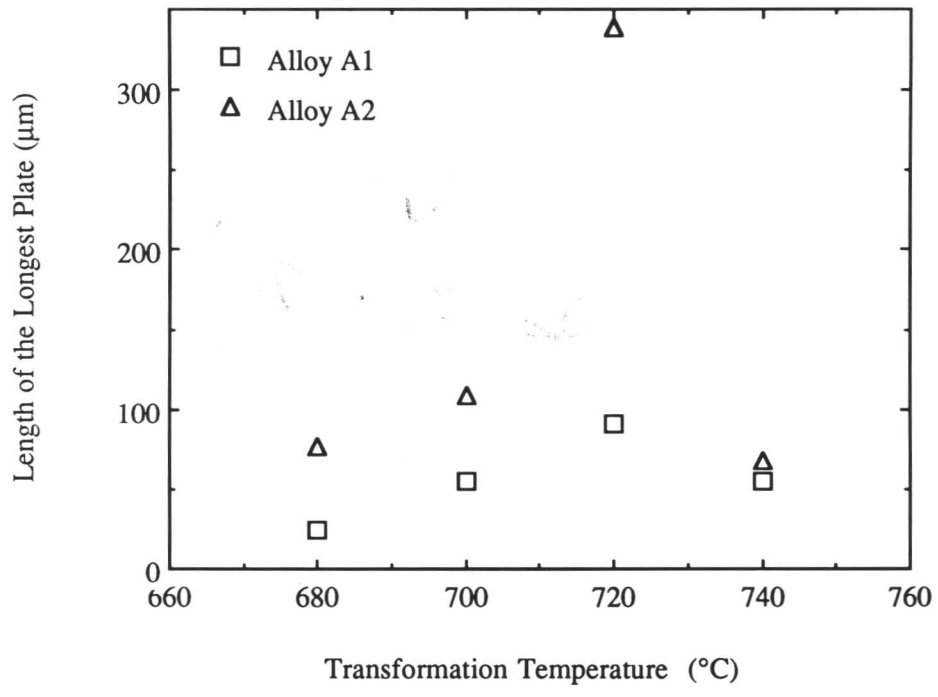

(b)

Fig. 10.16: *Continued .....*

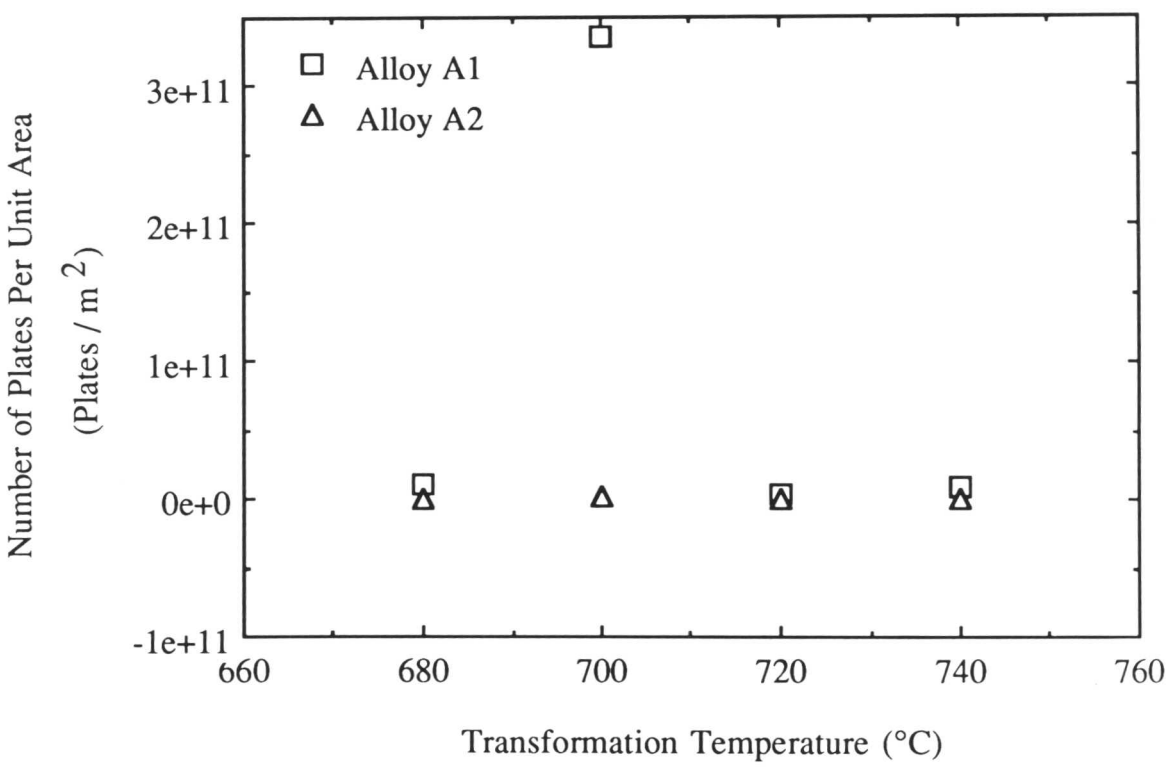

(c)

Fig. 10.16: (a) *Histogram showing the number of Widmanstätten ferrite plates per unit area, counted on metallographic samples observed using optical microscopy at a magnification of* $\times 100$*, as a function of the time at an isothermal transformation temperature of 720* ^{o}C. (b) *Length of the longest plate observed on a random section, as a function of the isothermal transformation temperature after holding at temperature for 264* hr. (c) *Number of plates per unit area, as a function of the transformation temperature after holding at temperature for 264* hr.

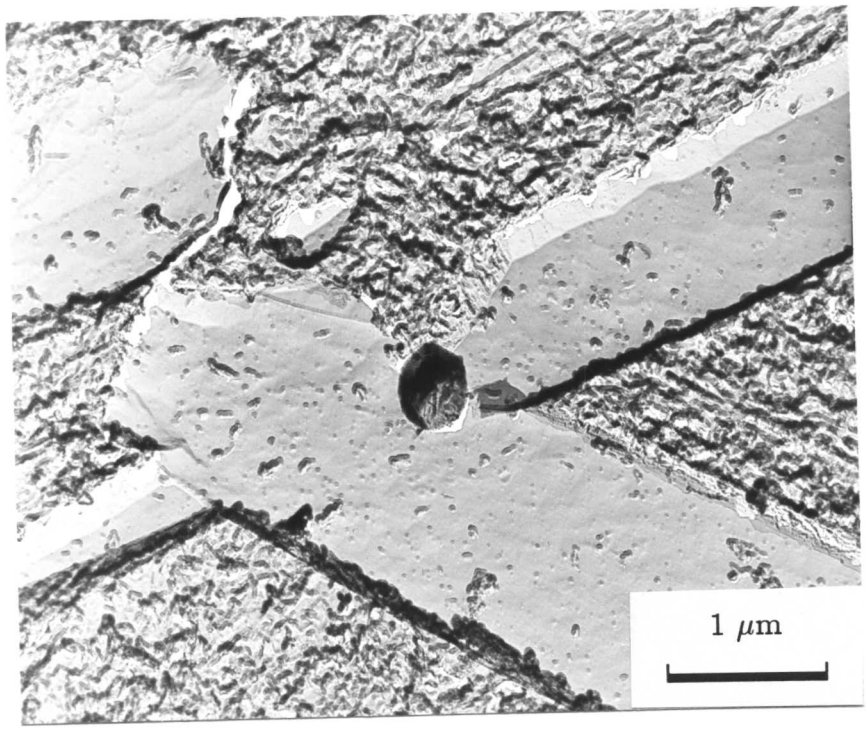

Fig. 10.17: *Carbon extraction replica micrograph showing plates of Widmanstätten ferrite apparently emanating from an inclusion nucleation site.*

Chapter 11
REAUSTENITISATION IN HIGH STRENGTH HARDENABILITY STEEL

There is now a need to conduct urgent experiments on the reaustenitisation behaviour of steels as an aid to the modelling of microstructure in welds. In multilayer weld deposits, the heat input associated with the deposition of new layers, reheats the underlying microstructure to temperatures where austenite formation can occur. The new austenite then cools and transforms back to a microstructure which can be rather different from that obtained immediately after weld deposition. Because many of the alloys used in the deposition of high-strength welds are designed to transform ultimately into bainitic microstructures, it is useful to study the reaustenitisation process by heating such microstructures. This chapter deals with the reaustenitisation process from a starting microstructure which is a mixture of bainite and residual austenite. The term residual austenite is used to represent the austenite which is left untransformed at the temperature where bainite is allowed to grow. Particular emphasis is placed on the mechanism and the kinetics of reaustenitisation process.

11.1 Material Selection

The steel selected for the present study is one which contains high silicon and manganese concentrations as the major alloying elements. The silicon retards the growth of cementite, so that a microstructure of just bainitic ferrite and residual austenite can be obtained by the transformation of austenite below the bainite-start (B_S) temperature [Hehemann, 1970]. Such alloys are becoming more prominent in industry, both as wrought materials [Bhadeshia and Edmonds, 1979] and in the form of high silicon cast irons [Rundman *et al.* 1988]. Manganese and molybdenum increase the incubation time for the formation of diffusional transformation products such as allotriomorphic ferrite, and generally raise the hardenability of the steel. The detailed chemical composition of the steel used in the present study is given in Table 11.1.

Table 11.1: *Chemical composition of the steel used in the present study.*

Steel	Chemical Composition (wt. %)						
	C	Si	Mn	Mo	Ti	Al	O (ppm)
A2	0.22	2.05	3.07	0.7	0.004	0.005	94

11.2 Experimental Procedures

11.2.1 *Heat Treatments*

High speed dilatometry was utilised to study the kinetics of reaustenitisation. All the samples were homogenised at 1250 °C for 3 days prior to dilatometric experiments, as discussed in Chapter 3 along with the other details of the heat treatment techniques. All heat treatments were performed in a Theta Industries high-speed dilatometer using homogenised, high purity, high hardenability steel, austenitised at 900 °C for 5 minutes, isothermally transformed at a temperature $T_i = 400$ °C for 2000 s to get a mixture of bainitic ferrite plus residual austenite and then, instead of cooling the specimens to ambient temperature, they were heated rapidly to an elevated temperature T_γ for isothermal reaustenitisation. The specimens were not cooled below 400 °C, in order to avoid the martensitic decomposition of the austenite. Schematic diagrams of the heat treatment cycles have already been shown in Fig. 3.1.

11.2.2 *Microscopy*

Specimens for optical and transmission electron microscopy were obtained from heat treated samples and prepared as discussed in Chapter 3. Thin foil samples were examined using a PHILIPS EM400T transmission electron microscope, equipped with a LINK EDX system to facilitate energy

11.3 Results

The general microstructure is illustrated in Fig. 11.1, and as expected, consisted of a mixture of bainitic ferrite, retained austenite and some martensite resulting from the decomposition of the residual austenite after cooling from the bainite formation temperature.

11.3.1 *Dilatometry*

The first detectable growth of austenite was found to occur at 660 °C as illustrated in Fig. 11.2, note that a length contraction is expected as ferrite transform to austenite. In all cases the transformation rate was initially rapid, but decreased with time at the isothermal reaustenitisation temperature T_γ so that the specimen length eventually stopped changing. The maximum relative length change as a function of T_γ is plotted in Fig. 11.3. The results showed that $\frac{\Delta L}{L}$ increases as T_γ increases from 660 °C to 740 °C and then remains essentially constant with the further increase in T_γ to 860 °C. The maximum degree of transformation to austenite thus increases from nearly zero at 620 °C to complete reverse transformation at

above 740 °C. It is also seen from the Fig. 11.3, that the rate of ferrite to austenite transformation increases with T_γ.

11.3.2 *Transmission Electron Microscopy*

The phenomenon of reaustenitisation can be monitored by observing the thickening of austenite layers using transmission electron microscopy (Figs. 11.4-11.11). Fig. 11.5 shows micrograph for reaustenitisation at 660 °C in which the ferrite subunits are parallel to each other and are separated by the austenite layers (now become martensite after cooling to ambient temperature). The thickness of the austenite films does not seem to increase significantly at 660 °C as expected from the dilatometric results (Fig. 11.3). As the isothermal reaustenitisation temperature increases, the austenite films become detectably thicker (Figs. 11.6-11.8). However the austenite layers still retain their general form as shown in Fig. 11.8 for reaustenitisation at 740 °C. Fig. 11.9 shows that there is some ferrite retained even after reaustenitisation at 780 °C. The electron micrographs in Figs. 11.10 and 11.11 demonstrate completely martensitic structures, indicating the completion of austenitisation following the 820 and 860 °C heat treatments This also confirms the dilatometric data (Fig. 11.3), that the maximum length change achieved beyond about 780 °C does not vary much with T_γ. A slight decrease is in fact expected as T_γ rises, even though the samples fully reaustenitise, because the difference in austenite and ferrite densities decreases with rising temperature.

11.3.3 *Microanalysis*

The microanalysis results are given in Table 11.2 and Figs. 11.12-11.16 illustrate the results from a range of isothermal reaustenitisation temperatures. They show that the degree of partitioning substitutional of alloying elements decreases with increasing austenitisation temperature.

11.3.4 *Hardness*

The hardness of each specimen was measured after the isothermal reaustenitisation and the results are plotted in Fig. 11.17. The results show that the hardness achieves a maximum value after austenitisation at about 780 °C.

Table 11.2: *EDX analysis of the (a) matrix and (b) ferrite. (All the specimens were austenitised at 900 °C for 5* min *and then transformed to bainite at 400 °C for 2000* s *prior to reaustenitisation).*

(a)

Temperature °C	EDX analysis (wt. %)			
	Fe	Mn	Si	Mo
620	93.7 ± 1.2	3.4 ± 0.7	2.1 ± 0.2	0.6 ± 0.3
660	93.6 ± 0.7	3.3 ± 0.5	2.1 ± 0.4	0.9 ± 0.5
680	94.2 ± 0.7	3.3 ± 0.4	1.9 ± 0.4	0.6 ± 0.3
700	94.1 ± 0.7	3.4 ± 0.6	1.9 ± 0.4	0.6 ± 0.5
860	94.1 ± 0.6	3.2 ± 0.3	1.9 ± 0.1	0.7 ± 0.4

(b)

Temperature °C	EDX analysis (wt. %)			
	Fe	Mn	Si	Mo
620	94.1 ± 0.7	2.7 ± 0.5	2.3 ± 0.3	0.9 ± 0.7
660	95.0 ± 0.9	2.4 ± 0.4	2.0 ± 0.4	0.5 ± 0.6
680	95.1 ± 0.9	2.3 ± 0.4	1.9 ± 0.4	0.6 ± 0.3
700	94.6 ± 0.7	2.5 ± 0.8	2.1 ± 0.5	0.7 ± 0.5
860	94.5 ± 0.7	2.4 ± 0.3	2.1 ± 0.2	0.9 ± 0.7

Table 11.3: *Effect of reaustenitisation temperature on partition coefficient.*

Temperature °C	Partition Coefficient $[K_i = \frac{K_i(\gamma)}{K_i(\alpha)}]$ (wt. %)		
	Mn	Si	Mo
620	1.2	0.9	0.7
660	1.3	1.0	1.7
680	1.4	0.9	0.9
700	1.3	0.9	0.9
860	1.3	0.9	0.7

11.4 Discussion

The results obtained in this study generally confirm the earlier published [Yang, 1987; Yang and Bhadeshia, 1987, 1990] on] experiments but provide additional microstructural detail. The Yang and Bhadeshia model shows that because isothermal transformation of austenite to bainite ceases prematurely before the austenite

achieves its equilibrium carbon concentration, there is a large temperature hysteresis before the reverse transformation to austenite become possible during heating from the bainite transformation temperatures. Any reverse transformation to austenite cannot occur until the sample is heated to an elevated temperature where the residual austenite composition becomes identical to the composition given by the Ae_3' phase boundary. This leads to a large hysteresis in the forward and reverse transformation temperatures for austenite, a hysteresis which is not found when the starting microstructure is instead a mixture of allotriomorphic ferrite and austenite [Tsuzaki *et al.* 1980]. This is evident from TEM micrographs with increasing thickness of austenite layers as shown in Fig. 11.18. A close examination of Fig. 11.19 shows that austenite layers become thicker they retain their layer like morphology between the ferrite sub units. This provides strong evidence that austenite grows by the normal movement of the approximately planar α/γ interface as assumed by Yang [1987].

11.4.1 *EDX Analysis*

The results of energy dispersive X-ray analysis of isothermally reaustenitised specimens show that the degree of partitioning of substitutional alloying elements, as indicated by the deviation of the partition coefficient K_i from unity, where

$$K_i = \frac{x_i^\gamma}{x_i^\alpha} \tag{11.1}$$

decreases with increasing reaustenitisation temperature (Fig. 11.16). As the driving force for reaustentisation increases, the transformation tends towards paraequilibrium or negligible partition-local equilibrium; this is illustrated clearly by the data for 700 °C. The concepts of paraequilibrium and local equilibrium have been discussed in Chapter 1. Paraequilibrium is state of constrained equilibrium in which the substitutional lattice is configurationally frozen with respect to the transformation interface. Hence, even though the transformation is diffusional in nature, the ratio (atom fraction of substitutional element (i)/atom fraction of iron) is the same in α and γ. Thus, the chemical potentials of the substitutional elements are not equal in the two phases. Carbon, which can diffuse faster, reaches equilibrium subject to this constraint. In negligible-partioning-local equilibrium (NPLE), equilibrium is maintained for all the transformation interface, but the concentration of substitutional element is essentially the same in all phases. The results also show that as thickness of the austenite layers increases with time at for a given T_γ, the partition coefficient K_i changes indicating that the concentrations of alloying

elements at the interface during the growth of austenite are not equilibrium concentrations. These results are qualitatively consistent with the dilatometric data. One of the factors for the increased rate of transformation at high T_γ is the fact that the degree of redistribution of alloying elements during transformation decreases with increasing T_γ.

11.4.2 *Carbon Concentration of the Residual Austenite*

The carbon content of the residual austenite when isothermal transformation ceases is very useful in understanding the transformation mechanism. Because of the relatively high silicon concentration in the steel used, the precipitation of cementite tends to be rather sluggish. Consequently, isothermal transformation to upper bainite generates a microstructure consisting of carbide-free bainitic ferrite and carbon-enriched residual austenite. It is then possible to estimate the carbon concentration x_γ of the residual austenite using a simple mass balance procedure, if the volume fraction of bainitic ferrite V_b is known

$$x_\gamma = \frac{\overline{x} - V_b \times x_\alpha}{1 - V_b} \tag{11.2}$$

where $\overline{x}$ is the average carbon concentration of the alloy and x_α is the carbon concentration of the bainitic ferrite. The volume fraction V_b can be calculated from the dilatometric data as discussed by Bhadeshia [1982]. The values of x_γ estimated by using the procedures just described here, for the point where isothermal transformation ceases at any given temperature, are plotted on the phase diagram presented in Fig. 11.20. The phase boundaries were calculated using the method given by Bhadeshia and Edmonds [1980]. The data presented in Fig. 11.20 confirm that the formation of upper bainite stops prematurely, well before the carbon concentration of the residual austenite reaches the paraequilibrium Ae'_3 phase boundary. This effect is known as the "incomplete reaction phenomenon"§ [Bhadeshia, 1985, Christian, *et al.* 1984]. After isothermal transformation to bainite at the temperature T_b has ceased, if the sample is rapidly heated to an isothermal temperature T_γ for reaustenitisation, the reverse transformation to austenite does not require any nucleation, simply the movements of already existing ferrite-austenite interfaces. Because the bainitic ferrite consist of ferrite sub units which are approximately parallel to each other. The thickness of austenite films measured by stereology is given in Fig. 11.18, which shows that as the reaustenitisation temperature increases the austenite films between bainitic ferrite become thicker and eventually consume

§ The incomplete reaction phenomenon has been discussed in detail in chapter 4.

all the bainitic ferrite transformed to austenite i. e., above 780 °C. This is also confirmed by the transmission electron microscopy.

11.4.3 *Macrohardness*

The hardness of the reaustenitised samples after quenching to ambient temperature has been found to initially increase as with the isothermal reaustenitisation temperature. This increase is expected since the amount of austenite (and hence martensite at austenitisation temperature) increases with T_γ. The maximum value of about 600 HV observed at around 780 °C beyond which sample becomes fully austenitic is more difficult to understand, but could arise because samples quenched from higher temperature undergo a greater degree of auto tempering of the martensite.

11.5 Theory for Reaustenitisation

In this section the thermodynamic model presented by Yang and Bhadeshia [1987] for the interpretation of the observations on reaustenitisation from a starting microstructure of bainite and retained austenite are analysed in the light of the results obtained in the present study. Since after the diffusionless growth of bainite, carbon is rapidly and spontaneously redistributed into the residual austenite with an accompanying reduction in free energy, the α_b/γ transformation in its original form is irreversible. The problem of reaustenitisation is therefore considerably different from the case of martensite to austenite in for example, shape memory alloys. It is noted that the formation of bainite ceases prematurely during isothermal transformation when the carbon content of the residual austenite reaches the T_o' curve (the phase diagram for the alloy is presented in Fig. 11.20). It follows that the carbon concentration x_γ of the residual austenite when the formation of bainite cease at T_b, is given by (point marked 'a' in Fig. 11.20)

$$x_\gamma = x'_{T_o}[T_b] \tag{11.3}$$

furthermore, it is noted that:

$$x_\gamma << x_{Ae'_3}[T_b] \tag{11.4}$$

where $x_{Ae'_3}[T_b]$ is marked "b" in Fig. 11.20. Thus, although the formation of bainite ceases at, because $x_\gamma << x_{Ae'_3}\ [T_b]$, the driving force for austenite to transform diffusionally to ferrite is still negative. Another way of expressing this is to say that the volume fraction of bainite present when its formation ceases at T_b is much

less than is required by the Lever rule. In fact, this remains the case until the temperature T is high enough *i.e.*, $T = T_\gamma$ to satisfy the equation:

$$x_\gamma = x_{Ae'_3}[T_b] \tag{11.5}$$

Hence, reaustenitisation will first occur at a temperature T_γ, as indicated in Fig. 11.20 (marked c), and as observed experimentally. Note that this is a direct consequence of the mechanism of the bainite transformation, which does not allow the transformation to reach completion. The theory goes further than explaining just the temperature at which the reverse transformation should begin. It also predicts that any temperature T greater than T_γ, the reverse $\alpha \rightarrow \gamma$ transformation should ceases as soon as the residual austenite carbon concentration x'_γ (initially x_γ reaches the Ae'_3 curve, i.e., when

$$x'_\gamma = x_{Ae'_3}[T_\gamma] \tag{11.6}$$

with the equilibrium volume fraction of austenite (at the temperature T_γ), V_γ, being given by:

$$V_\gamma[T_\gamma] = \frac{\overline{x}}{x_{Ae'_3}}[T_\gamma] \tag{11.7}$$

assuming that the carbon concentration of ferrite is negligible and $x_{Ae'_3}[T_\gamma] > \overline{x}$ when $x_{Ae'_3}[T_\gamma] = \overline{x}$, the alloy eventually becomes fully austenitic (point 'd' in Fig. 11.20) and If this condition is satisfied at $T = T_\gamma$ then all $T > T_\gamma$, the alloy transform completely to austenite. These concepts immediately explain the dilatometric data in which the degree of $\alpha \rightarrow \gamma$ transformation increase (from zero at 660 °C with the temperature of isothermal reaustenitisation, until the temperature 780 °C where the alloy transforms completely to austenite. The results obtained in present study thus generally confirm the Yang and Bhadeshia model for reaustenitisation of mixtures of bainitic ferrite plus residual austenite.

11.6 Conclusions

The kinetics of reaustenitisation in relatively high silicon concentrations has been studied by a combination of techniques such as high speed dilatometry, transmission electron microscopy, EDX analysis, stereology and macro hardness. It is found that the formation of austenite increases with increasing reaustenitisation temperatures and at 780 °C all the bainitic ferrite transformed to austenite. The transformation is initially rapid but slow at the end of reaction. The formation

of austenite was found to take place by the movements of planar ferrite/austenite interfaces. It is confirmed by measuring the thickness of the austenite films which increase during the reaustenitistion process. The results are generally consistent with the theory of reaustenitisation as proposed be Yang and Bhadeshia.

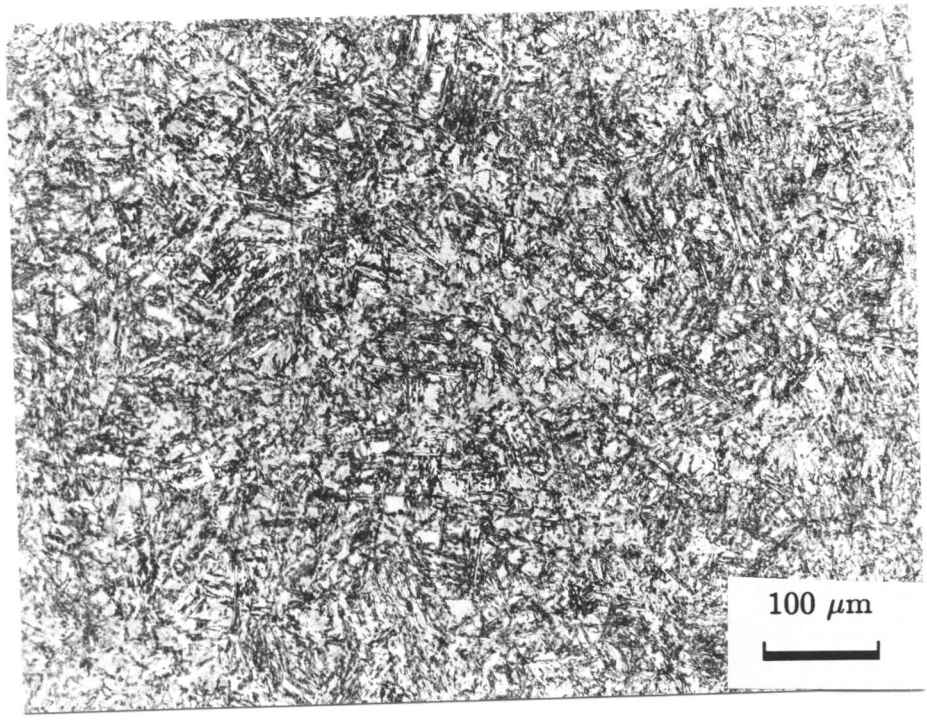

(a)

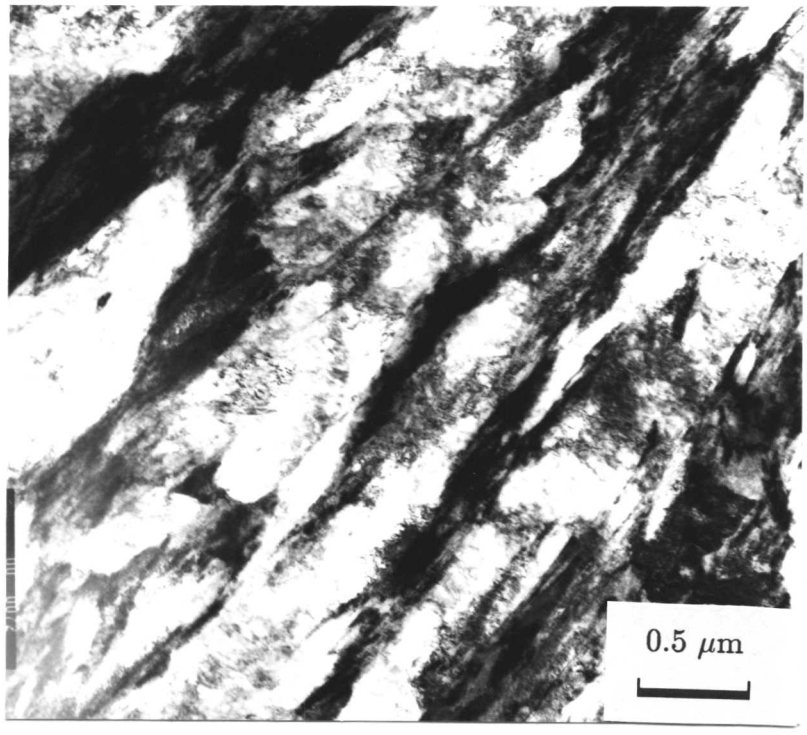

(b)

Fig. 11.1: *Typical mixed microstructure of bainitic ferrite, retained austenite and martensite after isothermal transformed at 400 °C for 2000* s *followed by water quenching. a) Optical micrograph. b) TEM micrograph.*

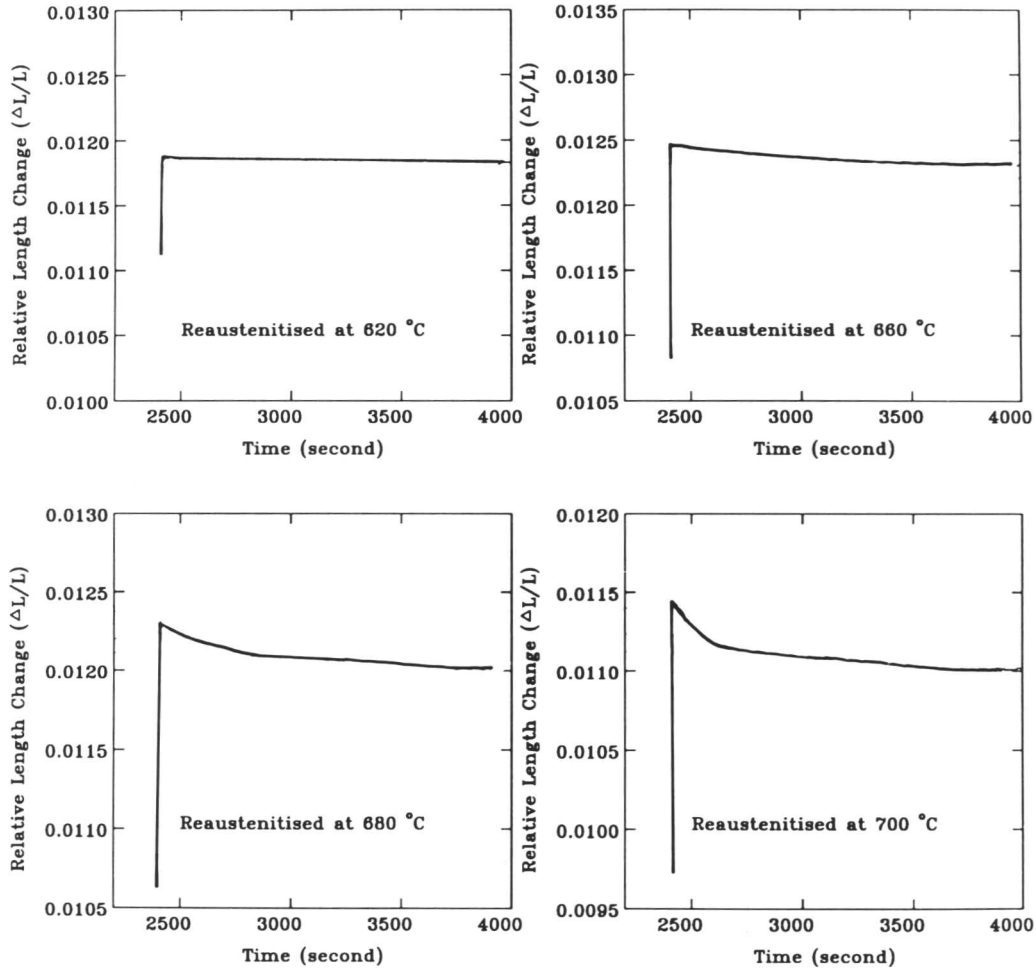

Fig. 11.2: *Continued .....*

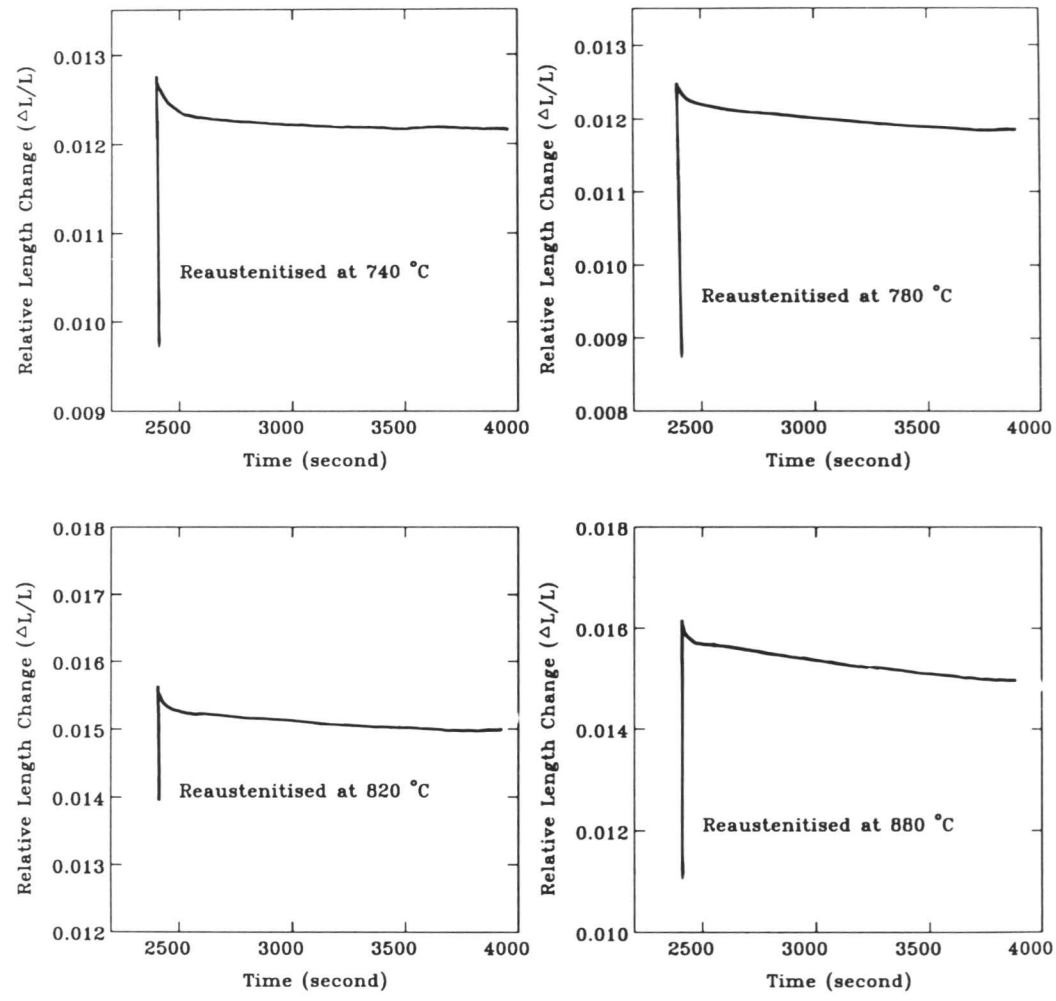

Fig. 11.2: *Isothermal reaustenitisation studied using dilatometry. The specimens were initially isothermally transformed to bainite at 400 °C for 2000* s *and then rapidly heated to the isothermal reaustenitisation temperature indicated on each figure.*

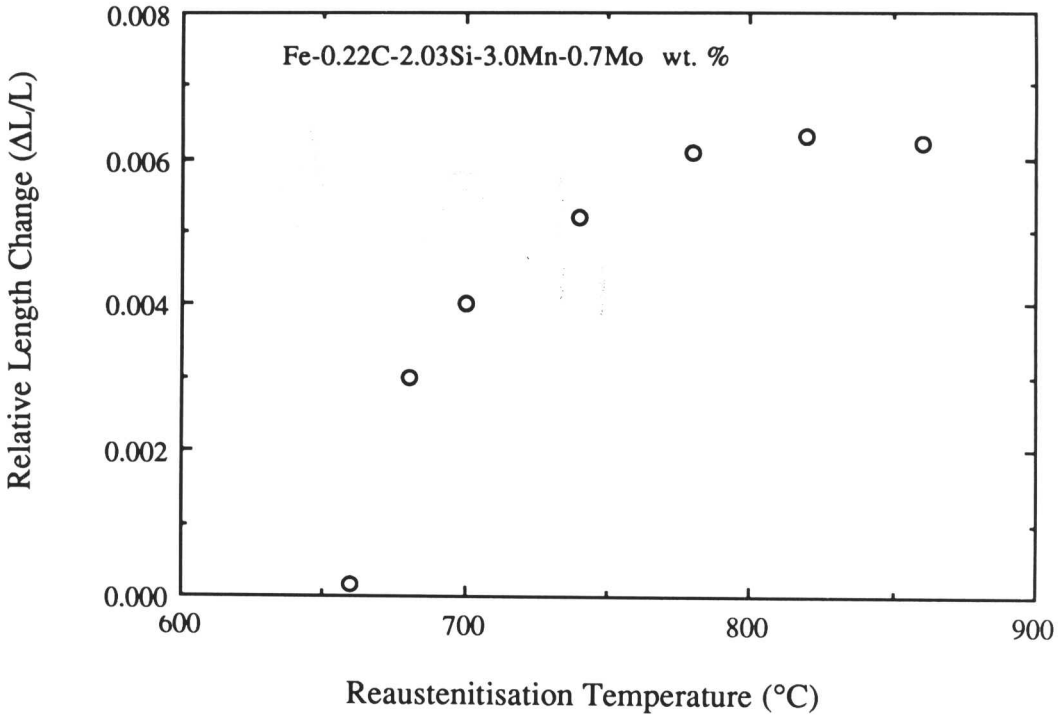

Fig. 11.3: *The maximum magnitude of the relative length change ($\frac{\Delta L}{L}$) increases with the reaustenitisation temperature (T_γ) and then attains an approximately constant value after the sample can achieved a fully austenitic state. Note that all the length changes are in fact negative.*

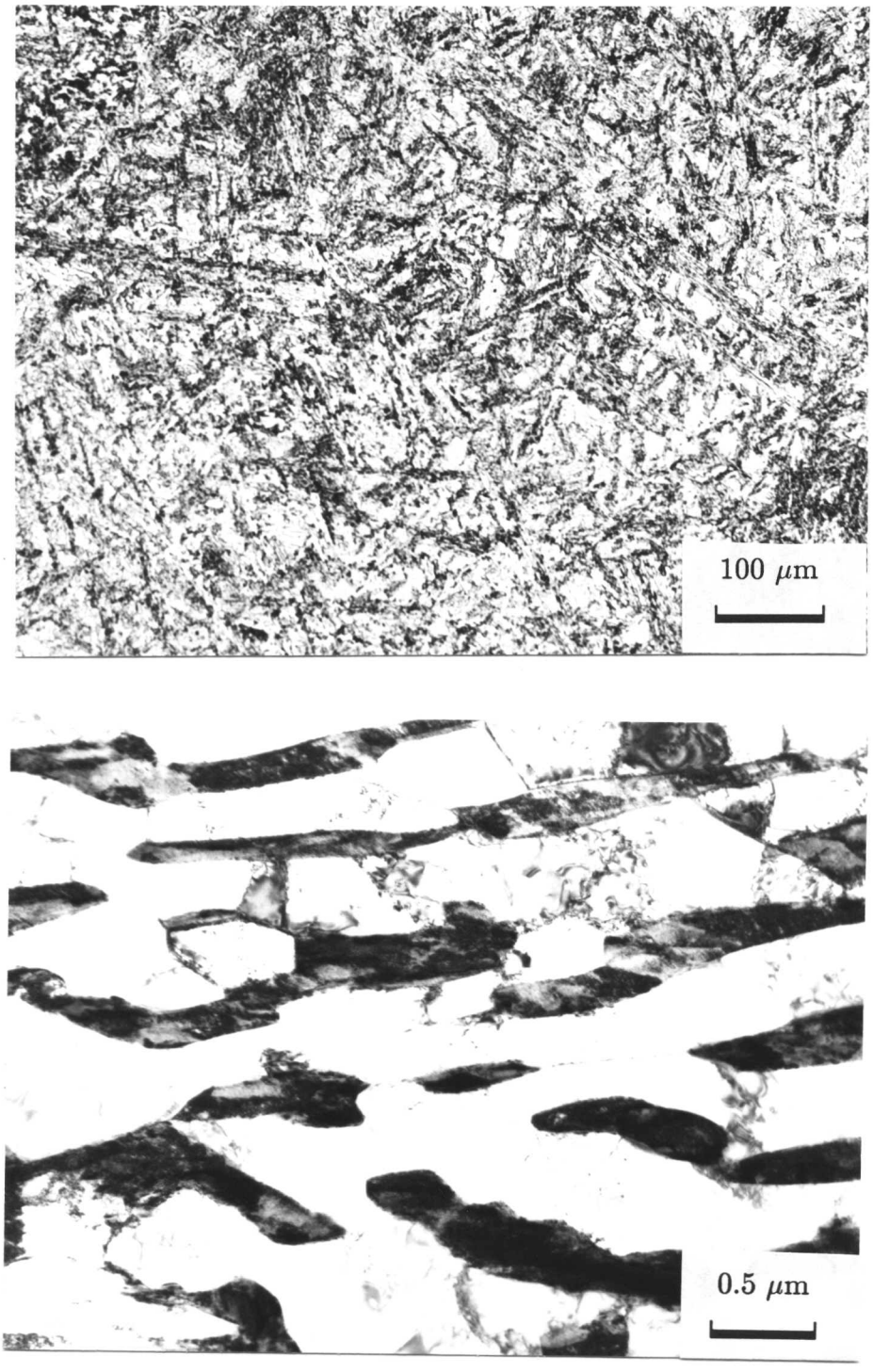

Fig. 11.4: *Microstructure of the specimen isothermally reaustenitised at 620 °C for 2000* s. *Note that there is some rounding of the bainite sub-units at their tips.*

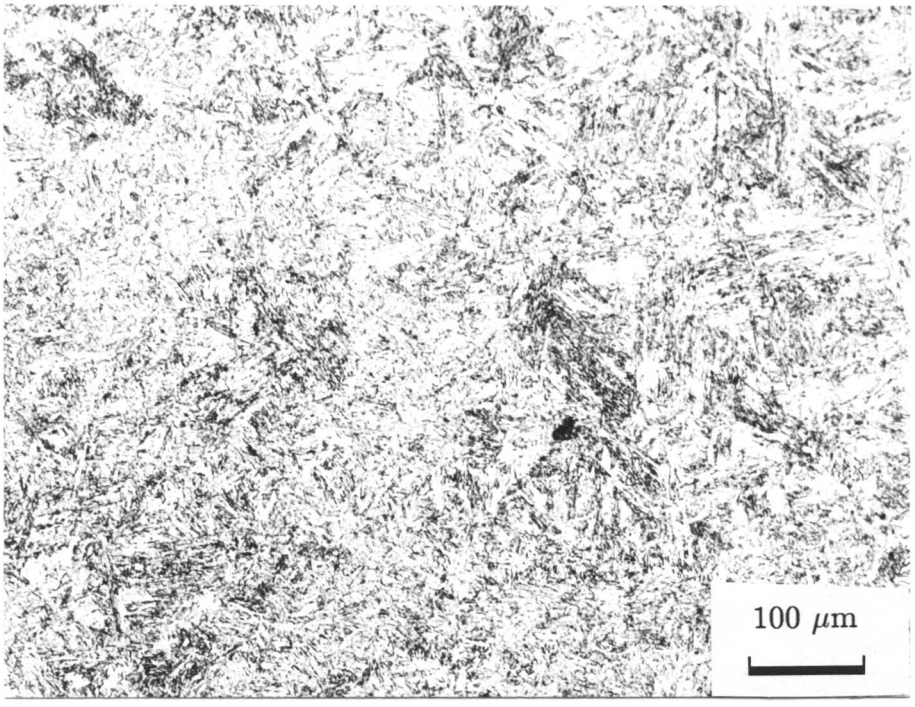

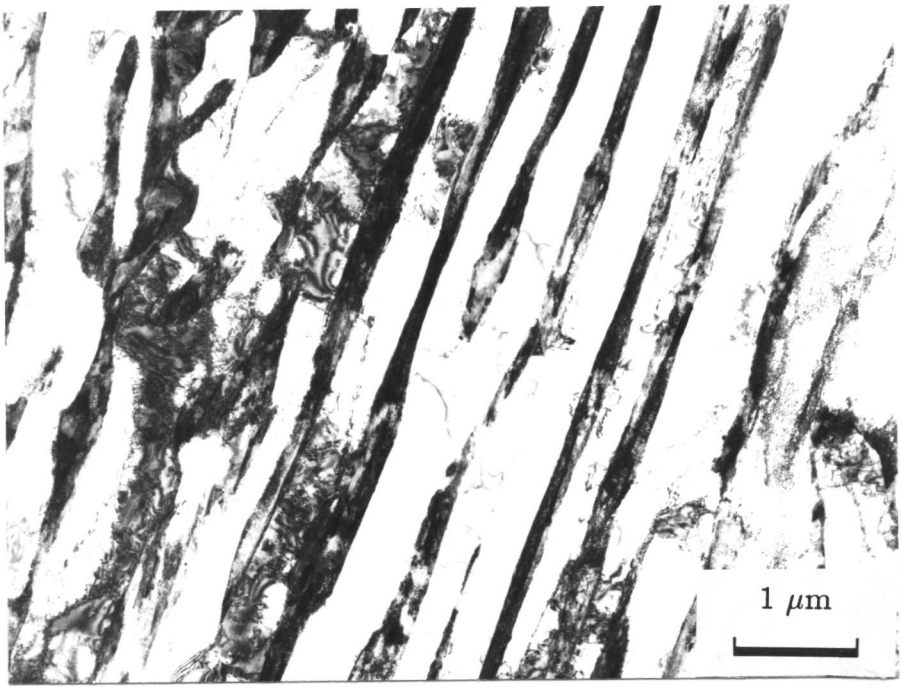

Fig. 11.5: *Microstructure observed at* T_γ*= 660 °C for 3000* s.

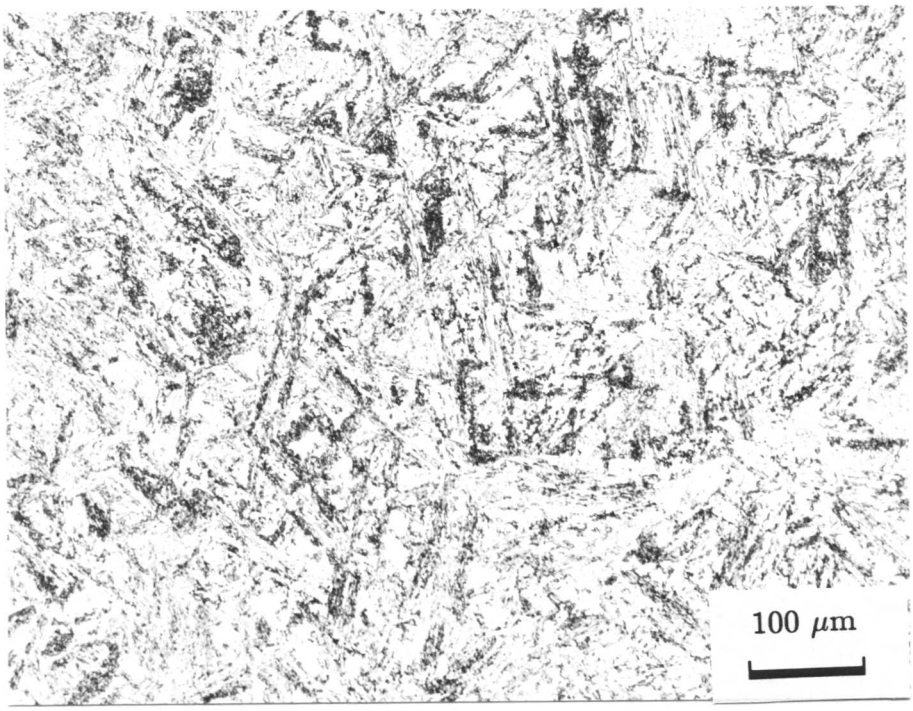

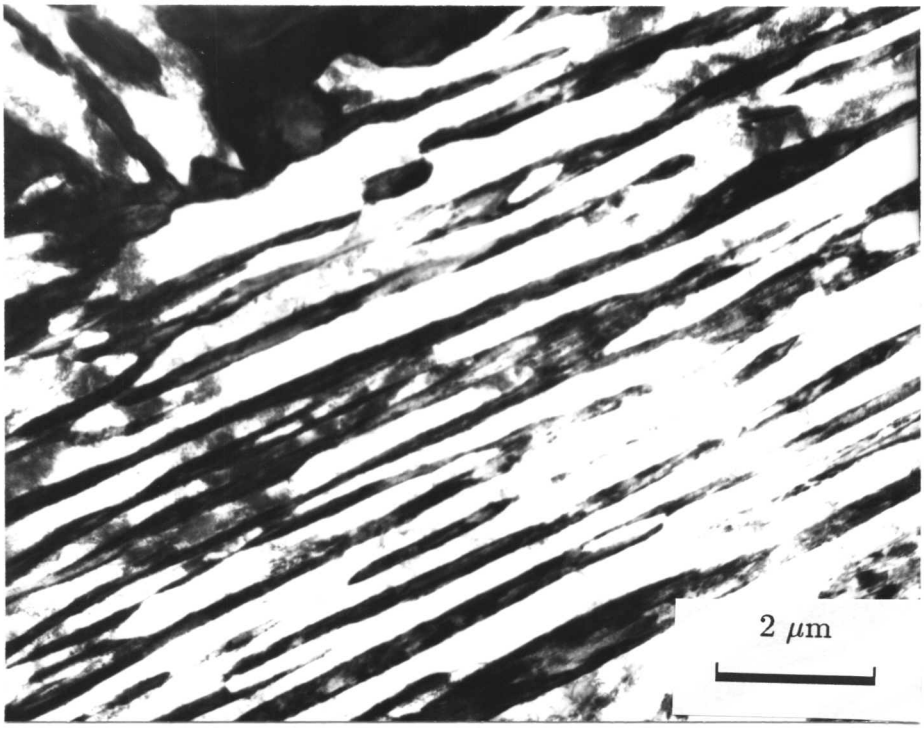

Fig. 11.6: *Microstructure observed after isothermal reaustenitisation at 680 °C for 2000* s.

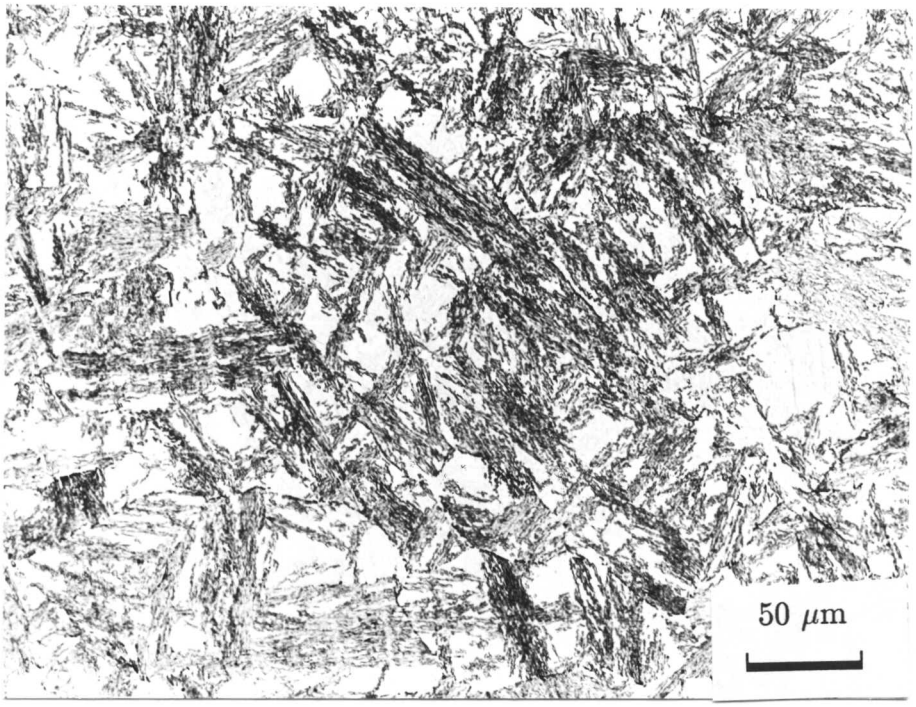

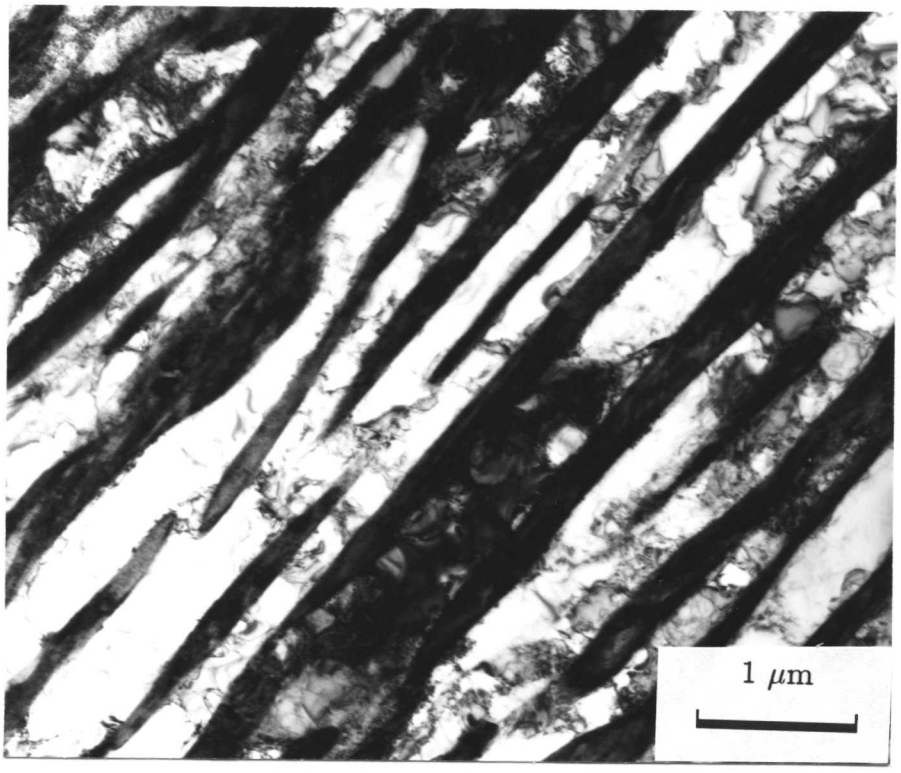

Fig. 11.7: *Thickening of the austenite films after reaustenitisation at 700 °C for 3000* s.

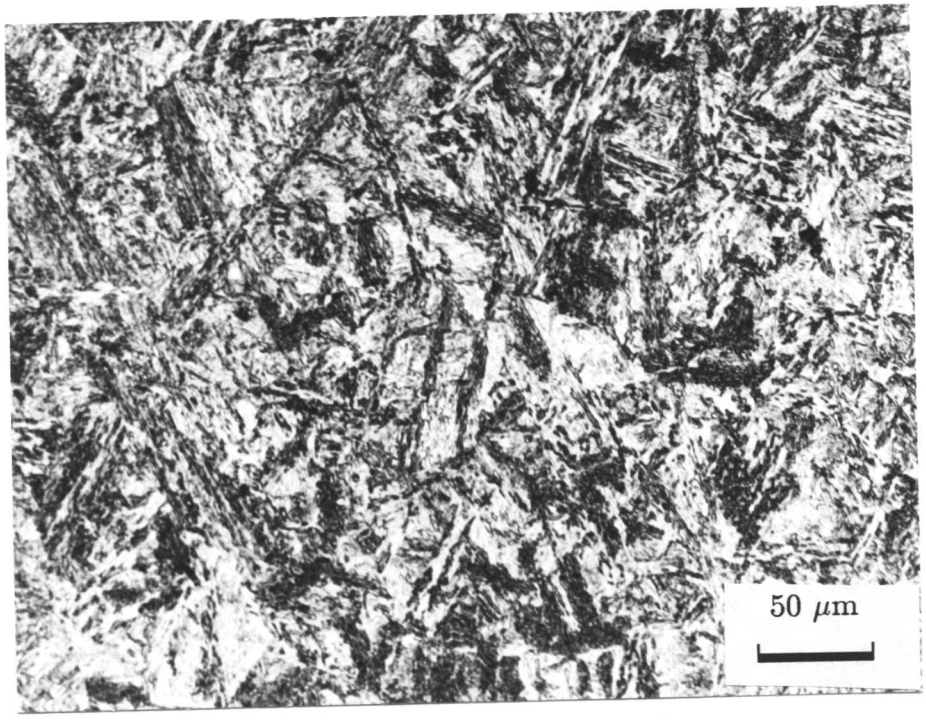

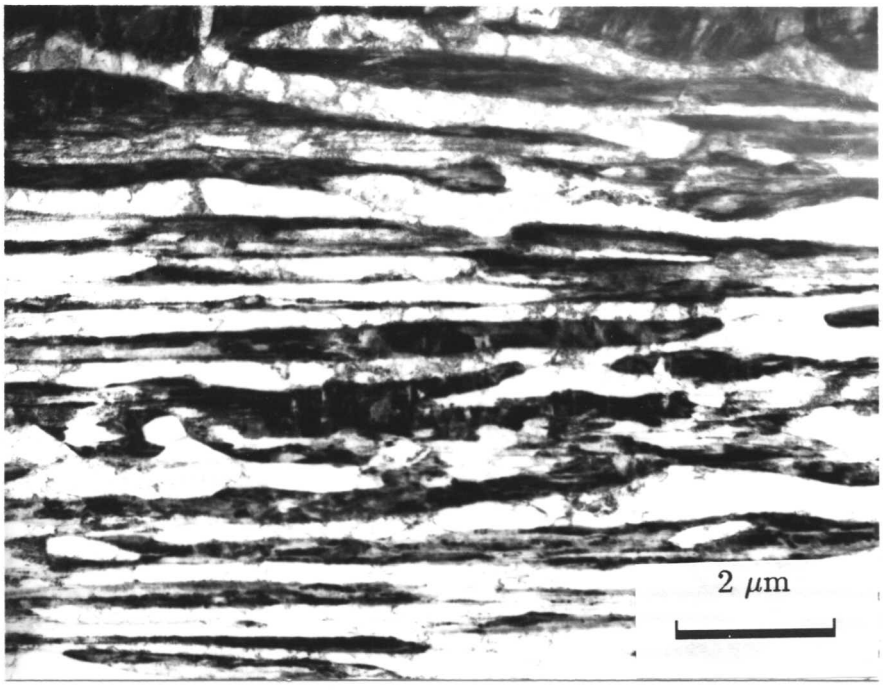

Fig. 11.8 : *The residual austenite films between bainitic ferrite subunits become thicker after isothermal reaustenitisation at 740 °C for 3000* s.

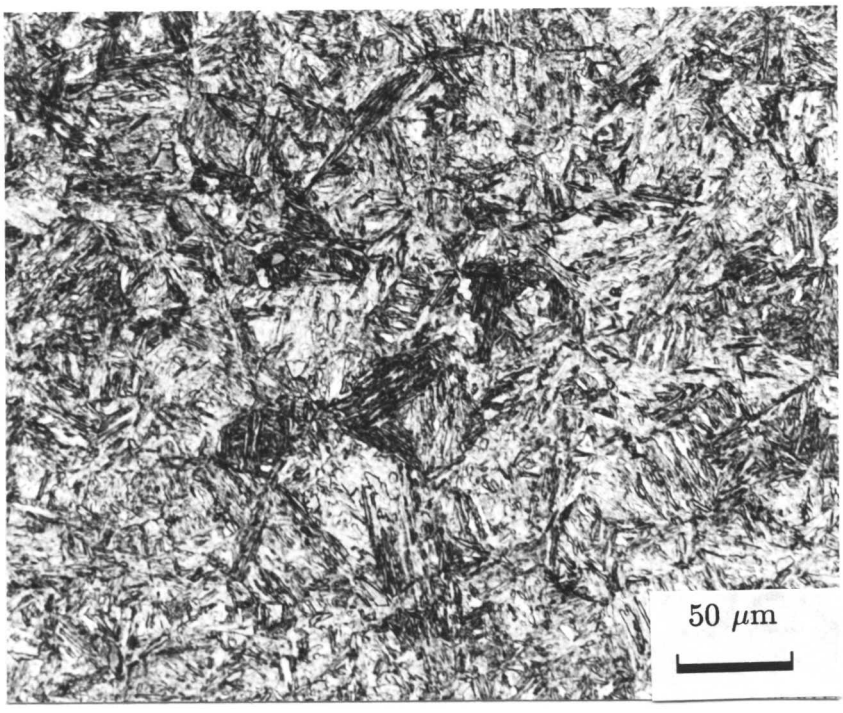

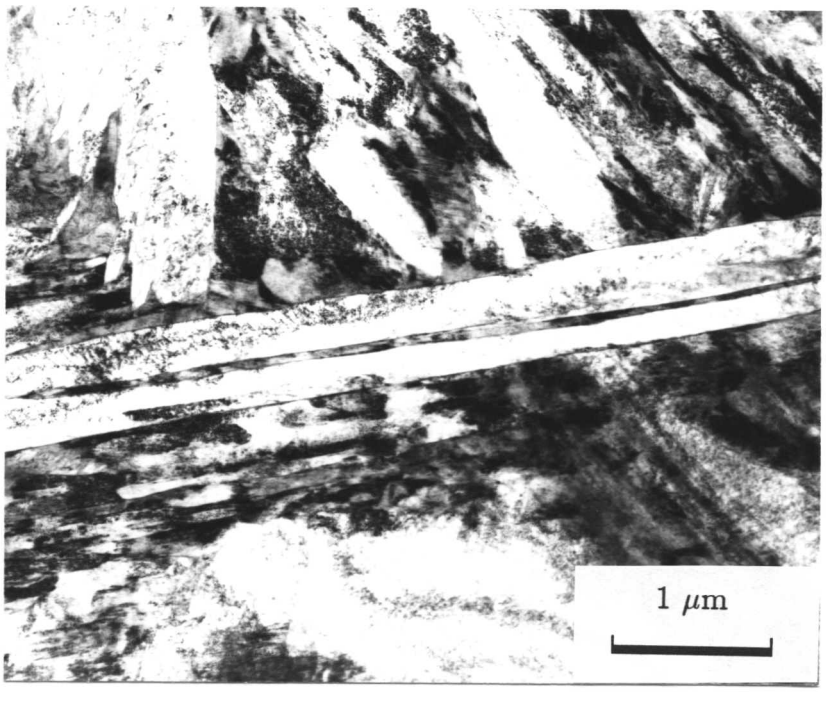

Fig. 11.9: *Showing that although most of the microstructure reaustenitised but still some of the ferrite subunits are present after isothermal reaustenitistion at 780 °C for 3000* s.

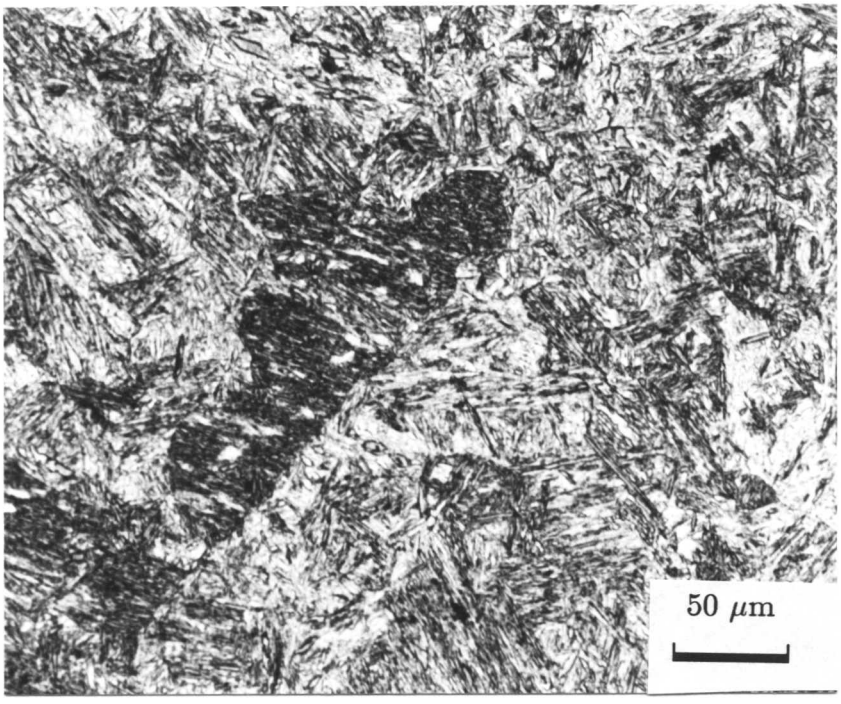

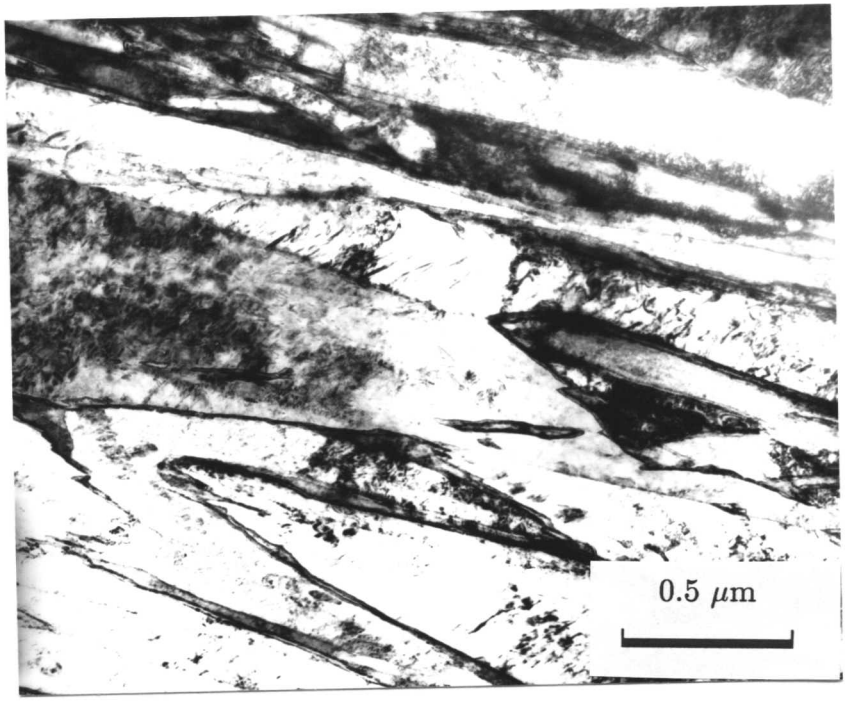

Fig. 11.10: *Microstructure observed after reaustenitistion at 820 °C for 3000* s.

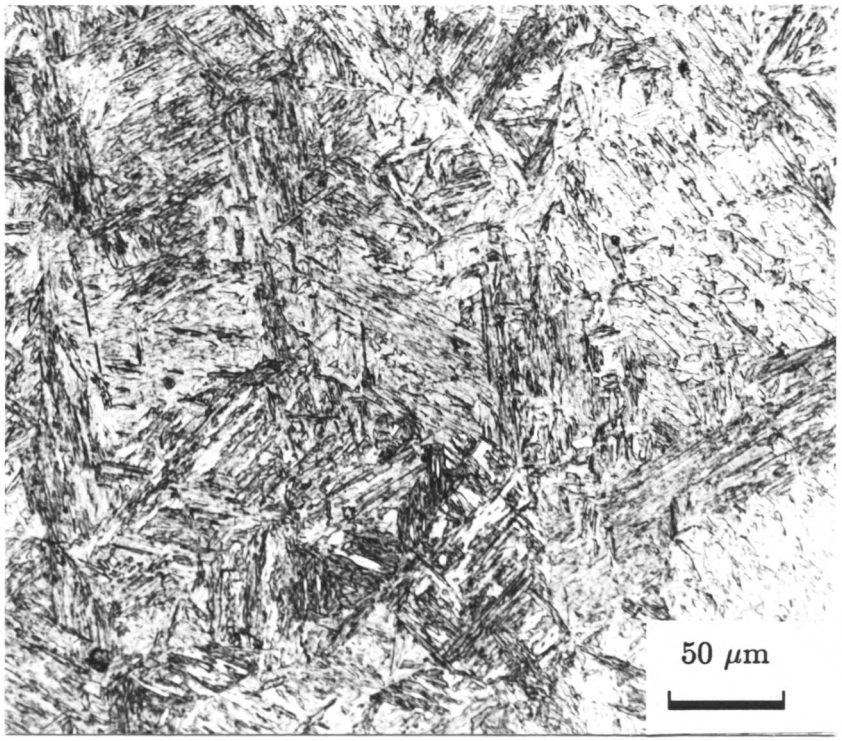

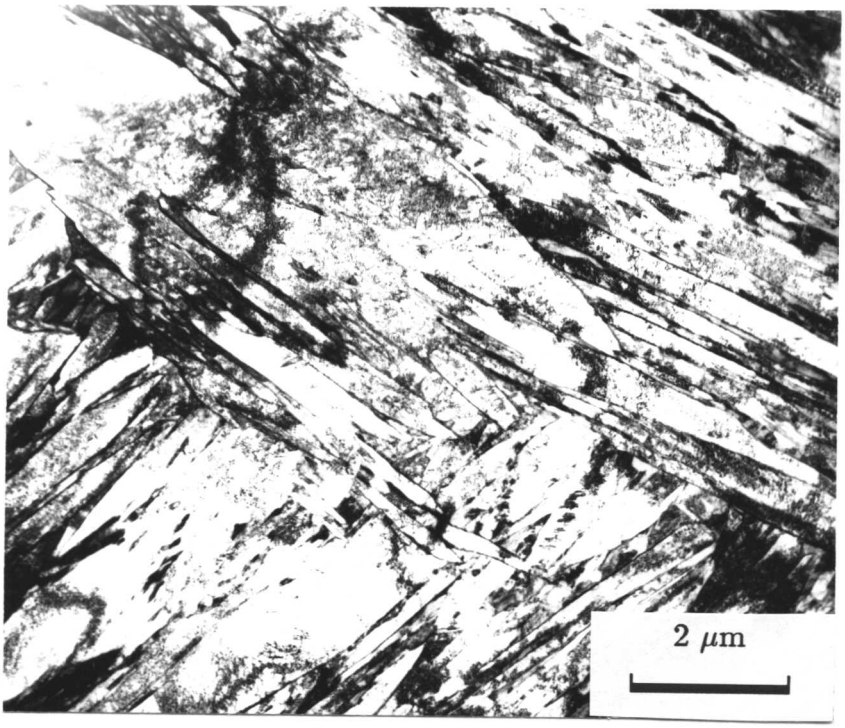

Fig. 11.11: *Showing that specimen completely reaustenitised after isothermal transformation at 860 °C for 3000* s.

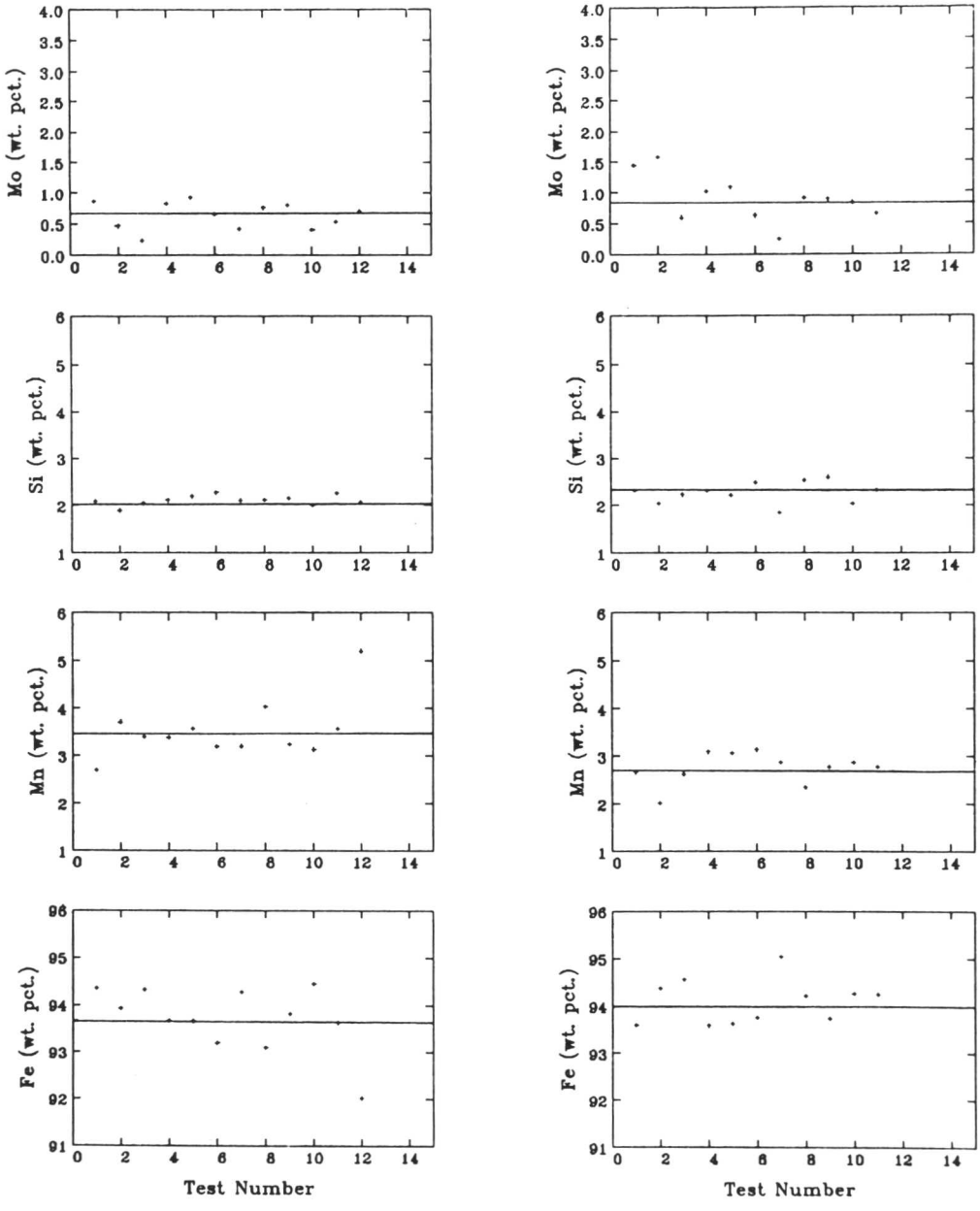

Fig. 11.12: *Microanalytical data obtained using energy dispersive X-ray analysis on PHILIPS 400T (T_γ = 620 °C).*

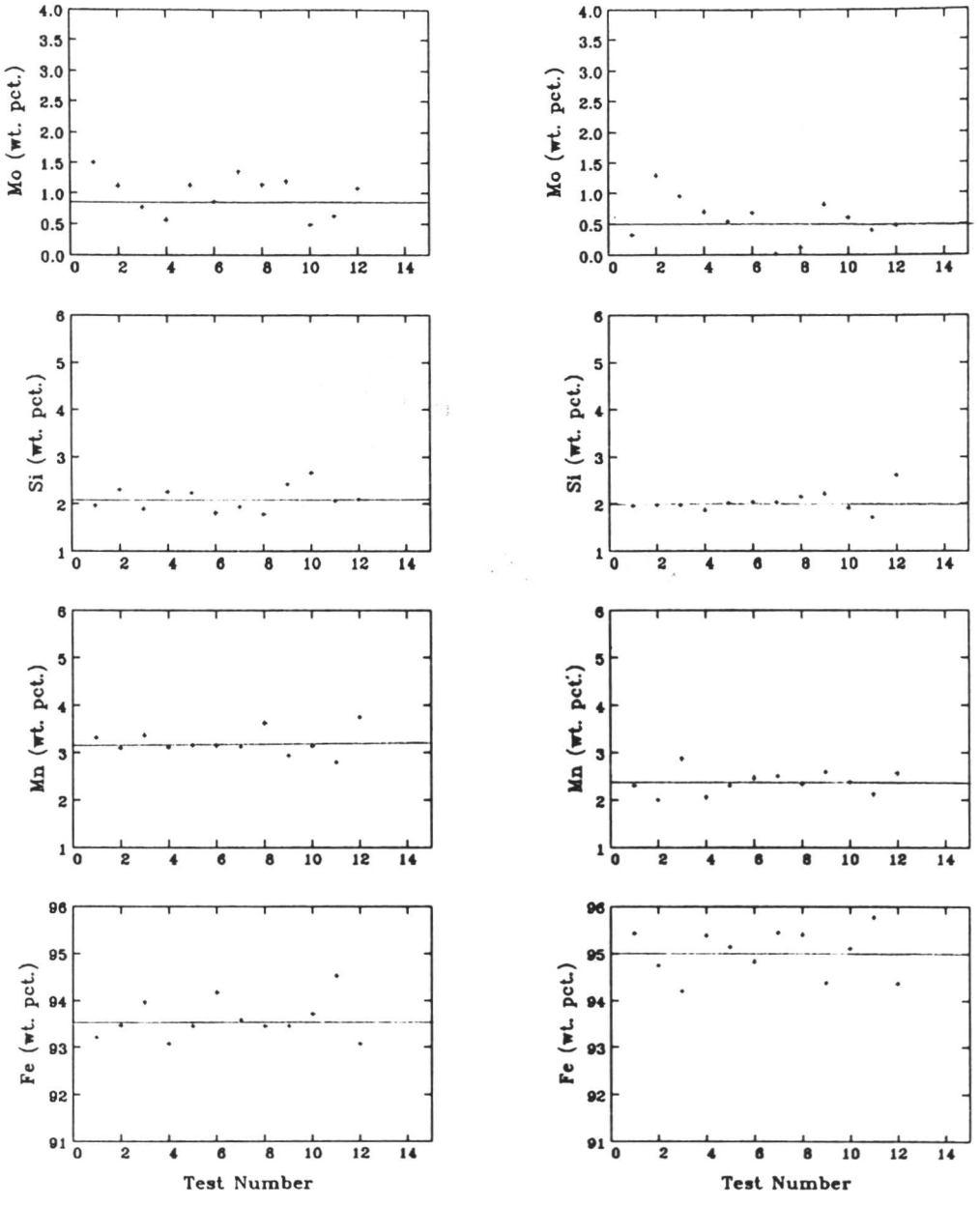

Fig. 11.13: *Microanalytical data obtained using energy dispersive X-ray analysis on PHILIPS* 400*T* (T_γ = 660 °*C*).

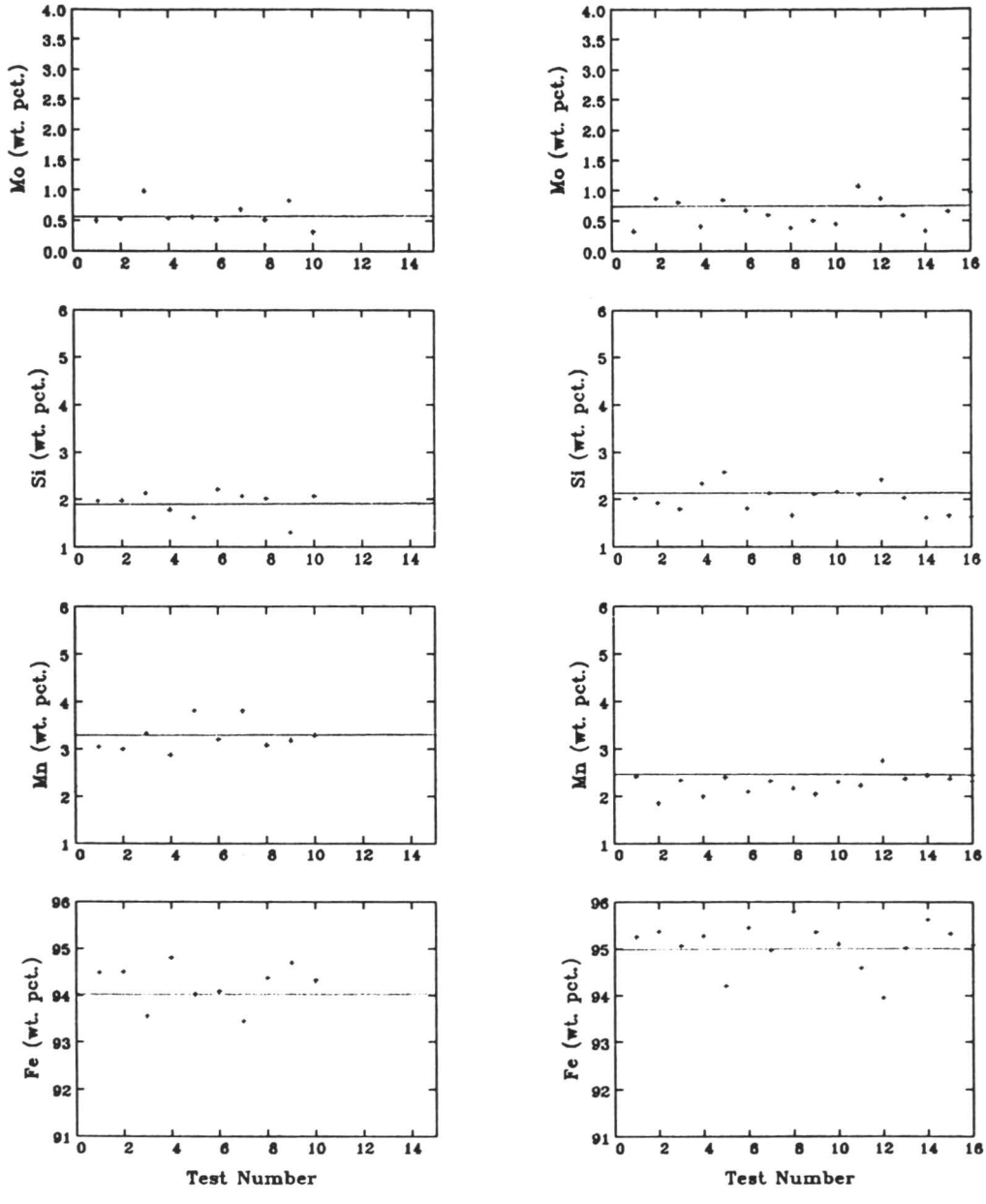

Fig. 11.14: *Microanalytical data obtained using energy dispersive X-ray analysis on PHILIPS 400T (T_γ = 700 °C).*

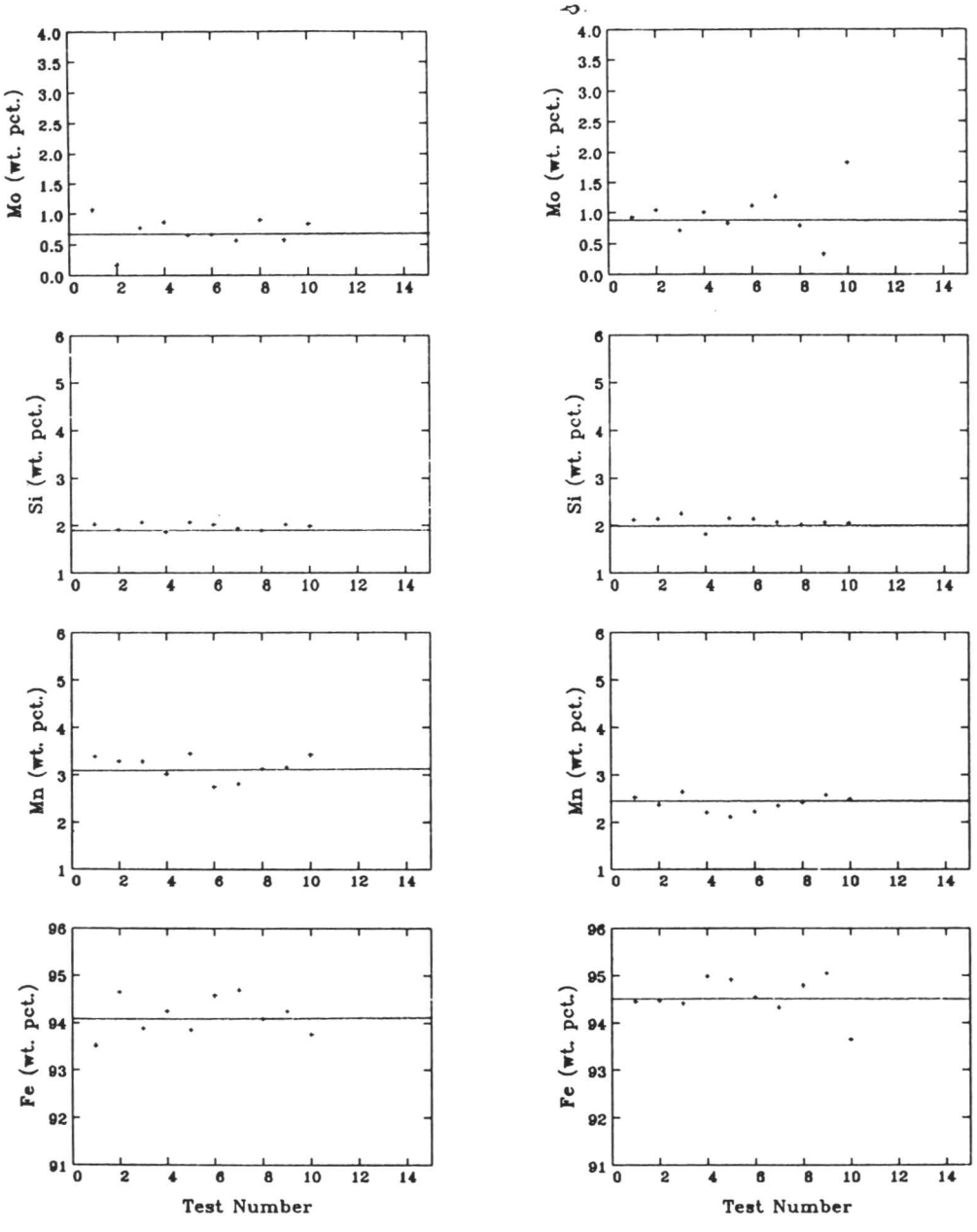

Fig. 11.15:*Microanalytical data obtained using energy dispersive X-ray analysis on PHILIPS* 400*T* (T_γ = *860 °C).*

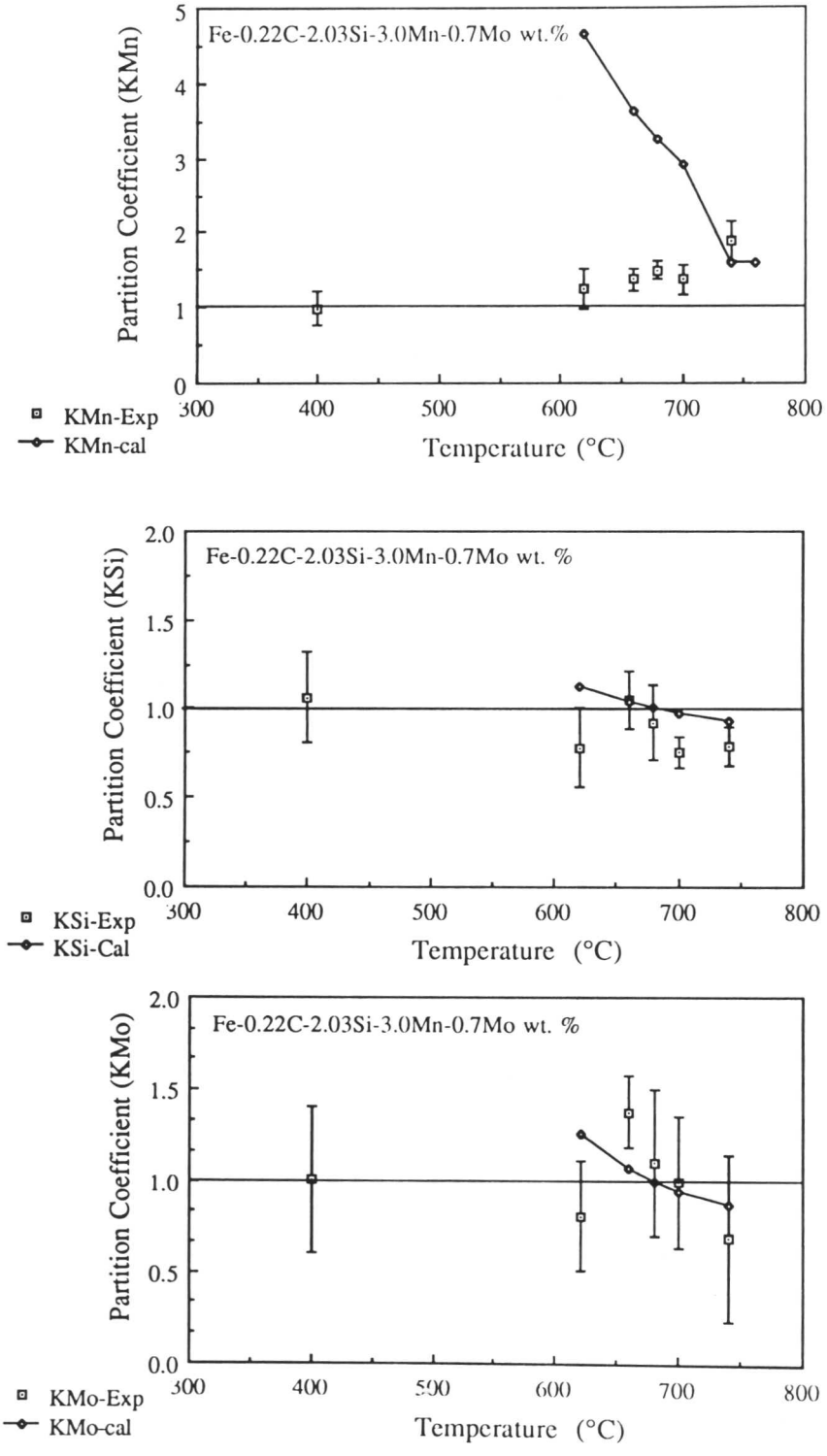

Fig. 11.16: *The effect of reaustenitisation temperature on the partition coefficient of manganese, showing that the degree of partitioning of manganese increases as the reaustenitisation temperature increases.*

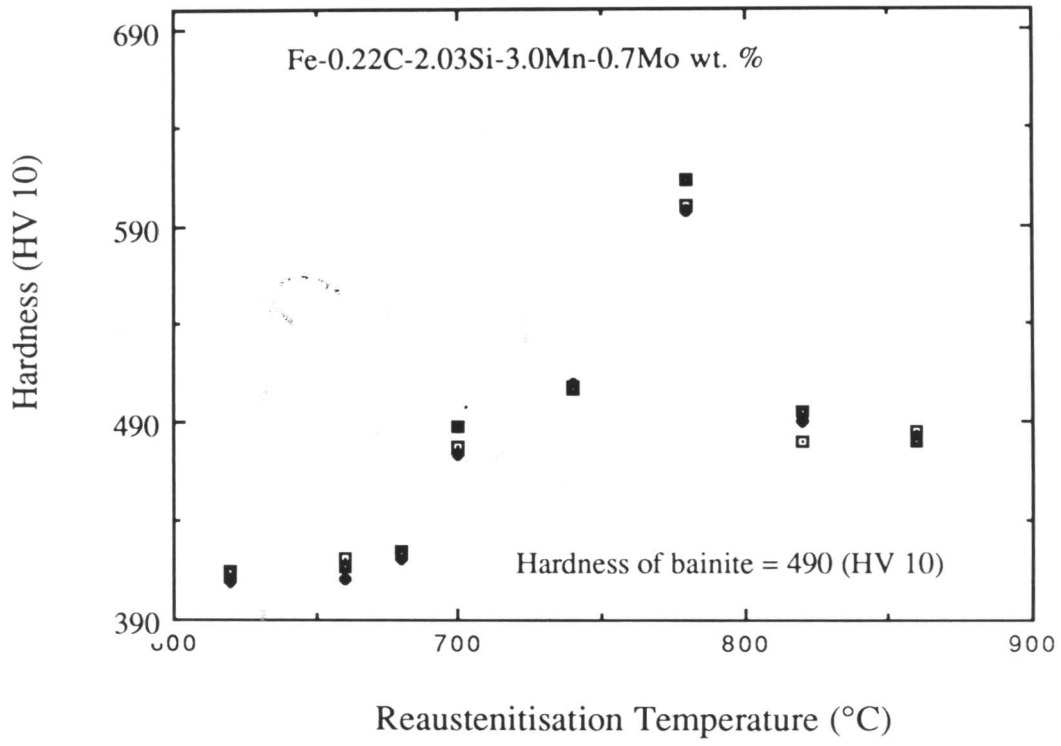

Fig. 11.17: *The effect of isothermal reaustenitisation temperature on the bulk hardness of the specimens.*

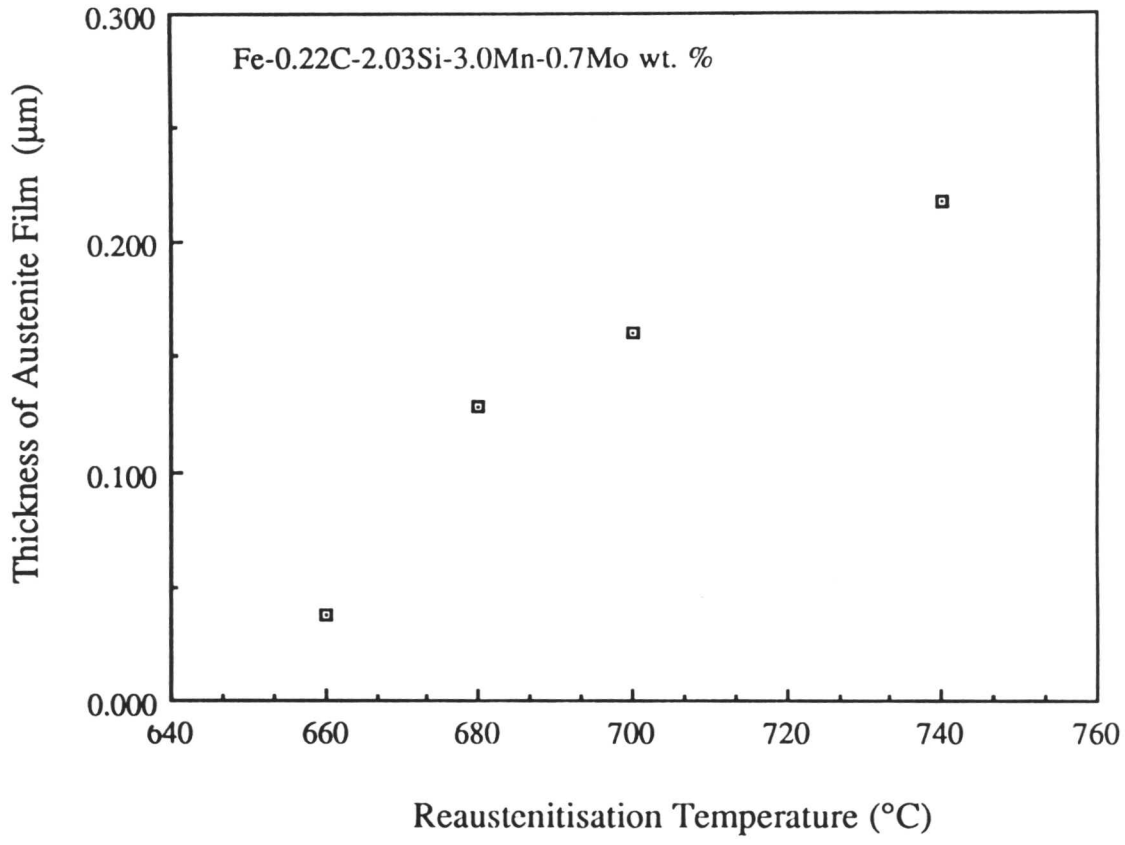

Fig. 11.18: *Measurement of the thickness of the residual austenite films. The thickness of austenite films increases with the increasing reaustenitisation temperature.*

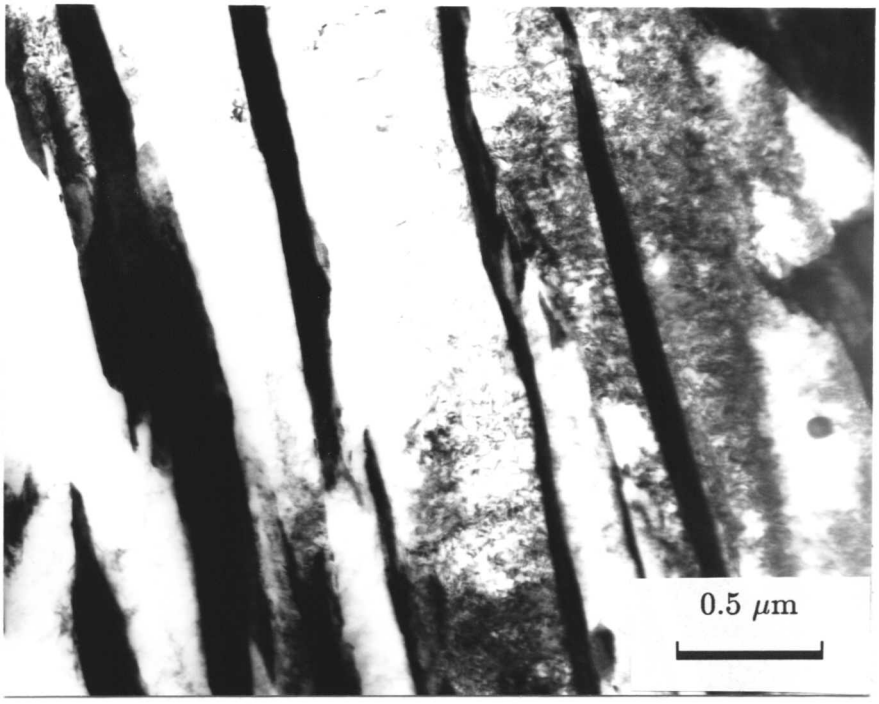

[$T = 400\ ^{o}\mathrm{C}$]

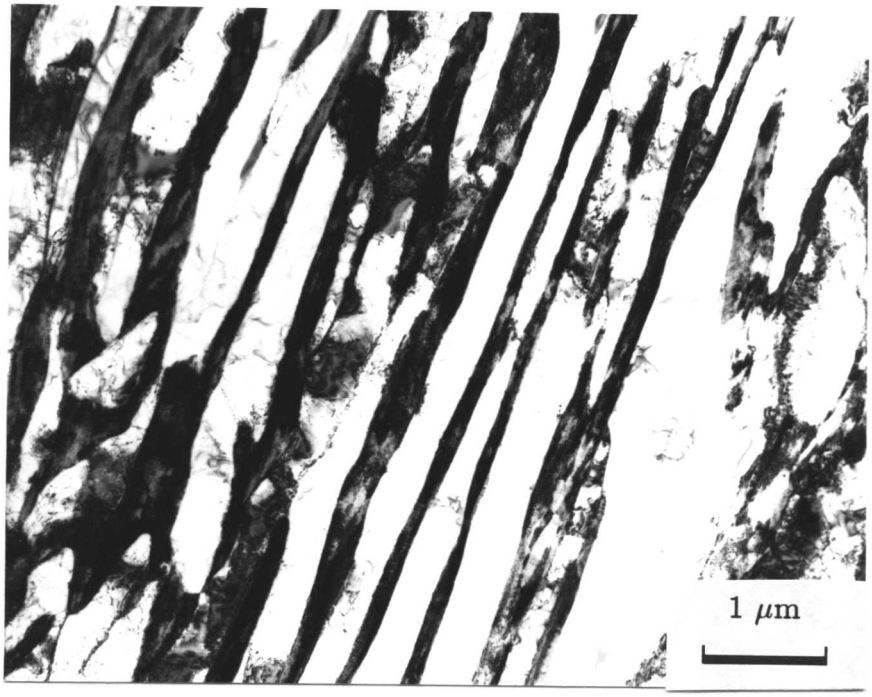

[$T_{\gamma} = 660\ ^{o}\mathrm{C}$]

Fig. 11.19: *Continued* .....

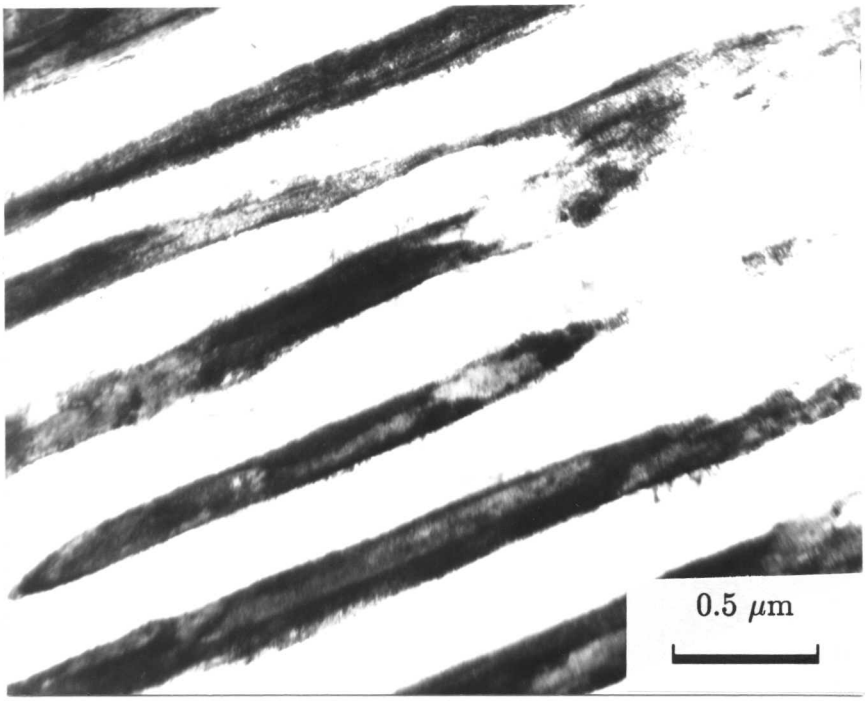

[$T_\gamma = 680\ ^o$C]

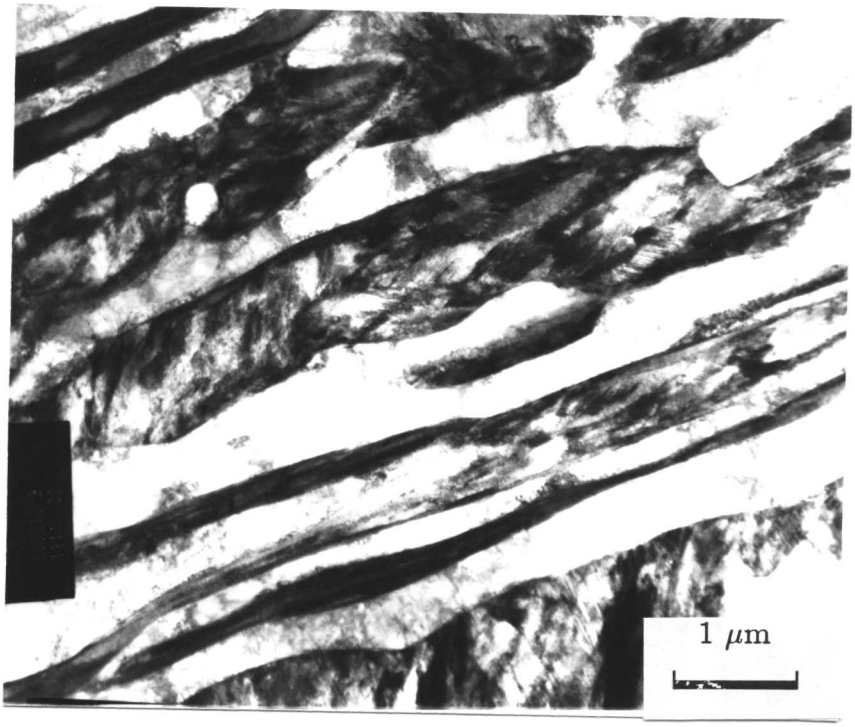

[$T_\gamma = 700\ ^o$C]

Fig. 11.19: *Continued .....*

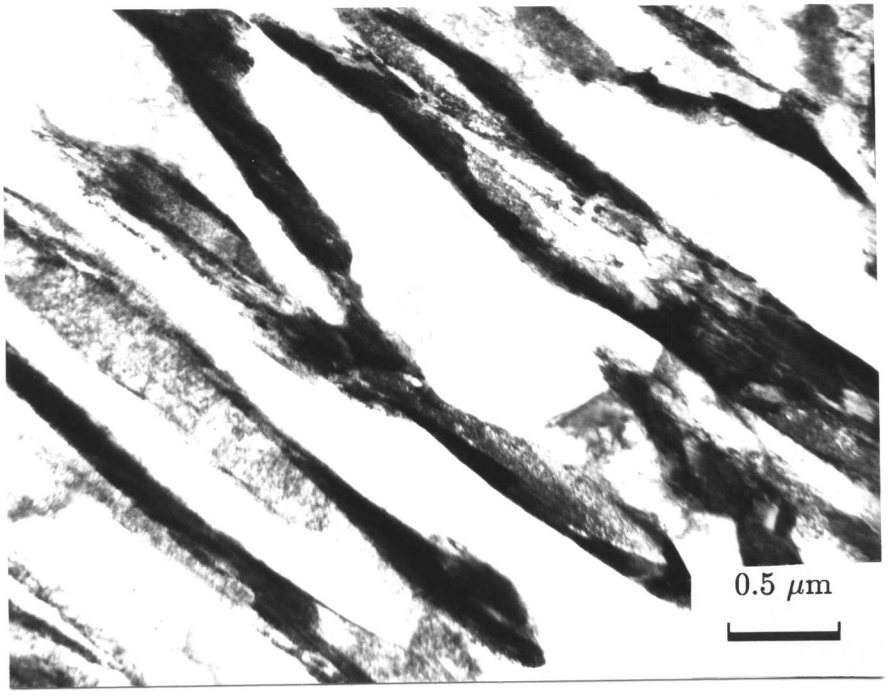

$[T_\gamma = 740\ ^\circ\mathrm{C}]$

Fig. 11.19: *TEM micrographs showing the thickening of austenite films after isothermal reaustenitisation for 3000* s *at temperatures indicated on each figure, note that the films remain parallel to the ferrite sub-units.*

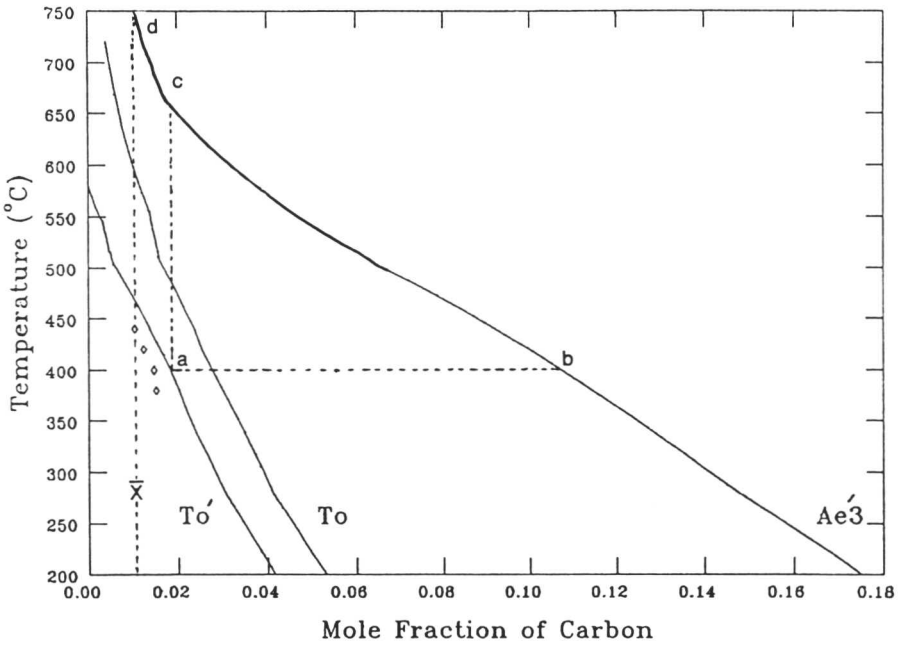

Fig. 11.20: *Calculated phase diagram with experimental data of carbon concentration of residual austenite at the termination of isothermal transformation. The para-equilibrium phase boundaries Ae'_3 and T_0 calculated as in [Bhadeshia and Edmonds, 1980].*

Chapter 12
SUGGESTIONS FOR FURTHER WORK

Nucleation Rate for Widmanstätten Ferrite: Some progress has been made in understanding the mechanism of Widmanstätten ferrite and bainite nucleation. Nevertheless, there is no experimental verification of the nucleation *rate*, and quantitative studies need to be pursued with vigour.

Although the linear relationship between the activation energy for nucleation and the chemical free energy change accompanying nucleation has been more or less verified, the slope and intercept of the experimental relation needs to be rigorously compared with theory. This cannot be done without extensive data on for example, dislocation (or interface) mobilities as a function of temperature.

Given the analogy between bainite and acicular ferrite, it should be possible to formulate the kinetic theory for acicular ferrite after accounting for its intragranular nucleation. Experiments are needed to verify the dependence of the activation energy for the nucleation of acicular ferrite on inclusions, on the chemical driving force. In particular, it is necessary to design and study samples in which the ratio of grain surface to intragranular nucleation densities varies. Monitoring the onset of a detectable degree of acicular ferrite formation then enables the free energy dependence to be deduced. It will be necessary to cover a range of alloys to give sufficient variation in the driving force at constant temperature. The theory will then be tested against experimental kinetic data on acicular ferrite in low–alloy steels.

Chaotic Microstructure in Ultrahigh–Strength Steel: One of the most exciting results to emerge from the work was the ability to induce the intragranular nucleation of ferrite plates in wrought steels containing extremely small quantities of nonmetallic particles. The dismantling of packets of parallel ferrite plates in bainitic or martensitic microstructures, into differently orientated chaotic acicular ferrite plates, improves toughness. The increased chaos can only be achieved by introducing inclusions as intragranular nucleation sites. The gain in toughness achieved in this manner overcomes any loss due to the presence of inclusions, in welds and low–strength steels. The same level of inclusions cannot however, be tolerated in ultrahigh–strength (UHS) steels ($\sigma_Y \geq 1300$ MPa) which typically contain oxygen at < 10 ppm. The research has shown that by eliminating the austenite grain surfaces as potential nucleation sites (by decorating them with a very thin layer of allotriomorphic ferrite), the very small oxygen concentration is

sufficient to nucleate acicular ferrite in UHS steel.

However, much further work is needed to make this idea into a viable proposition, since the heat treatments used were not realistic from a commercial point of view. Alloys need to be designed which are able to produce the required microstructure during continuous cooling transformations under near natural cooling conditions.

REFERENCES

Aaronson, H. I., Boswell, P. G. and Kinsman, K. R.: Mechanical Properties and Phase Transformations in Engineering Materials, eds. S. D. Antolovich, R. O. Ritchie and W. W. Gerberich, published by The Metallurgical Society of the AIME., Warrendale, Penn. USA., 1986, pp. 467.

Aaronson, H. I., Domain, H. A. and Pound, G. M.: *Thermodynamics of the Austenite→Proeutectoid Ferrite Transformation I, Fe-C Alloy* Trans. of Met. Soc. AIME, **236,** 1966a, pp. 753.

Aaronson, H. I., Domain, H. A. and Pound, G. M.: *Thermodynamics of the Austenite→Proeutectoid Ferrite Transformation II, Fe-C-X Alloy* Trans. of Met. Soc. AIME, **236,** 1966b, pp. 768.

Aaronson, H. I. and Domain, H. A.: *Partition of Alloying Elements between Austenite and Proeutectoid Ferrite or Bainite,* Trans. of Met. Soc. AIME, **236,** 1966, pp. 781-796.

Aaronson, H. I. and Wells, C.: *Sympathetic Nucleation of Ferrite,* Trans. of Met. Soc. AIME, **206,** 1956, pp. 1216-1223.

Abson, D. J., and Pargeter, R. J.: *Factors Influencing As-deposited Strength, Microstructure, and Toughness of manual Metal Arc Welds Suitable for C-Mn Steel Fabrications,* Int. Metals Reviews, **31,** 1986, pp. 141-194.

Allen, N. P., Peil, L. B. and Griffiths, W. T.: Second Rep. of the Alloy Steels Research Committee, ISI Spec. Rep. No. 24, 1939, pp. 369-390.

Babu, S. S. and Bhadeshia, H. K. D. H.: *Transition from Bainite to Acicular Ferrite in Reheated Fe-Cr-C Weld Deposits,* Materials Science and Technology, **6,** 1990, pp. 1005-1020.

Baeyertz, M.: *Effect of Initial Structure on Austenite Grain Formation and Coarsening,* Trans. ASM, **30,** 1942, pp. 458-490.

Baker, R. G. and Nutting, J.: *Tempering of* $2\frac{1}{4}\%$ *Cr-1%Mo Steel* Iron and Steel, **18,** 1959, pp. 606-612.

Barford, J. and Owen, W.: *The Effect of Austenite Grain Size and Temperature on the Rate of Bainite Formation,* JISI, 1961, pp. 146-151.

Barrite, G. S., Ricks, R. A. and Howell, P. R.: *Application of STEM/EDX to Study of Microstructral Developments in HSLA Steel Weld Metals,*

Becker, R. and Döring, W.: Ann. Phys., **24,** 1935, pp. 719.

Bhadeshia, H. K. D. H.: *The Thermodynamics of Steels: The Carbon-Carbon Interaction Energy,* Metal Sci., **14,** 1980, pp. 230-232.

Bhadeshia, H. K. D. H.: *A Rationalisation of Shear Transformations in Steels,* Acta Met., **29,** 1981a, pp. 1117-1130.

Bhadeshia, H. K. D. H.: *Diffusion of Carbon in Austenite,* Metal Science, **15,** 1981b, pp. 477-479.

Bhadeshia, H. K. D. H.: *Bainite: The Incomplete-reaction Phenomenon,* Proc. of Inter. Conf. on Solid-Solid Phase Transformations, Pittsburgh, USA., 1981b, pp. 1041-1048.

Bhadeshia, H. K. D. H.: *The Driving Force for Martensitic Transformation in Steels,* Metal Science, **15,** 1981c, pp. 175-177.

Bhadeshia, H. K. D. H.: *Thermodynamic Extrapolation and the Martensite-Start Temperature of Substitutionally-Alloyed Steels,* Metal Science, **15,** 1981d, pp. 178-180.

Bhadeshia, H. K. D. H.: *A Thermodynamic Analysis of Isothermal Transformation Diagrams,* Metal Science, **16,** 1982, pp. 159-165.

Bhadeshia, H. K. D. H.: *Bainite: Overall Transformation Kinetics,* J. De Physique, **43,** 1982, pp. C4-443-C4-448.

Bhadeshia, H. K. D. H.: *Diffusional Decomposition of Ferrite,* Prog. in Mater. Sci., **29,** 1985, pp. 325-328.

Bhadeshia, H. K. D. H.: *Diffusional Formation of Ferrite in Iron and its Alloys,* Prog. Mat. Sci., **29,** 1985, pp. 321-386.

Bhadeshia, H. K. D. H.: *Critical Assessment: Diffusion-controlled Growth of Ferrite Plates in Plain Carbon Steels,* Materials Science and Technology, **1,** 1985a, pp. 497-504.

Bhadeshia, H. K. D. H.: *Diffusional and Displacive Transformations,* Scripta Met., **21,** 1987a, pp. 1017-1022.

Bhadeshia, H. K. D. H.: *Worked Examples in the Geometry of Crystals,* Pub. by Inst of Metals, London, 1987b, pp. 26-25.

Bhadeshia, H. K. D. H.: CERL Report no. TPRD/L/3224/R87, 1988, pp. 5.

Bhadeshia, H. K. D. H.: *Kinetics of the Bainite Transformation,* ICOMAT 89, Int. Conf. on Martensitic Transformations, Sidney, Australia, 1989.

Bhadeshia, H. K. D. H.: Steel Technology International , ed. P. H. Scholes, Sterling Publications International, Ltd., London, UK., **1989,** pp. 289-294.

Bhadeshia, H. K. D. H.: Recent Trends in Welding Science and Technology, eds. S. A. David and J. Vitek, ASM International, Ohio, USA., 1989, pp. 189-198.

Bhadeshia, H. K. D. H. and Edmonds, D. V.: *The Bainite Transformation in Silicon Steels,* Metall. Trans., **10A,** 1979, pp. 895-907.

Bhadeshia, H. K. D. H. and Edmonds, D. V.: *The Mechanism of Bainite Formation in Steels,* Acta Met., **28,** 1980, pp. 1265-1273.

Bhadeshia, H. K. D. H. and Edmonds, D. V.: *Bainite in Silicon Steels: A New Composition-property approach-1,* Metal Science, **17,** 1983, pp. 411-419.

Bhadeshia, H. K. D. H. and Edmonds, D. V.: *Bainite in Silicon Steels: A New Composition-property Approach,*Metal Science, **17,** 1983, pp. 420-425.

Bhadeshia, H. K. D. H., Svennson, L. -E. and Gretoft, B.: *A Model for the Development of Microstructure in Low-Alloy Steel (Fe-Mn-Si-C) Weld Deposits,* Acta Met., **33,** 1985, pp. 1271-1283.

Bhadeshia, H. K. D. H., Svennson, L. -E.: *The Microstructure of Submerged-Arc Weld Deposits for High-Strength Steels,* J. of Materials Science, **1989,** 24, pp. 3180-3188.

Bhadeshia, H. K. D. H. and Waugh, A. R.: Acta Met., **30,** 1982a, pp. 775-784.

Bilby, B. A. and Christian, J. W.: *Martensitic Transformations,* Symp. on the Mechanism of Phase Transformations in Metals, Nov. 9th 1955, Inst. of Metals, London, UK., pp. 121-172.

Billy, J., Johnson, T., Loberg, B. and Easterling, K. E.: *Stress-Relief Heat Treatments of Submerged-Arc Weleded Microalloyed Steels,* Metals Technology **7,** 1980, pp. 67-78.

BISRA: *Atlas of Isothermal Transformation Diagram of B. S. En-Steels,* Special Report No. 56, 2nd ed. The Iron and Steel Inst. London, UK., 1956a.

BISRA: *Atlas of Isothermal Transformation Diagram of B. S. En-Steels,* Special Report No. 56, 2nd ed. The Iron and Steel Inst. London, UK., 1956b, pp. 11,

17-27, 33, 37-45, 57, 59, 83, 97, 107, 143, 151.

Brozzo, P., Buzzichell, G., Mascanzoni, A. and Mirabile, M.: *Microstructure and Cleavage Resistance of Low-Carbon Bainitic Steels,* Metal Science, **11,** 1977, pp. 123-129.

Bruke, J.: *The Kinetics of Phase Transformations in Metals,* Pergamon Press Ltd. UK., 1965a, pp. 98-104.

Bruke, J: *Mechanism of Phase Transformations in Metals,* Pub. by Pergamon Press, UK, 1965b, pp. 196-201.

Cai, X-L., Garratt-R, A.J. and Owen, W.S.: *The Development of Some Dual-Phase Steel Structure from Different Starting Microstructure,* Metall. Trans., **16A,** 1985, pp. 543-557.

Chadwick, G. A.: *Metallography of Phase Transformations,* Pub. by Butterworth and Co (Publishers) Ltd., 1972, pp. 188-191.

Chandel, R. S., Orr, R. F.,Gianetto, J. A., Mcgrath, J. T., Patchett, B. M. and Bicknell, A. C.: *The Microstructure and Mechanical Properties of Narrow Gap Welds in 2.25Cr-1Mo Steel, Report ERP/PMRL 85–16(OP–J) of the Physical Metallurgy Research Laboratories, CANMET, Energy, Mines and Resources Canada, Ottawa, Canada,* **1985,**

Christian, J. W.: *Accommodation Strains in Martensitic Formation and the Use of a Dilatation Parameter,* Acta Met., **6,** 1958, pp. 377-379.

Christian, J. W.: *Decomposition of Austenite by Diffusional Processes,* Proc. of Int. Conf. Philadelphia, Pennsylvania. ed. Zackay, V. F. and Aaronson, H. I., 1962, pp. 371-386.

Christian, J. W.: *Martensitic Transformations: A Current Assessment,* Symp. on Mechanism of Phase Transformations in Crystalline solids Univ. of Manchester, 3-5 July 1968, Monograph 33, Inst. of Metals London, UK., 1969, pp. 129-142.

Christian, J. W.: *The Theory of Phase Transformations in Metals and Alloys,* Pub. by Pergamon Press, UK. 1975a, pp. 6-14.

Christian, J. W.: *Theory of Transformations in Metals and Alloys, 2nd edition, Part I, Pergamon Press,* 1975b, pp. 180-181.

Christian, J. W.: *The Theory of Phase Transformations in Metals and Alloys,* Pub. by Pergamon Press. 1975c, pp. 482.

Christian, J. W. and Edmonds, D. V.: Phase Transformations in Ferrous Alloys', eds. A. R. Marder and J. I. Goldstein, A. S. M., Ohio, USA., 1984, pp. 293-325.

Christian, J. W. and Edmonds, D. V.: Proc. Int. conf. on Welding Metallurgy of Structural Steels, ed. J. Y. Koo, The Metallurgical Society of AIME, Warrendale, P. A., USA., 1987,

Chijiiwa, R., Tamehiro, H., Hirai, M., Matsuda, H. and Mimura, H.: *Offshore Mechanics and Arctic Engineering Conference (OMAE), Houston, Texas, USA.,* 1988 pp. 1-8.

Coates, D. E.: *Diffusional growth limitation and Hardenability,* Met. Trans., **4A,** 1973, pp. 2313-2325.

Conrad, H.: J. Metals, July 1973, pp. 582.

Cohen, M., Olson, G. B. and Clapp, P. C: *On the Classification of Displacive Phase Transformations,* Proc. of Int. Conf. on Martensitic Transformations ICOMAT Cambridge, Massachussetts, USA., 24-29 June, 1979, pp. 1-11.

Cottrell, S. A. and Ko, T.: *Effect of High-Temperature* JISI, March, 1953, pp. 224-229.

Cullity, B. D.: Elements of X-ray analysis diffraction, Addison-Wesley, Reading, N. Y. USA., 1978 pp. 356.

Davenport, E. S. and Bain, E. C.: *Transformation of Austenite at Constant Subcritical Temperature,* Trans. of Met. Soc. AIME, **90,** 1930, pp. 117-154,

Dirnfeld, S.F., Korevaar, B.M. and Spijker, F.B.: *The Transformation to Austenite in a Fine Grained Tool Steel,* Metall. Trans., **15,** 1974, pp. 1437-1444.

Dorn, J. E.: Dislocation Dynamics, McGraw Hill, New York, USA. 1968, pp. 27.

Dyson, D. J. and Holmes, B.: *Effect of Alloying Additions on the Lattice Parameter of Austenite,* JISI, **208,** 1970, pp. 469-474.

Dubé, C. A.: *Ph.D. Thesis,* Carnegie Inst. of Technology, Pittsburgh, P. A., USA, 1948.

Entwisle, A. R.: Materials Science J., **17,** 1968, pp. 153.

Ferrante, M. and Farrar, R. A.: *The Role of Oxygen Rich Inclusions in Determining the Microstructure of Weld Metal Deposits,* J. Mater. Sci., **17,** 1982, pp.

3293-3298.

Fisher, J. C.: Trans. of Met. Soc. AIME., **185,** 1949, pp. 688.

Fick, J. I. J. and Rogerson, J. H.: *The Effect of Post-Solidification Metallurgical Reactions on the Toughness of Weldments in Thick Structural Steel Plates,* Low Carbon Structural Steels for the Eighties, Institute of Metals, London, UK., **1977,** pp. IIIB-33-IIIB-50.

Fowler, R. H. and Guggenheim, E. A.: Statstical Thermodynamics, New York, Cambridge University Press, 1939.

Garcia, C.I. and DeArdo, A.J.: *Formation of austenite in 1.5 pct Mn Steels,* Metall. Trans., **12A,** 1981, pp. 521-530.

Garland, J. and Kirkwood, P. R.: *Towards Improved Submerged Arc Weld Metal,* Metal Constr., May, 1975, pp. 275-283

Glimour,J. B., Purdy, G. R. and Kirkaldy, J. S.: *Thermodynamics Controlling the Proeutectoid Ferrite Transformations in Fe-C-Mn Alloys,* Metall. Trans., **3A,** 1972, pp. 1455-1464,

Goodenow, R. H., Matas, S. J. and Hehemann, R. F.: *Growth Kinetics and the Mechanism of the Bainite Transformation* Trans. of Met. Soc. AIME., **227,** 1963, pp. 651-658.

Gordine, J. and Codd, I.: *The Influence of Silicon upto 1.5 wt% on the Tempering Characterstics of a Spring Steel,* J. I. S. I., **207,** 1969, pp. 461-467.

Graham, L. W. and Axon, H. J.: *The Effect of Austenitising Treatments on Formation of Lower Bainite in a Plain Carbon Steel,* JISI, April, 1959, pp. 361-365.

Grong, D. and Matlock, D. K.: *Microstructural Development in Mild and Low-Alloy Weld Metals,* Int. Met. Rev., **31,** 1986, pp. 27-48.

Habraken, J. and Economopoulos, M.: *Bainite Microstructures in Low-Carbon Alloy Steels,* Transformation and Hardenability in Steels, Climax Molybdenum Co. Ann Arbor, Michigan, USA, 1967, pp. 69-107,

Harrison, P. l. and Farrar, R. A.: *Influence of Oxygen-rich inclusions on the $\gamma - \alpha$ phase transformations in high-strength low-alloy steel(HSLA) welds,* J. Mater. Sci., **16,** 1981, pp. 2218-2226.

Harrison, P. l. and Farrar, R. A.: *Microstructural Development and Toughness of C-Mn and C-Mn-Ni Weld Metal part-1: Microstructural Development,* Metal

Constr., July, 1987, pp. 392R-399R.

Hayami, S. and Furukawa, T.: Proc. Microalloying Conf, Washington, D.C., 1975, pp. 78-87.

Hayami, S., Furukawa, T. Gondoh, H. and Takechi, H.: *Recent development in formable Hot- and Cold-rolled HSLA including Dual Phase Steels,* Formable HSLA and Dual Phase Steels, ed. Davenport, A.T., The Met. Society of AIME, 1979,

Hehemann, R. F.: *The Bainite Transformation,* Phase Transformations, ASM, Metals Park, Ohio, USA., 1970, pp. 307.

Hillert, M.: *Nuclear Composition- A Factor of Interest in Nucleation,* Acta Met., **1953,** 1, pp. 764-766.

Hillert, M.: Jernkontorets Ann., **141,** 1957, pp. 757,

Hillert, M., Nilsson, K. and Torndahl, L-E.: *Effect of alloying elements on the formation of austenite and dissolution of cementite,* Trans. J. I. S. I., **209,** 1971, pp. 49-66.

Homma, R.: *Studies on austenite grain of 3.5%Ni-Cr-Mo-V steel,* Trans. I. S. I. J., **14,** 1974, pp. 434-443.

Hornbogen, E.: International Materials Reviews, **34,** 1989, pp. 277-296.

Horvay, G. and Cahn, J. W.: *Dendritic and Spheroidal Growth,* Acta Met. **9,** 1961, pp. 695-705.

Hull, D.: *The Characterstics of the Martensitic Transformations,* Bull. Inst. Metals, **2,** 1954, pp. 134-139.

Hultgren, A.: *The Ac1 Range of Carbon Steels and Related Phenomenon,* Trans. Amer. Soc. for Steel Treaters, **16,** 1929, pp. 227-256.

Hultgren, A.: *Isothermal Transformation of Austenite,* Trans. ASM, **39,** 1947, pp. 915-1005,

Imagumbai, M., Chijiiwa, R., Aikawa, N., Nagumo, M., Homma, H., Matsuda, S. and Mimura, H.: HSLA Steels: Metallurgy and Applications, eds. J. M. Gray, T. Ko, Z. Shouhua, W. Baorong and X. Xishan, ASM International, Ohio, 1985, pp. 557-566,

Irani, J. J. and Honeycombe, R. W. K.: J. of Iron and steel Inst., 1955, pp.

826-833.

Irvine, K. J. and Pickering, F. B.: *The Tempering Characterstice of Low-Carbon Low-Alloy Steels,* JISI., 1960, pp. 137-153.

Ito, Y., Nakanishi, M. and Komizo, Y.: *Effect of Oxygen on Low Carbon Steel Weld Metal,* Metal Constr., Sept. 1982, pp. 472-478.

Judd, R.R. and Paxton, H.W.: *Kinetics of Austenite Formation from a Spheroidized Ferrite-Carbide Aggregate,* Trans. of Met. Soc. AIME., **242,** 1968, pp. 206-215.

Kaufman, L., Clougherty, E. V. and Weiss, R. J.: *The Lattice Stability of Metals- III Iron,* Acta Met., **11,** 1963, pp. 323-335.

Kenny, B. G., Kerr, H. W., Lazor, R. B. and Graville, B.: *Ferrite transformation Characterstics and CCT Diagrams in Weld Metals,* Metal Constr., June, 1985, pp. 374R-381R,

Kinoshita, S. and Ueda, T.: *Some Observation on the Formation of Austenite Grains,* Trans. I. S. I. J., **14,** 1974, pp. 411-418.

Kinsman, K. R. and Aaronson, H. I. : *Influence of Al, Co and Si upon the Kinetics of the Proeutectoid Ferrite Reactions,* Metall. Trans., **4A,** 1973, pp. 954.

Ko, T.: *The Formation of Bainite in an En 21 Steel,* JISI, September, 1953, pp. 16-18.

Krahe, P. R., Kinsman, K. R. and Aaronson, H. I.: *Influence of Austenite Grain Size upon the Widmanstätten-Start (W_S) Temperature for the Proeutectoid Ferrite Reactions,* Acta Met., **20,** 1972, pp. 1109-1121.

Lacher, J. R.: Proc. Cambridge Phil. Soc., **33,** 1973, pp. 518.

Law, N.C. and Edmonds, D.V.: *The Formation of Austenite in a Low-Alloy Steel,* Metall. Trans., **11A,** 1980, pp. 33-46.

Lenel, U.R. and Honeycombe, R.W.K.: *Formation of Austenite in Fe-10Cr-0.2C alloy,* Metal Science, **18,** 1984a, pp. 201-205.

Lenel, U.R. and Honeycombe, R.W.K.: *Morphology and Crystallography of Austenite Formed During Intercritical Annealing,* Metal Science, **18,** 1984b, pp. 503-510.

Levine, E. and Hill, D.C.: *Structure-Property Relationships in Low C Weld*

Metals, Metall. Trans. **8A,** 1977, pp. 1453-1463.

Lobo, J. A. and Geiger, G. H.: *Thermodynamics and Solubility of Carbon in Ferrite and Ferritic Fe-Mo Alloys,* Metall. Trans., **7A,** 1976a, pp. 1347-1357.

Lobo, J. A. and Geiger, G. H.: *Thermodynamics of in Austenite and Fe-Mo Austenite,* Metall. Trans., **7A,** 1976b, pp. 1359.

McLellan, R. B. and Dunn, W. W.: *A Quasi-Chemical Treatment of Interestitial Solid Solutions: Its Application to Carbon in Austenite,* J. Phys. Chem. Solids, **30,** 1969, pp. 2631-2637.

Magee, C. L.: *The Nucleation of Martensite,* Phase Transformations, A. S. M., Ohio, USA., 1970, pp. 115-156.

Matsuda, S., Inoue, T. and Ogasaswara, M.: Trans. Japan Inst. Metals, **9,** 1968, pp. 343.

Matsuda, S., Inoue, T. and Ogasaswara, M.: *Toughness and Effective Grain Size in Heat-Treamed Low-Alloy High-Strength Steels,* Trans. I. S. I. J., **12,** 1972, pp. 325.

Matsuda, S. and Okamura, Y.: *Microstructural and Kinetic Studies of Reverse Transformation in a Low-Carbon Low Alloy Steel,* Trans. I. S. I. J., **14,** 1974a, pp. 363-368.

Matsuda, S. and Okamura, Y.: *The Later Stage of Reverse Transformation in Low-Carbon Low Alloy Steel,* Trans. I. S. I. J., **14,** 1974b, pp. 444-449.

Mehl, R. F.: Hardenability of Alloys, ASM, Cleveland, OH, 1939, pp. 1.

Nakasugi, N., Matsuda, H. and Tamehiro, H.: *Ultra-Low Carbon Bainitic Steels for line pipes,* Steels for Line pipes and Pipeline Fittings, Metals Soc. London, UK., 1983, pp. 90-95.

Naylor, J. P. and Krahe, P. R.: *The Effect of the Bainite Packet Size on Toughness,* Metall. Trans., **5,** 1974, pp. 1699-1701.

Nehrenberg, A.E.: *The growth of austenite as related to prior structure,* Trans. of Met. Soc. AIME., J. of Metals, **1950,** 188, pp. 162-174.

Nelson, J. B. and Riley, D. P.: Proc. of Phys. Soc. London, **57,** 1945, pp. 126.

Nemoto, M.: High Voltage Electron Microscopy, Academic Press, New York, NY,

1974, pp. 230.

Nishioka, K. and Tamehiro, H.: Microalloying '88: International Symposium on Applications of HSLA Steel, Chicago, Illinois, USA, September 1988, pp. 1-9.

Oblak, J. M. and Hehemann, R. F.: Transformation and Hardenability in Steels, Climax Molybdenum. Ann Arbor, USA, 1967, pp. 15.

Ohmori, Y.: *The Precipitation of Molybdenum Carbides During the Isothermal Decomposition of an Fe-4.10% Mo-0.23% C Austenite,* Trans. ISIJ, **12,** 1972, pp. 350-376.

Ohmori, Y., Ohtani, H. and Kunitake, T.: *The Bainite in Low Alloy High Strength Steels,* Trans. I. S. I. J, **11,** 1971, pp. 250-259.

Ohmori, Y., Ohtani, H. and Kunitake, T.: *Tempering of the Bainite/Martensite Duplex Structure in a Low-Carbon Low-Alloy Steel,* Metal Science, **8,** 1974, pp. 357-366.

Olson, G. B. and Cohen, M.: *A Mechanism of Martensitic Nucleation: Part III, Kinetics of Martensitic Nucleation,* Metall. Trans., **7A,** 1976, pp. 1915-1923.

Olson, G. B. and Cohen, M.: Dislocations in Solids, ed. F. R. N. Nabarro, **7,** 1986, pp. 297.

Owen, W. S.: *The Effect of Silicon on the Kinetics of Tempering,* Trans. ASM, **46,** 1954, pp. 812-829.

Pati, S. R. and Cohen, M.: Acta Met., **17,** 1969, pp. 189

Pickering, F. B.: *The Structure and Properties of Bainite in Steels,* Transformation and Hardenability in Steels, Climax Molybdenum, Ann Arbor, USA., 1967, pp. 109-129.

Plichita, M.R. and Aaronson, H.I.: *Influence of Alloying Elements Upon the Morphology of Austenite Formed from Martensite in Fe-C-X Alloys,* Metall. Trans., **5,** 1974, pp. 2611-2613.

Porter, D. A. and Easterling, K. E.: *Phase Transformations in Metals and Alloys,* Pub. by Van Nortrand Reinhold (International) Berkshire, UK., 1988, pp. 142-147.

Purdy, G. R. and Hillert, M.: *On the Nature of the Bainite Transformation in Steels,* Acta Met., **32,** 1984, pp. 823-828.

Raghavan, V. and Cohen, M.: *Measurement and interpretation of Isothermal Martensitic Kinetics,* Metall. Trans., **2,** 1971, pp. 2409-2418.

Rao, M. M. and Winchell, P. G.: *Growth Rate of Bainite from Low-Carbon Iron-Nickel-Carbon Austenite,* Trans. of Met. Soc. AIME., J. of Metals, **239,** 1967, pp. 956-960.

Rashid, M. S. and Rao, B. V. N.: *Tempering Characterstics of a vanadium containing dual phase steel,* Fundamentals of dual phase steels, ed. Kot, R. A. and Branfit, B. L; Symp. proc. The Met. Soc. AIME Chicago, Feb. 23-24, 1981, pp. 249-264.

Ricks, R. A., Howell, P. R. and Barritte, G. S.: *The Nature of Acicular Ferrite in HSLA Steel Weld Metals,* J. Mater. Sci., **17,** 1982, pp. 732-740.

Roberts, M. J.: *Effect of Transformation Substructures on the Strength and Toughness of Fe-Mn Alloys,* Metall. Trans., **1,** 1970, pp. 3287-3294.

Roberts, G.A. and Mehl, R.F.: *The Mechanism and the Rate of Formation of Austenite from Ferrite-Cementite Aggregate,* Trans. ASM, **31,** 1943, pp. 613-650.

Rodrigues, P. and Rogerson, J. H.:*The Relationship between Welding Condition, Thermal Cycles and Microstructure on The Toughness of Weld Metals in Low Carbon Structure Steels,* Low Carbon Structural Steels for the Eighties, Institute of Metals, London, 1977, pp. IIIB-33-40

Rundman, K. B., Moore, D. J.,Hayrynen, K. L., Dubensky, W. J. and Rouns, T. N.: *The Microstructure and Mechanical Properties of Austempered Ductile Iron,* J. Heat Treating, **5,** 1988, pp. 79-95.

Savage, W. F. and Aaronson, A. H.: Welding Journal, **45,** 1966, pp. 85.

Sharma, R. C. and Purdy, G. R.: *Nucleation Limitation and Hardenability,* Metall. Trans., **4A,** 1973, pp. 2303-2311.

Shiflet, G. J., Bradley, J.R. and Aaronson, H. I.: *A Re-Examination of the Thermodynamics of the Proeutectoid Ferrite Transformation in Fe-C Alloys,* Metall. Trans., **9A,** 1978, pp. 999-1007.

Shih, C. H., Averlach, B. L. and Cohen, M.: Trans. of Met. Soc. AIME., **203,** 1955, pp. 183

Siller, R. H. and McLellan, R. B.: *The Variation with Composition of the Diffusivity of Carbon in Austenite,* Trans. of Met. Soc. AIME., **245,** 1969, pp.

697-700

Siller, R. H. and McLellan, R. B.: *The Application of First Order Mixing Statistics to the Variation of the Diffusivity of Carbon in Austenite,* Metall. Trans., **1,** 1970, pp. 985-988.

Simonen, E. P., Aaronson, H. I. and Trivedi, R.: *Lengthening Kinetics of Ferrite and Bainite Sideplates,* Metall. Trans., **4,** 1973, pp. 1239-1245.

Speich, G. R. and Cohen, M.: *The Growth Rate of Bainite,* **218,** 1960, pp. 1050-1059.

Speich, G.R.,Demarest, V.A. and Miller, R.L.: *Formation of Austenite During Intercritical Annealing of Dual-Phase Steels,* Metall. Trans., **12,** 1981, pp. 1419-1428.

Speich, G. R. and Leslie, W. C.: *Tempering of Steel* Metall. Trans. **3,** 1972, pp. 1043-1054.

Speich, G.R. and Szirmae, A.: *Formation of Austenite from Ferrite and Ferrite-Carbide Aggregates,* Trans. of Met. Soc. AIME., **245,** 1969, pp. 1063-1074.

Smith, R. and Nutting, J.: *The Tempering of Low-Alloy Creep-Resistant Steels Containing Chromium, Molybdenum, and Vanadium,* JISI., **187,** 1957, pp. 314-329.

Taylor, A. and Sinclair, H.: Proc. of Phys. Soc. London, **57,** 1945, pp. 126.

Tomita, Y. and Okabayashi, K.: *Improvement in Lower Temperature Mechanical Properties of 0.40pct C-Ni-Mo Ultrahigh Strength Steel with the Second Phase Lower Bainite,* Metall. Trans., **14A,** 1983, pp. 485-492.

Tomita, Y. and Okabayashi, K.: *Mechanical Properties of 0.40pct C-Ni-Mo High Strength Steel Having a Mixed Structure of Martensite and Bainite,* Metall. Trans., **1985,** 16A, pp. 73-82.

Trivedi, R.: *The Role of Interfacial Free Energy and Interface Kinetics During Growth of Precipitate Plates and Needles,* Metall. Trans., **1,** 1970, pp. 921-927.

Trivedi, R. and Pound, G. M.: *Effect of Concentration-Dependent Diffusion Coefficient on the Migration of Interphase Boundaries,* J. Appl. Phys., **38,** 1967, pp. 3569-3576.

Tsuzaki, K., Yamaguchi, K., Maki, T., and Tamura, I.: Tetsu to Hagane, **74,** 1984, pp. 1430-1437.

Umemot, M., Horiuchi, K. and Tamura, I.: *Transformation Kinetics of Bainite during Isothermal Holding and Continuous Cooling,* Trans. I. S. I. J., **22,** 1982, pp. 854-861.

Volmer, M. and Weber, A.: Z. Phys. Chem., **119,** 1926, pp. 227.

Watanabe, S. and Kunitake, T.: *On the Formation of Austenite Grains from Prior Martensitic Structure,* Trans. I. S. I. J., **16,** 1976, pp. 28-35.

Watanabe, S. and Kunitake, T.: *On the Formation of Austenite Grains from Prior Martensitic Structure* Tetsu-to-Hagan e, **61,** 1975, pp. 96.

Watson, J. D. and McDougall, P. G.: *The Crystallography of Widmanstätten ferrite,* Acta Met., **21,** 1973, pp. 961-973.

Widgrey, D. J.: Welding Journal **3,** 1975, pp. 57.

Winterton, K.: *The Effect of Overheating on The Transformation-Characteristic of a Nickel-Chromium-Molbdenum Steel,* JISI, **1,** 1945, pp. 79p-85p.

Yamamoto, K., Matsuda, S., Haze, T., Chijiiwa, R. and Mimura, H.: Residual and Unspecified Elements in Steel, ASM International, Ohio, USA, November 1987, pp. 1-24.

Yang, J. R.: *Development of Microstructure in High-strength Steel Weld Deposits,* Ph.D. Thesis, University of Cambridge, Cambridge, U.K., 1987.

Yang, J. R. and Bhadeshia, H. K. D. H.: *Thermodynamics of Acicular Ferrite Transformation in Low-Alloy Steel Weld Deposits,* Advances in Welding Technology and Science, ASM Metal Park, Ohio, USA, 1987a, pp. 187-191.

Yang, J. R. and Bhadeshia, H. K. D. H.: Proc. Int. conf. on Welding Metallurgy of Structural Steels, ed. J. Y. Koo, The Metallurgical Society of AIME, Warrendale, P. A., 1987, pp. 549-563.

Yang, J-R. and Bhadeshia, H.K.D.H.: The Bainite to Austenite Transformation, **Presented at Phase Transformation 1987 in press,** 1987b.

Yang, J-R. and Bhadeshia, H.K.D.H.: *Reaustenitisation in steel weld deposits,* Proc. of Int. Conf. on Welding Metallurgy of Structural Steels, Denver, 1987c.

Yang, J-R. and Bhadeshia, H. K. D. H.: *Reaustenitisation Experiments on Some High-Stregth,* Materials Sci. and Eng., **A118,** 1989, pp. 155-170.

Yang, J-R and Bhadeshia, H. K. D. H.: *Continuous Heating Transformation*

of Bainite to Austenite **1990,** in press.

Yang, D.Z., Brown, E.L., Matlock, D.K. and Krauss, G.: *Ferrite Recrystalisation and Austenite Formation in Cold-Rolled Intercritically Annealed Steels,* Metall. Trans., **16A,** 1985, pp. 1385-1391.

Yang, D.Z., Brown, E.L., Matlock, D.K. and Krauss, G.: *The Formation of Austenite at Low Intercritical Annealing Temperatures in a Normalized 0.08C-1.45Mn-0.21Si Steel,* Metall. Trans., **16A,** 1985, pp. 1523-1526.

Yi, J. J., Kim, I. S. and Chi H. S.: *Austenitisation During Intercritical Annealing of an Fe-C-Si-Mn Dual Phase Steel,* Metall. Trans., **16A,** 1985, pp. 1237-1245.

Zener, C.: Trans. of Met. Soc. AIME., **167,** 1946, pp. 550.